# Fibre Spinning:
# Model Analysis

**Renu Dhadwal**

*For my parents and brother*

# Contents

# List of Figures

# List of Tables

# Preface

The main objective of textile industries has been the production of long, thin polymer fibres. Fibre spinning is an important industrial process used in the manufacture of synthetic fibres such as Nylon. The problem of fibre spinning has been an area of interest for engineers, physicists, chemists and mathematicians alike since the past 50 years. Search for faster and more reliable manufacturing techniques, the demand for better quality and low cost-products and enormous progress in the field of rheology of polymeric fluids has initiated interest in the theoretical study of various manufacturing processes like the fibre spinning process. In this thesis, we study a particular kind of fibre spinning called *Melt spinning*. From now onwards we shall be always dealing with the melt spinning process.

**What is melt spinning?**

Melt spinning is one type of fibre spinning. In this process molten polymer is extruded from a pressurised reservoir through a small circular orifice called the spinneret. The liquid jet undergoes stretching, cooling and solidification. The solidified filament is wound up via a take-up device at a higher speed than the extrusion velocity to ensure that the fibre is stretched. The fibre is then subjected to other processing steps.

High speed, non-isothermal spinning is associated with a concentrated neck like deformation process (where the diameter of the fibre shows a sudden, sharp decrease forming a neck-like region) and the development of high tensile stresses which result in the so called flow-induced crystallization. As a result, the spun fibres can be vastly superior in quality, possessing better mechanical and transport properties.

To take into account effects of crystallization and to understand the necking phenomena better, it has been inevitable for engineers to come up with models that couple the continuum equations with the microstructure. Typically,

the coupling takes place through the stress tensor which has an equivalent description in terms of the microstructural variables that describe the conformation of polymer molecules. There have been several attempts in this regard. One outstanding work is that of Doufas, McHugh and Miller (in sequel abbreviated as DMM model), [12] wherein the Giesekus constitutive model has been used to model the nonlinear viscoelastic effects. The DMM model consists of two ordinary differential equation (ODE) systems which are coupled by boundary conditions at the interface which is the point of onset of crystallization. This gives rise to a free boundary value problem where the point of onset of crystallization is unknown and a part of the solution. One ODE system describes the melt spinning equations before the onset of crystallization and we abbreviate this system as BOC. The other system describing the phase after the onset of crystallization will be called AOC.

## Objective and outline of the thesis

The purpose of this PhD thesis is to apply the model of Doufas ,McHugh and Miller to a specific industrial application (data from the company *Freudenberg & Co.*) and to perform a mathematical analysis. The outline and summary of the work is given as follows:

- In Chapter 1, we start with a brief overview of polymeric fluids, their viscoelastic (non-Newtonian) behaviour and kinetic theory of polymeric fluids. Then we describe the basic equations of melt spinning.

- In the Chapter 2, we give a brief description of the model which we have chosen for our analysis, the DMM model.

  However when applied to the empirical data, the DMM model has to be modified with respect to the air drag term and with respect to the interface condition at the free boundary. In the original work of Doufas et al [12], a linear air drag term with Bingham number is employed. For our purposes, the employment of Bingham number is not appropriate. Bingham plastics require a yield stress to deform. The fibres under consideration exhibit viscoelastic behaviour without yield stress. Thus, an alternative air drag term with a quadratic dependence on axial velocity is used.

  Concerning the interface condition at the boundary proposed by Doufas *et al*, discontinuity in the tensile stress is encountered. In the DMM model, the boundary condition for the strain rate at the interface (point of onset of crystallization) is taken from the calculations

from the previous stage. This assumes continuity of the strain rate at the point of onset of crystallization. There seems to be no valid explanation for such an assumption. Such an assumption implies the discontinuity of tensile stress at that point which is dubious from the physical point of view. On the other hand, we observe that from the simple physical law of force balance, the tensile forces on one side of the point of onset of crystallization should balance those on the other side. This force balance provides us with the correct boundary condition at the point of onset of crystallization.

- In Chapter 3, a mathematical analysis of the DMM model is performed. For the analysis, we treat the two sets of ODE systems in their respective domains separately. Through a local analysis of a simplified model, we show that even for the simplified model, the existence of a global solution for ODE system BOC is not guaranteed. In fact it even predicts the breakdown of the model in some cases. Thus, only a maximal solution for the initial value problem (IVP) BOC can exist. We define what we call a *physically acceptable solution* for both phases BOC and AOC and show that by choosing a restricted set of initial conditions for IVP BOC, a physically acceptable solution for the phase AOC exists under certain conditions. For this we prove the positive definiteness of the conformation tensor.

- In Chapter 4, we use Hamiltonian mechanics to analyse the basic equations of melt spinning excluding crystallization. The Hamiltonian for the 1-d viscoelastic fibre is found and it is shown that the cross sectionally averaged equations of melt spinning (excluding the temperature equation) along with the constitutive microstructural equations can be derived from the Hamiltonian. For this we derive the correct expression of the Poisson brackets for the 1-d, compressible, uniaxial extensional flow of a viscoelastic fluid.

- In Chapter 5, we present the numerical algorithm used to carry out the simulations. A shooting method is used to solve DMM numerically. Starting with a set of boundary conditions at the spinneret, the point of onset of crystallization is determined by solving the ODE system BOC. Afterwards the ODE system AOC is solved. The final velocity of the fibre is determined. Shooting method relies on the interpolation of this final velocity and the prescribed final velocity. At least two aspects make the numerical simulations challenging. First of all the set of initial conditions yielding physically acceptable solutions is quite limited (This topic is discussed in more details in Chapter 3). Second,

even for a physically acceptable solution the orders of magnitude of the ODE system coefficients vary a lot. This makes it necessary to employ efficient implicit methods for solving the ODEs. Matlab routines are used with appropriate choices of the control parameters. We show the results of the simulations for different take-up velocities. In this chapter we also demonstrate with the help of numerical experiments the sensitivity of the equations with respect to the initial conditions and order of magnitudes of the parameters.

- In Chapter 6, we show the simulation results done on four sets of data provided by the company *Freudenberg & Co.* Experimental profiles are used to do comparisons.

We conclude the thesis with some final remarks.

# Chapter 1

# Introduction to Polymer Fibres

*This chapter is intended to give a brief overview of the basic notions of polymers, viscoelastic fluids, various constitutive models, kinetics of polymers and finally the basic equations of melt spinning. The material for this chapter has been taken mainly from [4],[10] and [27].*

## 1.1 Polymer fluids

A polymer is a macromolecule. Macromolecules are large molecules made up of many small structural units. Polymer fluids are macromolecular fluids. There are many differences between macromolecular fluids like concentrated polymer melts and fluids composed of small molecules, like water. The molecular weight of macromolecules is very high and usually all the molecules of a polymer do not have the same weight. Polymer molecules assume a tremendous number of configurations even at equilibrium. In flow, the distribution of the configurations is significantly altered with the result that stretching and alignment of the molecules can cause the flow properties to change. For example, in the process of melt spinning, such stretching and alignment enhances crystallization and is responsible for the tremendous change in the material properties of the fibre. Due to the special structure of polymer fluids, Newtonian fluid dynamics fails to describe these fluids which are abundantly found in nature and are of great importance in our everyday life. Therefore, in the next section we discuss non-Newtonian fluids.

### 1.1.1 Non-Newtonian fluids

In order to understand what Non-Newtonian fluids are, we first define Newtonian fluids.

**Newtonian fluids** are defined as isotropic fluids with the shear stress $\boldsymbol{\tau}$ proportional to the deformation rate $\mathbf{D}$:

$$\boldsymbol{\tau} = \mu\mathbf{D}$$

where $\mu$ denotes the viscosity of the fluid [15]. For Newtonian fluids viscosity is constant. This class of fluids includes many "simple" liquids and gases (low molecular weight), e.g. water, air.

**Non-Newtonian fluids** are those fluids for which the relation between the shear stress and the deformation rate is not linear. Therefore, the viscosity is not a constant. It could depend on the shear stress or the deformation rate or other variables like temperature $T$ and other material properties. One could express the relation between the shear stress and deformation rate as:

$$\boldsymbol{\tau} = \mu(\mathbf{D}, T, ...)\mathbf{D}$$

[10]. The viscosity could increase (shear thickening) or decrease (shear thinning) respectively with increase in shear rate (deformation rate). Often in engineering literature, deformation rate is referred to as the shear rate or rate of strain. We will sometimes use the expression shear rate where we find that the meaning is better conveyed by this term.

### 1.1.2 Viscoelasticity

Viscoelastic fluids are one class of non-Newtonian fluids. As implied by the name, viscoelastic materials exhibit both viscous and elastic properties in varying degrees. For a purely viscous material the internal stresses are a function only of the instantaneous deformation rate. For a purely elastic material the stresses are a function only of the instantaneous deformation. But for a viscoelastic material, internal stresses are a function not only of the instantaneous deformation but also the entire history of deformation. Therefore, viscoelastic fluids are often called *fluids with memory* since the previous deformations influence the present state of stress. This influence of time on the relation between stress and strain can be described either by a differential equation involving derivatives of stress and/or strain with respect to time or by an integral equation with time as the variable.

**Properties of viscoelastic fluids**

The properties of viscoelastic fluids are quite different from those of Newtonian fluids and give rise to very interesting phenomena. Some of the main properties are described below, [19].

- Shear rate dependent viscosity
  The viscosity of a non-Newtonian fluid is not constant as stated before, but depends on the flow state of the liquid, that is the local shear rate. In most cases, the viscosity of a polymer solution decreases with increasing shear rate exhibiting the *shear thinning* behaviour.

- Normal stress differences
  Viscoelastic fluids exhibit normal stresses in contrast to Newtonian fluids. Normal stress differences play a very important role in the modelling of many industrial processes like melt spinning, film blowing etc. They are responsible for effects such as the Die-swell behaviour in fibre spinning.

- Memory and stress relaxation
  Viscoelastic fluids display memory. This can be seen when a viscoelastic material is subjected to sudden deformation and then kept fixed in that state. One observes that the stresses relax or decay to zero with a characteristic *relaxation time* (time taken for the stresses to relax). An elastic body would hold the tension once developed where as a viscous fluid would exert the stress only during the short time in which it is deformed. Therefore the relaxation time of a purely elastic solid is infinity and that of a purely viscous liquid is zero. For a viscoelastic fluid it lies in between 0 and $\infty$.

## 1.1.3   Examples of constitutive models

There are several rheological models that relate the stress in a viscoelastic material to its deformation rate. The models are either differential or integral equations. We explain below some of the differential viscoelastic models.

**Linear viscoelastic models**

- **Maxwell model**
  Maxwell model is the simplest and the oldest model describing vis-

coelastic effects. It is usually seen as the mechanical analog of a spring-dashpot model connected in series, [10]. The spring represents the elastic element and the dashpot represents the viscous element. Let $F$ represent the force acting on the spring and $x_s$ the resulting displacement. Then, we have $F = Kx_s$, where $K$ is the Hookean spring constant. Similarly, let $x_d$ represent the extension of the dashpot in response to applied force $F$. Then we have, $F = Ldx_d/dt$ for some constant of proportionality $L$. The total displacement is given by the sum of the two displacements as :

$$x = x_s + x_d$$

Differentiating the above with respect to time we have,

$$\frac{dx}{dt} = \frac{1}{K}\frac{dF}{dt} + \frac{F}{L}$$

This can be written as:

$$F + \lambda\frac{dF}{dt} = L\frac{dx}{dt}$$

where $\lambda = L/K$. If we assume the spring force to be analogous to the shear stress in an elastic material and the displacement analogous to the resulting shear strain and similarly, the force acting on the dashpot analogous to the shear stress and the resulting extension analogous to the deformation rate for a Newtonian fluid in shear, then the above derived equation results in the Maxwell model for viscoelastic fluids. In particular, the 3-d Maxwell model is given by:

$$\boldsymbol{\tau} + \lambda\frac{\partial\boldsymbol{\tau}}{\partial t} = -\mu(\nabla\mathbf{u} + \nabla\mathbf{u}^T)$$

where $\boldsymbol{\tau}$ represents the shear stress, $\mathbf{u}$ is the shear strain and the relaxation time has been defined as $\lambda = \mu/G$ with $\mu$ being the viscosity and $G$ the shear modulus. In the limiting case of $\lambda \to 0 \quad (G \to \infty)$, the model reduces to that of a Newtonian fluid. In the limiting case $\lambda \to \infty$, the model reduces to that of an elastic solid.

By using convected coordinates, one can get the so called *Upper Convected Maxwell model* which is given by:

$$\boldsymbol{\tau} + \lambda\check{\boldsymbol{\tau}} = 2\mu\mathbf{D}$$

where the convected derivative is denoted by the inverted hat on top of the tensor $\boldsymbol{\tau}$ and is in general defined as:

$$\check{\boldsymbol{A}} = \frac{\partial \boldsymbol{A}}{\partial t} + \mathbf{v} \cdot \nabla \boldsymbol{A} - (\nabla \mathbf{v} \cdot \boldsymbol{A} + \boldsymbol{A} \cdot \nabla \mathbf{v}^{\mathbf{T}}). \qquad (1.1)$$

for any second order tensor $\mathbf{A}$. There exist several other linear viscoelastic models like the Oldroyd model and the Voigt model. Details of these models can be found in any book about viscoelastic fluids [10], [27] and [4]. But linear viscoelastic models cannot describe the nonlinear effects of viscoelasticity. In melt spinning, one example of a nonlinear effect is the so called *strain hardening* behaviour where there is a sudden increase in the tensile stress of the fibre with increase in deformation rate. This is closely related to the necking phenomena observed in melt spinning. The extrudate die swell is also attributed to nonlinear viscoelastic behaviour. Hence we investigate some nonlinear viscoelastic models.

**Nonlinear viscoelastic models**

Among the several nonlinear viscoelastic models, we mention the one which we will be using.

- **Giesekus model** [2]
  Giesekus model has been derived from molecular theory. It is a nonlinear model which can describe a large number of material properties of polymer fluids in both shear and elongational flows. In terms of macroscopic variables of shear stress and deformation rate it takes the following form.

$$\boldsymbol{\tau} + \lambda \check{\boldsymbol{\tau}} + \alpha \boldsymbol{\tau} \cdot \boldsymbol{\tau} = 2\mu \mathbf{D} \qquad (1.2)$$

  where $0 \leq \alpha \leq 1$ is a model parameter.

- **Other models** Among other nonlinear models we mention the Phan-Thien-Tanner (PTT) model which is derived from molecular theory of networks of entangled polymers. More information about this and other models can be found in literature, [2],[23].
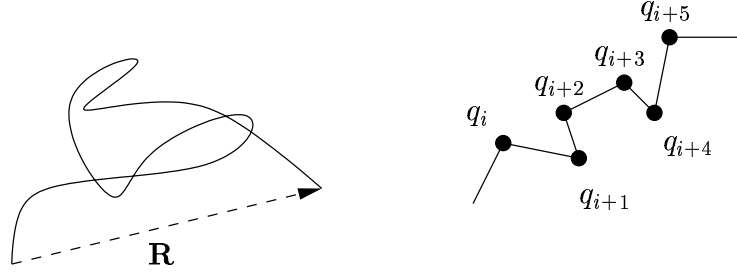
Figure 1.1: Left: *Polymer molecule with end-to-end vector* **R**. Right: *Segment of a polymer chain showing atoms and bonds.*

## 1.2   Micro-structure of polymer fluids

The polymer is assumed to be a flexible single chain molecule. In equilibrium, the polymer molecules are coiled into a small spherical shape where the conformational entropy is maximal. In flow conditions, this shape may get deformed, stretched. The forces trying to bring it back to equilibrium exert an extra force which is called the extra stress. Non-equilibrium statistical mechanics of polymer chains leads to constitutive equations which relate this extra stress to the flow field.

The coordinates of the atoms (say $n$) of the molecule and the corresponding momenta are denoted by $(\mathbf{q_i}, \mathbf{p_i})$, $i = 1, ..., n$ respectively, see Fig.1.1. The conformation of a single chain is given by the coordinates and momenta of all atoms $(\mathbf{Q}, \mathbf{P}) = \{(\mathbf{q_i}, \mathbf{p_i}), i = 1, ..., n\}$. The distance between the two ends of the polymer chain is given by the vector $\mathbf{R}$ which is also called the *end-to-end vector*. The set of all possible conformations constitutes the phase space of the polymer. From statistical mechanics, one gets the distribution function $\Psi(\mathbf{Q}, \mathbf{P})$ over this phase space. Then one can define any averaged quantity over the phase space as

$$< B >= \int B(\mathbf{Q}, \mathbf{P}) \Psi(\mathbf{Q}, \mathbf{P}) \; d(\mathbf{Q}, \mathbf{P}).$$

The *end-to-end distance* $R =< \mathbf{R} \cdot \mathbf{R} >^{1/2}$ is a measure of the average elongation of the polymer chain, caused by the flow field.

The *conformation tensor* **c** defined as $\mathbf{c} =< \mathbf{R} \otimes \mathbf{R} >$ is a symmetric positive definite tensor. From here we also see that

$$\mathrm{tr} \; \mathbf{c} =< \Sigma_i R_i^2 >= R^2$$

where tr represents the trace of tensor **c**.

**Remark 1.1** *At the macroscopic level, the conformation tensor can be understood to be equivalent to the strain tensor, [27], [2].*

### 1.2.1 Linear elastic dumbbell model
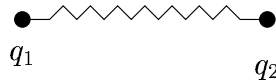


Figure 1.2: *Elastic dumbbell model*

The simplest model that gives a qualitative idea of the polymer chain dynamics is the *linear elastic dumbbell* model, [14]. The polymer chain is represented by two beads connected by a Hookean spring. When the beads move relative to the fluid, they experience a frictional force called the hydrodynamic drag $\zeta$. For concentrated polymer melts, the hydrodynamic drag has to take into account the frictional force due to the neighbouring beads (molecules).

## 1.3 Constitutive models in terms of micro-structure

The constitutive models mentioned in the previous section can also be derived from molecular theory using Hamiltonian mechanics, [2]. There are some models which have been in fact originally derived from network theory of polymer chains. One of these models is the Giesekus model. But these models have an equivalent macroscopic (continuum) description too.

### 1.3.1 Giesekus model

The Giesekus model at the molecular level takes into account the hydrodynamic interaction between neighbouring molecules in a concentrated solution. This is done by modifying the hydrodynamic drag parameter $\zeta$ suitably [2]. This introduces a nonlinearity in the model. But for this reason Giesekus

model is appropriate to model concentrated polymer melts. In terms of the conformation tensor **c**, the constitutive equation is written as

$$\check{\mathbf{c}} = -\frac{4k_BT}{\zeta}\left((1-\alpha)\mathbf{I} + \alpha\frac{K}{k_BT}\mathbf{c}\right)\cdot\left(\frac{K}{k_BT}\mathbf{c} - \mathbf{I}\right) \tag{1.3}$$

where $\alpha$ is a mobility parameter (also mentioned in the macroscopic version) with the constraint $0 \leq \alpha \leq 1$, $K$ denotes the Hookean spring constant, $k_B$ is the Boltzmanns constant and $T$ denotes the absolute temperature. For $\alpha = 0$, the equation reduces to the Maxwell model, [2].

## 1.3.2    FENE models

Most constitutive equations suffer from the drawback that having been derived from the elastic dumbbell model for polymer molecule, these equations cannot describe a strong flow such as uniaxial elongational flow. The class of *Finitely Extensible Nonlinear Elastic* (FENE) models take into account the finite extension of the polymer chains. In the linear elastic dumbbell model, the spring force is given by

$$\mathbf{F} = \left(\frac{3k_BT}{N_0l^2}\right)\mathbf{R} \tag{1.4}$$

Here $N_0$ denotes the number of links of length $l$ in a polymer chain. **R** is the end-to-end vector between the two ends of the chain. But this is valid only for small deformations of $R/N_0l$ where $R$ denotes the magnitude of **R** and $R/N_0l$ represents the extension of the polymer chain with respect to its length. For $R/N_0l \approx 1$, the force should increase infinitely since the molecule is stretched to its maximum. This can be taken into account by using a modified spring law:

$$|\mathbf{F}| = F = \frac{k_BT}{l}L^{-1}\left(\frac{R}{N_0l}\right) \tag{1.5}$$

[27], where the Langevin function $L$, is

$$L(x) = \coth(x) - \frac{1}{x}. \tag{1.6}$$

Let $e = R/N_0l$. Then, Eq.(1.5) can be re-written as

$$F = \frac{L^{-1}(e)}{3e}KR.$$

Denote $E := L^{-1}(e)/(3e)$. Then $F = EKR$ where $K = 3k_BT/(N_0l^2)$. This modified spring force law can be used in other constitutive equations like the Giesekus model (Eq.1.3) in order to take into account the finite extensibility of chains. This has been done in the model of Doufas, McHugh and Miller which will be explained in details in the next chapter.

**Relation between macroscopic stress and microscopic conformation tensor**

There is a relation between the macroscopic stress $\boldsymbol{\tau}$ and the microscopic variable $\mathbf{c}$. To determine the stress in a polymeric fluid at the microscopic level, one has to take into account the flux of $n$ number of dumbbells across a fixed element and the tension exerted by these dumbbells straddling a plane [27]. Then, the expression for the stress is:

$$\boldsymbol{\tau} = n < \mathbf{F} \otimes \mathbf{R} > -nk_BT\mathbf{I}$$

where $\mathbf{F}$ is the spring force and $nk_BT$ is the melt shear modulus. After substituting Eq.(1.4), the following relation is obtained for stress in terms of the conformation tensor

$$\boldsymbol{\tau} = nK\mathbf{c} - nk_BT\mathbf{I}.$$

Having given a brief overview of polymers, we move on to describe the basic equations of melt spinning.

# 1.4  Fundamental equations of melt spinning

The basic governing equations of melt spinning are typically 1-d differential equations accompanied by the appropriate boundary and/or initial conditions. Usually one is not interested in the time dependence and therefore steady state equations are used more often. In this section, we present a brief outline of the derivation of the fundamental equations of melt spinning as done by Hans Peter Langtangen in [20]. A schematic diagram of the process of melt spinning is shown in Fig.1.3. In the figure, the take-up velocity is denoted by $v_L$ at the take-up roll, $T_a$ denotes the temperature of the cooling air. The term *Freeze point* denotes the point where the fibre completely solidifies. When crystallization is taken into account then this point also

represents the point where crystallization is complete. Just before the freeze
point one sees the contraction of the fibre diameter. It is in the form of a
neck and therefore this phenomena is also called the *necking phenomena*.
However, in this section effects like necking or crystallization have not been
taken into account. This section is meant only to give an idea of the simple,
basic equations of melt spinning.

The molten polymer that comes out of the spinneret is assumed to be a
continuum fluid. The motion of any fluid is described by the equations of
conservation of mass, momentum and energy.

Let $\rho$ be the density of the polymer, $\mathbf{v}$ the velocity, $\boldsymbol{\sigma}$ the stress tensor, $\mathbf{g}$
gravity, $U$ the internal energy, $\mathbf{q}$ the heat flux and $Q$ the heat source.
Then the balance laws are given by:

- Equation of mass :

$$\frac{D}{Dt}\rho = 0 \tag{1.7}$$

- Equation of momentum:

$$\rho\frac{D\mathbf{v}}{Dt} = \nabla \cdot \boldsymbol{\sigma} + \rho\mathbf{g} \tag{1.8}$$

- Equation of energy:

$$\rho\frac{DU}{Dt} = \boldsymbol{\sigma} : \mathbf{D} - \nabla \cdot \mathbf{q} + Q \tag{1.9}$$

where $\mathbf{D}$ is the deformation rate tensor defined as $\mathbf{D} = (\nabla\mathbf{v} + (\nabla\mathbf{v})^T)/2$.
The material derivative $D/Dt$ is given by:

$$\frac{D}{Dt} = \frac{\partial}{\partial t} + \mathbf{v} \cdot \nabla.$$

Later, we shall assume only steady state equations.

According to Fourier's law, heat flux is proportional to the temperature gra-
dient

$$\mathbf{q} = -k\nabla T \quad k > 0 \tag{1.10}$$

where $k$ is the heat conduction coefficient.
Density $\rho$ is assumed to be constant. The internal energy $U$ can be approx-
imated by $C_pT$ where $C_p$ is the specific heat capacity at constant pressure.
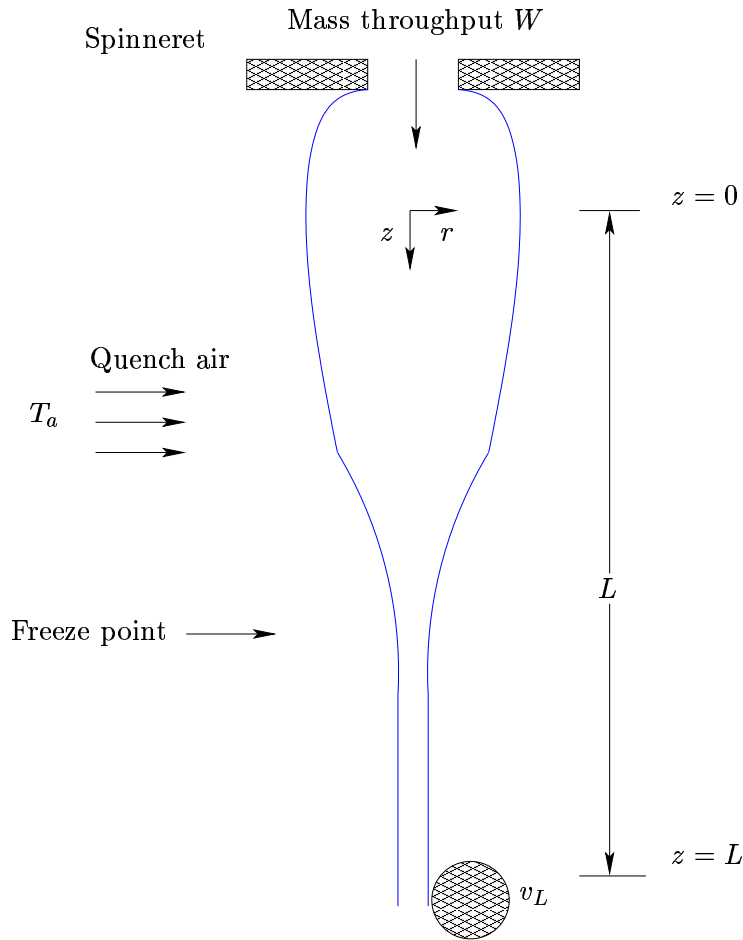
Figure 1.3: *Sketch of melt spinning process*

The enthalpy change due to phase transition from an amorphous phase to semi-crystalline phase is denoted by $c$. A phenomenological model for $c$ is

$$c = \rho \Delta H \frac{D\phi}{Dt}$$

where $\Delta H$ is the specific heat of fusion of a perfect crystal and $\phi$ is the degree of crystallinity.

Using the above relations, (1.9) can be written as

$$\rho C_p \frac{DT}{dt} = \boldsymbol{\tau} : \mathbf{D} - \nabla \cdot (k\nabla T) + c \tag{1.11}$$

where the shear stress $\boldsymbol{\tau}$ denotes the deviatoric part of the stress tensor, i.e $\boldsymbol{\sigma} = -p\mathbf{I} + \boldsymbol{\tau}$.

## 1.4.1    Coordinate system

For further work, an appropriate coordinate system is chosen. Due to the elongational nature of polymer flow, there is axisymmetry, which can be exploited by employing cylindrical coordinate system. Introducing the cylindrical coordinates $(r, \theta, z)$, the velocity can be written as

$$\mathbf{v} = v_r \mathbf{i_r} + v_\theta \mathbf{i_\theta} + v_z \mathbf{i_z},$$

where $\mathbf{i_r}, \mathbf{i_\theta}, \mathbf{i_z}$ are the unit vectors in the $r, \theta$ and $z$ directions respectively.

From rotational symmetry, $v_r = v_r(r, z)$, $v_\theta = 0$, and $v_z = v_z(r, z)$. Since the radial variations in the $z$ component of the velocity are assumed to be negligible as compared to the axial variations, $v_z$ is a function only of $z$. Then,

$$\mathbf{v}(r, z) = v_r(r, z)\mathbf{i_r} + v_z(z)\mathbf{i_z}.$$

## 1.4.2    Uniaxial elongational flow

Consider the mass balance equation in the differential form:

$$\frac{1}{r}\frac{\partial(r\rho v_r)}{\partial r} + \frac{\partial \rho v_z}{\partial z} = 0 \tag{1.12}$$

The flow field in the melt spinning process can be considered to be a uniaxial, elongational flow, with axial position dependent elongation rate. Integrating (1.12) with respect to $r$ one gets a relation between the radial component of velocity and the axial component, [20]

$$v_r(r, z) = -\frac{1}{2}\frac{dv_z}{dz}r.$$

Then deformation rate tensor $\mathbf{D}$ has the following diagonal components:

$$
\begin{aligned}
D_{zz} &= \frac{dv_z}{dz} \\
D_{rr} &= \frac{\partial v_r}{\partial r} = -\frac{1}{2}\frac{dv_z}{dz} \\
D_{\theta\theta} &= \frac{v_r}{r} = -\frac{1}{2}\frac{dv_z}{dz}.
\end{aligned}
$$

Vanishing of other components can be concluded from dimensional analysis. Scaling the radial variable $r$ by radius at the spinneret $R_0$ and $z$ by the

typical length of the fibre $L$, one observes that the typical scale of $\partial v_r / \partial z$ is $R_0 / L$. Since from slender body approximation $R_0 / L \ll 1$, one can assume that $\partial v_r / \partial z = 0$. Then $\mathbf{D}$ takes the following form:

$$
\begin{aligned}
\mathbf{D} &= \tfrac{1}{2}(\nabla \mathbf{v} + (\nabla \mathbf{v})^T) \\[2mm]
&= \begin{pmatrix}
-\frac{1}{2}\frac{dv_z}{dz} & 0 & 0 \\
0 & -\frac{1}{2}\frac{dv_z}{dz} & 0 \\
0 & 0 & \frac{dv_z}{dz}
\end{pmatrix}
\end{aligned}
\tag{1.13}
$$

Stress tensor in cylindrical coordinates is

$$
\boldsymbol{\sigma} = \begin{pmatrix}
\sigma_{rr} & \sigma_{\theta r} & \sigma_{zr} \\
\sigma_{r\theta} & \sigma_{\theta\theta} & \sigma_{z\theta} \\
\sigma_{rz} & \sigma_{\theta z} & \sigma_{zz}
\end{pmatrix}.
$$

It is symmetric and since $\boldsymbol{\sigma} = p\mathbf{I} + 2\mu\mathbf{D}$, it has a diagonal form. For non Newtonian fluids, the viscosity $\mu$ depends on $\mathbf{D}$. In general, the viscosity will depend on the temperature and other material properties of the polymer.

Consider a particular volume $V$, representing a fibre section of infinitesimal thickness $dz$. Using the steady state and incompressibility assumptions to Eqs.(1.7), (1.8) and (1.11), the resulting equations are integrated over $V$ with boundary $\partial V$. After applying the divergence theorem the following equations are obtained.

$$
\int_{\partial V} \rho \mathbf{v} \cdot \mathbf{n} d\Gamma = 0
\tag{1.14}
$$

$$
\int_{\partial V} \rho(\mathbf{v} \otimes \mathbf{v}) \cdot \mathbf{n} d\Gamma = \int_{\partial V} \boldsymbol{\sigma} \cdot \mathbf{n} d\Gamma - \int_V \rho \mathbf{g} dV
\tag{1.15}
$$

$$
\int_{\partial V} \rho C_p T(\mathbf{v} \cdot \mathbf{n}) d\Gamma = \int_{\partial V} k\nabla T \cdot \mathbf{n} d\Gamma + \int_V \boldsymbol{\tau} : \mathbf{D} dV + \int_V c \, dV
\tag{1.16}
$$

The outward unit normal $\mathbf{n}$ of the free surface $r = R(z)$ is given as

$$
\mathbf{n} = \frac{\nabla(r - R(z))}{\| \nabla(r - R(z)) \|} = \frac{i_r - R'(z)i_z}{\sqrt{1 + R'(z)^2}}
$$

Radius of the fibre at $z$ is denoted by $R(z)$ and its derivative with respect to $z$ by $R'(z)$.

### 1.4.3    Boundary conditions on the surface

The boundary conditions on the surface $r = R(z)$ are the following:

- $\mathbf{v} \cdot \mathbf{n} = 0$.

- Stress conditions
  Let $\tau_n = (\boldsymbol{\tau} \cdot \boldsymbol{n}) \cdot \mathbf{n}$ denote the normal stress component of the fluid at the boundary $r = R(z)$ and $\tau_t$ the corresponding tangential stress component. Then,

$$\tau_t = -\sigma_T.$$

  where $\sigma_T$ is the surface shear stress due to the friction between the polymer and the surrounding air.

$$\tau_n = -p_a - \sigma_s\big(\kappa_r + \kappa_z\big)$$

  where $p_a$ denotes the atmospheric pressure, $\sigma_s$ denotes the surface tension and $\kappa_r$ and $\kappa_z$ are radii of curvature in the $r$ and $z$ directions respectively. Here, $\kappa_r = 1/R(z)$ and $\kappa_z \sim R''$. Again from scaling arguments one concludes that $\kappa_z$ is small and hence can be neglected.

- Temperature conditions

$$-k\nabla T.\mathbf{n} = \beta(T - T_a)$$

  where $T_a$ is the temperature of the surrounding air and $\beta$ is the heat transfer coefficient.

After integrating over the volume and applying the boundary conditions at the free surface, one performs averaging over the cross section of the fibre to obtain the final equations of melt spinning. Let $D = 2R$ be the diameter of the fibre and $A = \pi R^2$, the corresponding cross-sectional area. Then the final equations of melt spinning can be written as:

$$W = \frac{\pi \rho v_z D^2}{4} \tag{1.17}$$

$$W\frac{dv_z}{dz} = -\pi D \sigma_T + \frac{\pi \sigma_s}{2}\frac{dD}{dz} + \frac{d}{dz}A(\tau_{zz} - \tau_{rr}) + A\rho g \tag{1.18}$$

$$\rho C_p v_z \frac{dT}{dz} = \frac{-4}{D}k(T - T_a) + (\tau_{zz} - \tau_{rr})\frac{dv_z}{dz} + \rho \Delta H v_z \frac{d\phi}{dz} \tag{1.19}$$

Here $W$ denotes the mass throughput per unit time. Therefore the first equation simply states that the mass throughput is constant along the spinline. In the second equation, the first term on the right hand side represents the force due to shear stress at the fibre surface (air drag for example), the second term represents the force due to surface tension, the third term represents the average tensile force and the last term, the force due to gravity. In the third equation, the first term represents the exchange of heat between the air and fibre surface, the second term describes the heat released due to viscous dissipation and third term denotes the latent heat of crystallization.

To close the system a viscoelastic constitutive model is needed that relates the shear stress to the deformation rate. One can choose any viscoelastic model from the many existing ones. e.g Maxwell model, Giesekus etc.

The unknown variables are $v_z$,$T$,$\tau_{zz}$ and $\tau_{rr}$ where evolution equations of $\tau_{zz}$ and $\tau_{rr}$ are given by the viscoelastic model. This system has to be closed by appropriate boundary conditions. Typically the velocity and temperature are prescribed at the spinneret exit and a take up velocity is prescribed at the end of the fibre. One usually has to guess the initial condition for the stress variables. Therefore, shooting technique has to be applied to solve the boundary value problem.

# Chapter 2

# The Two-phase Model

*In this chapter we give a brief description of the two phase model of Doufas, McHugh and Miller, [11]. Later we present some modifications of the macroscopic model.*

The model of Doufas, McHugh and Miller (DMM), couples the balance laws for fluids with the microstructural equations of the polymer. It is a steady state model. The balance laws of mass, momentum and energy take into account effects such as air drag, inertia, surface tension, gravity, exchange of heat with surrounding air and viscous dissipation. The microstructural equations are the constitutive viscoelastic equations that describe the evolution of the microstructure, (see Section 1.3). In the process of melt spinning at high speeds, the polymer molecules are stretched and aligned, giving rise to the process of crystallization. Therefore, the microstructure has two components, the amorphous phase and the semi-crystalline phase. The amorphous phase is described by a modified Giesekus model. The Giesekus model is suitably modified by introducing finite extensibility of polymer chains, as described in Section 1.3.2. In the semi-crystalline phase the polymer molecules are modelled as rigid rods that grow and orient in the flow field. The reason for having two separate phases is that in high speed spinning, with increase in strain rate, tensile stresses shoot up indicating rigid behaviour of polymer molecules. By modelling the molecules as rigid rods in this phase, the necking phenomenon can be captured. The model can be divided into two parts: The part before the onset of crystallization (BOC) and the part after the onset of crystallization (AOC).

## 2.1  Before the onset of crystallization

Before the onset of crystallization the polymer is amorphous. The polymer in its molten state can be thought of as consisting of $n$ nonlinear elastic dumbbell molecules. Each of the molecule chains is assumed to consist of $N_0$ structural units or statistical links of length $l$. Let $\mathbf{R}$ denote the end-to-end distance vector between the two end points of a chain. The tensor $\mathbf{c} = <\mathbf{R} \otimes \mathbf{R}>$ represents the configuration of the melt.

### 2.1.1  Amorphous phase

The rheological behaviour of the melt is modelled by a modification of the single-mode Giesekus model, Eq.(1.3):

$$\check{\mathbf{c}} = -\frac{4k_b T}{\zeta}\left((1-\alpha)\mathbf{I} + \alpha\frac{K}{k_B T}\mathbf{c}\right) \cdot \left(\frac{K}{k_B T}\mathbf{c} - \mathbf{I}\right) \tag{2.1}$$

with the definition of the convected derivative as given by Eq.(1.1). Here, $\zeta$ denotes the hydrodynamic drag between the beads of the molecules. To take into account the finite extensibility of chains, a modified spring law (FENE) is used as explained in Section 1.3.2. By defining $\lambda_a = \zeta/4K$ the following final evolution equation for the conformation tensor is obtained:

$$\check{\mathbf{c}} = -\frac{1}{\lambda_a(T)}\frac{k_B T}{K}((1-\alpha)\mathbf{I} + \alpha\frac{K}{k_B T}E\mathbf{c}) \cdot (\frac{K}{k_B T}E\mathbf{c} - \mathbf{I}) \tag{2.2}$$

where $k_B$ is the Boltzmann constant, $K$ is the Hookean spring constant, $\lambda_a$ is the characteristic relaxation time of the melt and $E$ is the non-linear spring force factor given by $E = L^{-1}(e)/3e$ where $L^{-1}$ is the inverse Langevin function and $e = (\mathrm{tr}\mathbf{c})^{1/2}/N_0 l$. Expanding the convected derivative term and considering only the steady state so that partial derivatives with respect to time vanish, the following evolution equations for the components of the conformation tensor $c_{zz}$ and $c_{rr}$ are obtained:

$$v_z\frac{dc_{zz}}{dz} = 2c_{zz}\frac{dv_z}{dz} - \frac{1}{\lambda_a(T)}\frac{k_B T}{K}(1 - \alpha + \alpha\frac{K}{k_B T}Ec_{zz})(\frac{K}{k_B T}Ec_{zz} - 1) \tag{2.3}$$

$$v_z\frac{dc_{rr}}{dz} = -c_{rr}\frac{dv_z}{dz} - \frac{1}{\lambda_a(T)}\frac{k_B T}{K}(1 - \alpha + \alpha\frac{K}{k_B T}Ec_{rr})(\frac{K}{k_B T}Ec_{rr} - 1) \tag{2.4}$$

**Remark 2.1** $\mathbf{c}$ *is a diagonal tensor with* $c_{rr} = c_{\theta\theta}$.

### 2.1.2   Extra stress

The extra stress tensor for the melt in terms of the microstructural variables is according to [4]:

$$\boldsymbol{\tau} = nKE\mathbf{c} - nk_BT\mathbf{I} \qquad (2.5)$$

The melt shear modulus $G$ is given in terms of microstructure as $G = nk_BT$ and is assumed to be constant along the spinline. The calculation of the stress from the kinetic theory of concentrated polymer fluids can be found in [27].

## 2.2   Onset of crystallization

As explained before, each polymer chain is assumed to be made up $N_0$ structural units called statistical links. During flow, due to the influence of cooling air and increasing stress, some of these links (say $N$) break away and align themselves. This starts the process of crystallization. It is observed experimentally that crytallization starts approximately when the temperature of the polymer melt reaches its melting temperature. It should be noted that the temperature at the exit of the spinneret is much higher than the melting temperature.

The degree of crystallization is given as $x = N/N_0$. The absolute degree of crystallinity, defined as the ratio of the mass of pure crystalline material over the total mass of the system is given as $\phi = x\phi_\infty$, where $\phi_\infty$ is the degree of crystallinity within the semi-crystalline phase. That is, mass of the pure crystalline material over mass of semi-crystalline phase.

## 2.3   After the onset of crystallization

After the onset of crystallization, the polymer melt has two phases: Amorphous phase and Semi-crystalline phase.

## 2.3.1   Amorphous phase

The untransformed melt phase is simulated as a single-mode Giesekus fluid as
before but with corrections to the Hookean spring constant and $e$ as follows

$$
\begin{aligned}
K &= \frac{3k_B T}{N_0(1-x)l^2} \\
e &= \frac{1}{1-x}\sqrt{\frac{c_{zz}+2c_{rr}}{3N_0}}
\end{aligned}
\tag{2.6}
$$

The crystallinity dependent relaxation time is modelled by

$$
\lambda_a(x,T) = \lambda_{a,0}(T)(1-x)^2
$$

where $\lambda_{a,0}$ is the temperature dependent relaxation time in the absence of
crystallization, see Appendix A.

## 2.3.2   Semi-crystalline phase

The semi-crystalline phase is modelled as a collection of rigid rods that grow
and orient in the flow field. The structural variable representing the orienta-
tion of the rigid rods is given by the orientation tensor $\mathbf{S} \equiv <\mathbf{u}\otimes\mathbf{u}> -1/3\ \mathbf{I}$,
where $\mathbf{u}$ is the unit vector along the rod axis and $\mathbf{I}$ is the identity tensor.
It is a second order trace-less tensor with $S_{rr} = S_{\theta\theta}$. The bracket in the
definition of $\mathbf{S}$ denotes an average with respect to the distribution function
of the semi-crystalline phase. The evolution equation for $\mathbf{S}$ reads as follows:

$$
\check{\mathbf{S}} = -\frac{\sigma}{\lambda_{sc}(x,T)}\mathbf{S} + \frac{1}{3}(\nabla\mathbf{v}+(\nabla\mathbf{v})^T) - 2(\nabla\mathbf{v})^T:\mathbf{U}
\tag{2.7}
$$

where $\mathbf{U}$ is a fourth order tensor, $\mathbf{U} :=<\mathbf{u}\otimes\mathbf{u}\otimes\mathbf{u}\otimes\mathbf{u}>$. We refer to
[11] and [14] for details. Here $\sigma$ is the anisotropic drag parameter such that
$0 < \sigma \leq 1$. The relaxation time is modelled as

$$
\lambda_{sc}(x,T) = \lambda_{sc,0}(T)\exp(Fx) \simeq c\lambda_{a,0}(T)\exp(Fx).
\tag{2.8}
$$

The model parameters $c$ and $F$ are determined experimentally.

### 2.3.3   Extra stress

The extra stress contributed by the semi-crystalline phase is

$$\boldsymbol{\tau_{sc}} = 3nk_BT \; (\mathbf{S} + 2\lambda_{sc}(\nabla\mathbf{v})^T : \mathbf{U}). \qquad (2.9)$$

The first term on the RHS of Eq.(2.9) represents the elastic contribution to the stress and the second term is the so called viscous contribution to the stress.

A closure approximation by Advani and Tucker is used to evaluate the expression $(\nabla\mathbf{v})^T : \mathbf{U}$ in equations (2.7) and (2.9).

$$\begin{aligned}
\nabla(\mathbf{v})^T : \mathbf{U} \cong (1-w) &\left( \frac{1}{15}(\nabla\mathbf{v} + (\nabla\mathbf{v})^T) + \frac{1}{7}\bigg[ ((\nabla\mathbf{v})^T : \mathbf{S}) \; \mathbf{I} \right. \\
&+ \mathbf{S} \cdot (\nabla\mathbf{v} + (\nabla\mathbf{v})^T) + (\nabla\mathbf{v} + (\nabla\mathbf{v})^T) \cdot \mathbf{S} \bigg] \bigg) \\
&+ w((\nabla\mathbf{v})^T : \mathbf{S}) \; (\mathbf{S} + \frac{1}{3}\mathbf{I})
\end{aligned} \qquad (2.10)$$

where $w = 1 - 27\det(\mathbf{S} + 1/3 \; \mathbf{I})$, see [1], [11] for details.

### 2.3.4   Rate of crystallization

The rate of crystallization is modelled using the Avrami equation and following the Hamiltonian bracket formalism, [11]. It reads as:

$$\frac{Dx}{dt} = mK_{av}(T)[-\log(1-x)]^{(m-1)/m}(1-x)\exp\left(\psi\frac{\mathrm{tr}\tau}{G}\right) \qquad (2.11)$$

where $\psi$ and $m$ are dimensionless constant model parameters and $K_{av}$ is also a parameter depending on the temperature, see Eq.(5) in Appendix A. The total stress tensor is given by $\boldsymbol{\tau} = \boldsymbol{\tau_a} + \boldsymbol{\tau_{sc}}$.

*We have described the microstructural models very briefly. For further details we request the reader to refer to the corresponding cited literature.*

## 2.4  Modifications in the macroscopic model

We introduce our modifications in the macroscopic model.

**Force due to air drag**

In the DMM model a linear relationship has been used to model the air drag. We make a modification by using the air drag force with a quadratic dependence on velocity. The force due to air drag is expressed as

$$F = -\frac{1}{2}\rho_a C_d (v_z - v_d)^2$$

where $\rho_a$ is the density of the air, $C_d$ is the air drag coefficient and $v_d$ the downward component of the air velocity. The air drag coefficient $C_d$ depends on the Reynolds number Re: $C_d = 0.37\mathrm{Re}^{-0.61}$ where $\mathrm{Re} = (v_z D \rho_a)/\mu_a$ with $\mu_a$ being the viscosity of the air, [20], [29].

Introducing the new air drag force into the momentum equation the following modified momentum equation is obtained:

$$W\frac{dv_z}{dz} = -\frac{1}{2}\pi D \rho_a C_d (v_z - v_d)^2 + \frac{\pi s}{2}\frac{dD}{dz} + \frac{d}{dz}A(\tau_{zz} - \tau_{rr}) + A\rho g. \quad (2.12)$$

**Force balance at the point of onset of crystallization**

The differential equation system arising from the model is a nonlinear, coupled system of differential equations with boundary conditions at the spinneret, at the end of the spinline and at the point of onset of crystallization $\xi$. In the phase BOC, the ODE system consists of variables $v_z$, $T$, $c_{zz}$ and $c_{rr}$ and in the phase AOC, variables $v_z$, $dv_z/dz$, $c_{zz}$, $c_{rr}$, $S_{zz}$ and $x$. In the model, the boundary condition for the variable $dv_z/dz$ at $\xi$ is taken from the calculations from the previous phase (BOC). This assumes the continuity of $dv_z/dz$ at the point of onset of crystallization. There seems to be no valid explanation for such an assumption. Such an assumption implies the discontinuity of tensile stress at $\xi$ which is questionable from the physical point of view. On the other hand, we observe that from the simple physical law of force balance, the tensile forces on one side of the point of onset of crystallization should balance those on the other side. In the momentum equation, $A(\tau_{zz} - \tau_{rr})$ denotes the tensile force at any arbitrary position $z$. Since the cross sectional area $A$ is continuous at $\xi$, this means that the tensile stresses themselves should also be continuous:

Let $[0, \xi)$ denote the domain before the onset of crystallization and $(\xi, 1]$, the domain after the onset of crystallization. Introduce non-dimensionalised variables $\boldsymbol{\tau}^* = \boldsymbol{\tau}/G$, $\mathbf{c}^* = \mathbf{c}K/k_BT$, $v_z^* = v_z/v_0$, $z^* = z/L$ and $\mathrm{De}_{sc} = v_0\lambda_{sc}/L$ where $\mathrm{De}_{sc}$ represents the Weisenberg number of the semi-crystalline phase. The stress difference before the onset of crystallization, i.e for $z \in [0, \xi)$, is given by

$$\tau_{zz}^* - \tau_{rr}^* = E(c_{zz}^* - c_{rr}^*).$$

The stress difference after the onset of crystallization, i.e for $z \in (\xi, 1]$ is given by

$$\begin{aligned}\tau_{zz}^* - \tau_{rr}^* =& E(c_{zz}^* - c_{rr}^*) + \frac{9}{2}S_{zz} \\ &+ 6\mathrm{De}_{sc}[(1 - w)(\frac{3}{15}\frac{dv_z^*}{dz^*} + \frac{6}{14}\frac{dv_z^*}{dz^*}S_{zz}) + \frac{9}{4}w\frac{dv_z^*}{dz^*}S_{zz}^2].\end{aligned}$$

where $w = 1 - 27\det(\mathbf{S} - 1/3\mathbf{I})$.
From the continuity of the stress difference at the point $\xi$, for $\epsilon > 0$, we have

$$\lim_{\epsilon \to 0}(\tau_{zz}^*(\xi - \epsilon) - \tau_{rr}^*(\xi - \epsilon)) = \lim_{\epsilon \to 0}(\tau_{zz}^*(\xi + \epsilon) - \tau_{rr}^*(\xi + \epsilon))$$

Substituitng the boundary values of $S_{zz}$ and $x$ which are $S_{zz}(\xi) = 0$ $x(\xi) = 0$, we get,

$$E(\xi)(c_{zz}^*(\xi) - c_{rr}^*(\xi)) = E(\xi)(c_{zz}^*(\xi) - c_{rr}^*(\xi)) + \frac{6}{5}\mathrm{De}_{sc}(\xi)\frac{dv_z^*}{dz^*}(\xi). \qquad (2.13)$$

Continuity of $E$ which is a function of $c_{zz}$, $c_{rr}$ and $x$ is easy to see from its definition in Sections 2.1.1 and 2.3.1. Moreover, $\mathrm{De}_{sc}(\xi) \neq 0$ for $c \neq 0$. Parameter $c$ is always chosen to be non-zero since a zero relaxation time would indicate a totally viscous or rigid behaviour of the melt. Hence, Eq.(2.13) is satisfied if and only if $dv_z^*/dz^*(\xi) = 0$. This gives us the correct boundary condition for the strain rate at $\xi$ which is

$$\frac{dv_z^*}{dz^*}(\xi) = 0.$$

## 2.5   Non-dimensionalised evolution equations

The final system consists of Eqs.(1.17), (1.18), (1.19) and the steady state microstructural evolutions equations for $c_{zz}$, $c_{rr}$, $S_{zz}$ and $x$ given by Eqs.(2.2), (2.7) and (2.11) with the appropriate changes for the semi crystalline phase as mentioned in Section 2.3.1. Dimensionless variables are introduced as follows, [11]:

- Axial distance $z^* = \frac{z}{L}$,   gradient operator $\nabla^* = \frac{\nabla}{L}$

- Axial velocity $v_z^* = \frac{v_z}{v_0}$,   Temperature $T^* = \frac{T}{T_0}$

- Conformation tensor $\mathbf{c}^* = \frac{\mathbf{c}K}{k_B T}$,   Extra stress tensor $\boldsymbol{\tau}^* = \frac{\tau}{n k_B T} = \frac{\tau}{G}$

- Inertia $D_1 = \frac{\rho v_0^2}{G}$,   Air drag $D_2 = \frac{C_d v_0^3 L \rho_a}{2G} \sqrt{\frac{\rho \pi}{W v_0}}$;

**Remark 2.2** *The air drag term is different from the one originally used by Doufas et al. The original $D_2$ is given as $D_2 = \frac{\pi \mu_a B L \rho v_0^2}{GW}$*

- Gravity $D_3 = \frac{gL\rho}{G}$,   Surface tension $D_4 = \left(\frac{\pi \sigma_s^2 \rho v_0}{4 W G^2}\right)^2$

- Heat convection $D_5 = \left(\frac{4\pi L^2 k^2}{\rho C_p^2 v_0 W}\right)^{1/2}$,   Viscous dissipation $D_6 = \frac{G}{\rho C_p T_0}$

- Latent heat of crystallization $D_7 = \frac{\Delta H_f \phi_\infty}{C_p T_0}$

- Relative velocity of air $v_r = \frac{v_d}{v_0}$ where $v_d$ is the downward component of the air velocity

- Relative temperature of air $T_r = \frac{T_a}{T_0}$

- Weisenberg number of amorphous phase $De_a = \frac{v_0 \lambda_a}{L}$

- Weisenberg number of semi-crystalline phase $De_{sc} = \frac{v_0 \lambda_{sc}}{L}$

- Crystallization number $K^* = \frac{K_{av} L}{v_0}$

Heat capacity $C_p$ depends on temperature and crystallinity and the heat diffusion coefficient $k$ depends on velocity. The formulae for calculating them are given in Appendix A. Models for other quantities like $\Delta H_f$ and $\mu_a$ are also given in Appendix A. The system of ODEs for the phase BOC can be written in terms of the dimensionless variables as follows:

- Momentum balance

$$D_1 \frac{dv_z^*}{dz} = \frac{d}{dz}\left[\frac{\tau_{zz}^* - \tau_{rr}^*}{v_z^*}\right] - D_2 \frac{(v_z^* - v_r)^2}{\sqrt{v_z^*}} + \frac{D_3}{v_z} - D_4 \left(v_z^*\right)^{-3/2} \frac{dv_z^*}{dz^*} \quad (2.14)$$

- Energy balance

$$\frac{dT^*}{dz^*} = -D_5 (v_z^*)^{-1/2} (T^* - T_r) + D_6 \frac{\tau_{zz}^* - \tau_{rr}^*}{v_z^*} \frac{dv_z^*}{dz^*} \qquad (2.15)$$

- Evolution equations for the conformation tensor

$$\frac{dc_{zz}^*}{dz^*} = 2\frac{c_{zz}^*}{v_z^*} \frac{dv_z^*}{dz^*} - \frac{1}{v_z^* De_a} ((1-\alpha) + \alpha E c_{zz}^*)(E c_{zz}^* - 1) \qquad (2.16)$$

$$\frac{dc_{rr}^*}{dz} = -\frac{c_{rr}^*}{v_z^*} \frac{dv_z^*}{dz^*} - \frac{1}{v_z^* De_a} ((1-\alpha) + \alpha E c_{rr}^*)(E c_{rr}^* - 1) \qquad (2.17)$$

These equations are supplemented by the relation

$$\boldsymbol{\tau}^* = E\mathbf{c}^* - \mathbf{I}. \qquad (2.18)$$

The ODE system for phase AOC is the following:

- Momentum balance is given by Eq.(2.14) but with the stress relation as given in Eq.(2.24).

- Energy balance

$$\frac{dT^*}{dz^*} = -D_5 (v_z^*)^{-1/2} (T^* - T_r) + D_6 \frac{\tau_{zz}^* - \tau_{rr}^*}{v_z^*} \frac{dv_z^*}{dz^*} + D_7 \frac{dx}{dz^*} \qquad (2.19)$$

- Evolution equations for the conformation tensor

$$\frac{dc_{zz}^*}{dz^*} = 2\frac{c_{zz}^*}{v_z^*} \frac{dv_z^*}{dz^*} - \frac{1-x}{v_z^* De_a} ((1-\alpha) + \alpha \frac{E}{1-x} c_{zz}^*)(\frac{E}{1-x} c_{zz}^* - 1) \quad (2.20)$$

$$\frac{dc_{rr}^*}{dz} = -\frac{c_{rr}^*}{v_z^*} \frac{dv_z^*}{dz^*} - \frac{1-x}{v_z^* De_a} ((1-\alpha) + \alpha \frac{E}{1-x} c_{rr}^*)(\frac{E}{1-x} c_{rr}^* - 1) \quad (2.21)$$

- Evolution equation for the orientation tensor

$$\frac{dS_{zz}}{dz^*} = 2\frac{S_{zz}}{v_z^*} \frac{dv_z^*}{dz^*} - \frac{\sigma}{v_z^* De_{sc}} S_{zz} + \frac{2}{3} \frac{1}{v_z^*} \frac{dv_z^*}{dz^*} - 2\frac{1-w}{v_z^*} \left(\frac{2}{15} + \frac{11}{14} S_{zz}\right) \frac{dv_z^*}{dz^*}$$
$$- 3\frac{w}{v_z^*} S_{zz} \left(S_{zz} + \frac{1}{3}\right) \frac{dv_z^*}{d_z^*} \qquad (2.22)$$

where $w = 1 - 27\det(S + \frac{1}{3}\mathbf{I})$. By definition $S_{zz}$ is dimensionless.

- Evolution equation for the rate of crystallization

$$\frac{dx}{dz^*} = \frac{1}{v_z^*} mK^* [\log(1-x)]^{(m-1)/m}(1-x)\exp(\psi \mathrm{tr}\boldsymbol{\tau}^*) \qquad (2.23)$$

  where tr represents the trace of tensor $\boldsymbol{\tau}^*$. By definition $x$ is also dimensionless.

**Remark 2.3** *Parameter m is always taken to be 1 in this model, [11], [12] which simplifies the equation. In future we use the simplified equation for all our analysis and simulations.*
These equations are supplemented by the relation

$$\boldsymbol{\tau}^* = \frac{E}{1-x}\mathbf{c}^* - \mathbf{I} + 3\mathbf{S} + 6De_{sc}(\nabla^*\mathbf{v}^*)^T : \mathbf{U}. \qquad (2.24)$$

## 2.6    Boundary conditions

- Boundary conditions at the spinneret exit, i.e. at $z^* = 0$ are,

$$v_z^*(0) = 1, \quad T^*(0) = 1, \quad \tilde{h}(c_{zz}^*(0), c_{rr}^*(0)) = 0.$$

  More about the form of $\tilde{h}$ will be found in Chapters 3 and 5.

- Condition for finding $\xi$,

$$T^*(\xi) = T_m$$

  where $T_m$ = melting temperature of the polymer/initial temperature.

- Boundary condition at $z^* = \xi$,

$$v_z^*(\xi-) = v_z^*(\xi+), \quad T^*(\xi-) = T^*(\xi+),$$
$$c_{zz}^*(\xi-) = c_{zz}^*(\xi+), \quad c_{rr}^*(\xi-) = c_{rr}^*(\xi+),$$
$$\frac{dv_z^*}{dz^*}(\xi) = 0, \quad S_{zz}(\xi) = 0, \quad x(\xi) = 0.$$

- Boundary condition at $z^* = 1$

$$v_z^*(1) = v_l$$

  where $v_l$ is the draw ratio which is defined as $v_l = v_L/v_0$. Here, $v_L$ and $v_0$ denote the prescribed final and initial velocities respectively.

**Remark 2.4** *The correlations for material properties of polymer and models for physical properties of the quench air are given in Appendix A.*

# Chapter 3

# Mathematical Analysis Part I

*In this chapter we perform a mathematical analysis of the model equations given by Eqs.(2.14)-(2.24).*

Thomas Hagen has done a thorough mathematical analysis of non-stationary equations of melt spinning with a viscous constitutive law, [17]. He shows the extensions of his results to the viscoelastic case also. However, he does not take into account microstructural equations and crystallization. Effects like surface tension, air drag, gravity and inertia in the momentum equation have been neglected. Neglecting inertia in the momentum equation is an important assumption since then, the momentum equation can be integrated and the result can be inserted in the mass balance and heat equations. He assumes that the temperature is monotonically decreasing such that the system can be written with $T$ as the independent variable. In our problem, the numerics show that the temperature is not always monotonically decreasing throughout the spinline. For high speed spinning, there is an increase in the temperature owing to the release of latent heat of crystallization. Therefore in our case this assumption is not realistic. Moreover, the model that we are treating takes into account all the mentioned effects in the momentum equation and has many parameters which depend on the solution. These parameters induce singularities in the ODE system. Our model has a complex coupling with microstructure. There are two different systems of ODEs in different domains which are coupled through boundary conditions at the interface. Hence, the techniques of Hagen cannot be applied to our problem. We find enough hints from the numerics and the physics of the problem about the sensitivity of the model equations with respect to the parameters, initial conditions and even the differential equation coefficients.

In the following section we write down the ODE systems in explicit form.

# 3.1    Mathematical formulation of the problem

### 3.1.1    ODE system BOC

ODE system BOC is represented by Eqs.(2.14), (2.15), (2.16) and (2.17) along with (2.18). We write this system in the form

$$\mathbf{A}(\mathbf{x})\mathbf{x}' = \tilde{\mathbf{f}}(\mathbf{x})$$

where $\mathbf{x} = [v_z, T, c_{zz}, c_{rr}]$. Coefficient matrix $\mathbf{A}(\mathbf{x})$ is given by

$$\mathbf{A}(\mathbf{x}) = \begin{pmatrix} A_{11} & 0 & A_{13} & A_{14} \\ A_{21} & A_{22} & 0 & 0 \\ A_{31} & 0 & A_{33} & 0 \\ A_{41} & 0 & 0 & A_{44} \end{pmatrix}$$

where

$$A_{11} = D_1 x_1^2 + E(x_3 - x_4) + D_4 x_1^{1/2}, \quad A_{13} = -(x_1 p(x_3 - x_4) + E x_1),$$
$$A_{14} = -(2x_1 p(x_3 - x_4) - E x_1), \quad A_{21} = -D_6 E(x_3 - x_4)$$
$$A_{22} = x_1, \quad A_{31} = -2x_3,$$
$$A_{33} = x_1, \quad A_{41} = x_4$$
$$A_{44} = x_1$$

The right hand side function vector $\tilde{\mathbf{f}}$ reads as follows:

$$\tilde{\mathbf{f}} := \begin{pmatrix} D_3 x_1 - D_2(x_1 - v_r)^2 x_1^{3/2} \\ -D_5 x_1^{1/2}(x_2 - T_r) \\ -\frac{1}{D_{e_a}}((1 - \alpha) + \alpha E x_3)(E x_3 - 1) \\ -\frac{1}{D_{e_a}}((1 - \alpha) + \alpha E x_4)(E x_4 - 1) \end{pmatrix}$$

where,

$$p = \frac{3E^2 \sinh^2(3eE) - Ee^{-2}(\sinh^2(3eE) - (3eE)^2)}{6N_0(\sinh^2(3eE) - (3eE)^2)}.$$

The factor $E$ is as defined in Chapter 2.

$$E = \frac{L^{-1}(e)}{3e} \tag{3.1}$$

$$e = \sqrt{\frac{x_3 + 2x_4}{3N_0}} \tag{3.2}$$

with $L^{-1}$ being the inverse Langevin function, see Eq.(1.6).

For $\det \mathbf{A}(\mathbf{x}) \neq 0$, we get the differential equation system in the following explicit form:

$$\mathbf{x}' = \mathbf{A}(\mathbf{x})^{-1}\tilde{\mathbf{f}}(\mathbf{x}) = \mathbf{f}(\mathbf{x}). \tag{3.3}$$

## 3.1.2 ODE system AOC

ODE system AOC is given by Eq.(2.14), (2.19), 2.20), (2.21), (2.22) and (2.23) along with Eq.(2.24). By substituting Eq.(2.24) in (2.14) we get a second order differential equation for the variable $v_z$. By introducing $w = dv_z/dz$ we reduce this equation to a system of first order differential equations. Finally, the complete system of ODEs can be written in the form

$$\mathbf{B}(\mathbf{u})\mathbf{u}' = \tilde{\mathbf{g}}(\mathbf{u})$$

where $\mathbf{u} := (\mathbf{x}, \mathbf{y})$ with $\mathbf{x}$ as defined in Section 3.1.1 and $\mathbf{y} = [w = dv_z/dz, S_{zz}, x]$. Coefficient matrix $\mathbf{B}(\mathbf{u})$ reads as follows:

$$\mathbf{B}(\mathbf{u}) = \begin{pmatrix} 1 & 0 & 0 & 0 & 0 & 0 & 0 \\ 0 & 1 & 0 & 0 & 0 & 0 & B_{27} \\ 0 & 0 & 1 & 0 & 0 & 0 & 0 \\ 0 & 0 & 0 & 1 & 0 & 0 & 0 \\ 0 & B_{52} & B_{53} & B_{54} & B_{55} & B_{56} & B_{57} \\ 0 & 0 & 0 & 0 & 0 & 1 & 0 \\ 0 & 0 & 0 & 0 & 0 & 0 & 1 \end{pmatrix}$$

where

$$B_{27} = -D_7, \quad B_{52} = -6x_1 \mathrm{De}_{sc}(1-q)\frac{3}{7}y_2 - \frac{27}{2}x_1 \mathrm{De}_{sc}\, q\, y_2^2$$

$$B_{53} = -6(1-q)\frac{v_0}{L}\,\mathrm{dTlam}\, x_1 - \frac{27}{2}x_1 q y_2^2 y_1 \frac{v_0}{L}\mathrm{dTlam},$$

$$B_{54} = -\frac{x_1}{1-y_3}\left(p_1(x_3-x_4)+E\right),$$

$$B_{55} = -\frac{x_1}{1-y_3}\left(2p_1(x_3 - x_4) - E\right),$$

$$B_{56} = \frac{-9}{2}x_1 + 243x_1\mathrm{De}_{sc}\left(\frac{1}{5} + \frac{3}{7}y_2\right)y_1\left(\frac{-y_2}{2} + \frac{1}{3}\right)y_2$$

$$- \frac{18}{7}x_1y_1\mathrm{De}_{sc}(1-q) - 27x_1y_1q\mathrm{De}_{sc}y_2$$

$$B_{57} = -x_1\left(\frac{p_2}{1-y_3}(x_3 - x_4) - \frac{E(x_3 - x_4)}{(1-y_3)^2}\right) - 6x_1\frac{v_0}{L}\mathrm{dxlam}y_1\left(\frac{1}{5} + \frac{3}{7}y_2\right)$$

$$- \frac{27}{2}x_1qy_2^2y_1\mathrm{dxlam}\frac{v_0}{L}.$$

where,

$$q = 1 - 27\left(y_2 + \frac{1}{3}\right)\left(-\frac{1}{2}y_2 + \frac{1}{3}\right)^2$$

$$\mathrm{dTlam} = \frac{\partial\lambda_{sc}}{\partial x_2}$$

$$p_1 = \frac{3E^2\sinh^2(3eE) - Ee^{-2}(\sinh^2(3eE) - (3eE)^2)}{6N_0(1-y_3)^2(\sinh^2(3eE) - (3eE)^2)}$$

$$p_2 = \frac{3e^2E^2\sinh^2(3eE) - E(\sinh^2(3eE) - (3eE)^2)}{(1-y_3)(\sinh^2(3eE) - (3eE)^2)}$$

$$\mathrm{dxlam} = \frac{\partial\lambda_{sc}}{\partial y_3}.$$

The RHS vector function $\tilde{\mathbf{g}}$ is given by:

$$\tilde{\mathbf{g}} := \begin{pmatrix} y_1 \\ -D_5x_1^{-1/2}(x_2 - T_r) + D_6\frac{\tau_{zz} - \tau_{rr}}{x_1}y_1 \\ 2\frac{x_3}{x_1}y_1 - \frac{1-y_3}{De_a}\left((1-\alpha) + \alpha\frac{E}{1-y_3}x_3\right)\left(\frac{E}{1-y_3}x_3 - 1\right) \\ -\frac{x_4}{x_1}y_1 - \frac{1-y_3}{De_a}\left((1-\alpha) + \alpha\frac{E}{1-y_3}x_4\right)\left(\frac{E}{1-y_3}x_4 - 1\right) \\ -y_1(\tau_{zz} - \tau_{rr}) - D_1y_1x_1^2 - D_2(x_1 - v_r)^2x_1^{3/2} + D_3x_1 - D_4x_1^{1/2}y_1 \\ 2\frac{y_2}{x_1}y_1 - \frac{\sigma}{x_1De_{sc}}y_2 + \frac{2}{3}\frac{y_1}{x_1} - 2\frac{1-q}{x_1}\left(\frac{2}{15} + \frac{11}{14}y_2\right)y_1 - 3\frac{y_1}{x_1}y_2\left(y_2 + \frac{1}{3}\right)y_1 \\ \frac{1}{x_1}K^*(1-y_3)\exp(\psi\mathrm{tr}) \end{pmatrix}$$

where, $\mathrm{tr} = (E/(1-y_3))(x_3 + 2x_4) - 3 + 9\mathrm{De}_{sc}\,y_2\,y_1$.

For $\det\mathbf{B}(\mathbf{u}) \neq 0$, the following system is obtained:

$$\mathbf{u}' = \mathbf{B}^{-1}(\mathbf{u})\tilde{\mathbf{g}}(\mathbf{u}) = \mathbf{g}(\mathbf{u}) \qquad (3.4)$$

Combining Eqs.(3.3) and (3.4) we can describe the DMM model as a *Free boundary value problem*. Let $\xi$ denote the point of onset of crystallization. Then,

$$\mathbf{x}' \;=\; \mathbf{f}(\mathbf{x}) \qquad \text{for } z \in [0, \xi(\mathbf{x_0})) \tag{3.5}$$

$$\begin{aligned} \mathbf{x}' &\;=\; \mathbf{g}(\mathbf{x}, \mathbf{y}) \quad \text{for } z \in (\xi(\mathbf{x_0}), 1] \\ \mathbf{y}' &\;=\; \mathbf{h}(\mathbf{x}, \mathbf{y}) \end{aligned} \tag{3.6}$$

where $\mathbf{f} : \mathbb{R}^4 \to \mathbb{R}^4$, $\mathbf{g} : \mathbb{R}^7 \to \mathbb{R}^4$, $\mathbf{h} : \mathbb{R}^7 \to \mathbb{R}^3$ and $\mathbf{x_0}$ denotes the boundary condition of $\mathbf{x}$ at $z = 0$.

The boundary conditions can be described as in Section 2.6:

- At $z = 0$,    $x_1(0) = 1$,    $x_2(0) = 1$,    $\tilde{h}(x_3(0), x_4(0)) = 0$, where

$$\tilde{h} := \coth\left(\frac{3}{e_0 N_0}\right) - \frac{e_0 N_0}{3} - e_0 \tag{3.7}$$

  and $e_0 = \sqrt{\frac{x_3(0) + 2x_4(0)}{3 N_0}}$. More details about this boundary condition can be found in Chapter5.

- $\quad x_3(\xi) = T_m$.

- At $z = \xi$,    $x(\xi+) = x(\xi-)$,    $y(\xi) = 0$.

- At $z = 1$,    $x_1(1) = v_l$,    $v_l \in \mathbb{R}^+$.

We give below vector functions $\mathbf{f}$, $\mathbf{g}$ and $\mathbf{h}$ explicitly:

$$\begin{aligned} f_1 :=& \frac{1}{\text{Den}}\left((D_3 x_1 - D_2(x_1 - v_r)^2 x_1^{3/2}) + x_1(px_3 - px_4 + E)\text{term}_1 + \right. \\ & \left. x_1(2px_3 - 2px_4 - E)\text{term}_2\right) \end{aligned} \tag{3.8}$$

$$\begin{aligned} f_2 :=& \frac{-D_6 E(x_3 - x_4)}{x_1 \text{Den}}(D_3 x_1 - D_2(x_1 - v_r)^2 x_1^{\frac{3}{2}}) - D_5\sqrt{x_1} \\ & + \frac{D_6 E(x_3 - x_4)}{\text{Den}}(\text{term}_1(px_3 - px_4 + E) \\ & + \text{term}_2(2px_3 - 2px_4 - E)) \end{aligned} \tag{3.9}$$

$$
f_3 := \frac{-2x_3}{x_1 \text{Den}} \left( D_3 x_1 - D_2 (x_1 - v_r)^2 x_1^{\frac{3}{2}} \right) + \frac{\text{term}_2}{\text{Den}} \left( 2x_3 (2px_3 - 2px_4 - E) \right)
$$

$$
+ \frac{\text{term}_1}{\text{Den}} \left( D_1 x_1^2 + E x_3 - 2E x_4 + D_4 \sqrt{x_1} + 2x_3 px_4 - 2px_4^2 \right) \quad (3.10)
$$

$$
f_4 := \frac{x_4}{x_1 \text{Den}} \left( D_3 x_1 - D_2 (x_1 - v_r)^2 x_1^{\frac{3}{2}} \right) - \frac{\text{term}_1}{\text{Den}} (px_3 - px_4 + E)
$$

$$
- \frac{\text{term}_2}{\text{Den}} \left( -D_1 x_1^2 + E x_3 + E x_4 - D_4 \sqrt{x_1} + 2px_3^2 - 2x_3 px_4 \right) \quad (3.11)
$$

where,

$$
\text{Den} = \left( -D_1 x_1^2 + E x_3 + 2E x_4 - D_4 \sqrt{x_1} + 2p(x_3 - x_4)^2 \right) x_1^2
$$

$$
\text{term}_1 = \frac{(1 - \alpha + \alpha E x_3)(E x_3 - 1)}{x_1 \text{De}_a}
$$

$$
\text{term}_2 = \frac{(1 - \alpha + \alpha E x_4)(E x_4 - 1)}{x_1 \text{De}_a}
$$

The vector function **g** is defined by:

$$
g_1 := y_1 \tag{3.12}
$$

$$
g_2 := \frac{-D_5}{\sqrt{x_1}} (x_2 - T_r) + D_6 \frac{E(x_3 - x_4)}{x_1} y_1 + D_7 \frac{1}{x_1} K^* (1 - y_3) \exp(\psi \text{tr}) \tag{3.13}
$$

$$
g_3 := 2 \frac{x_3}{x_1} y_1 - \frac{1 - y_3}{x_1 \text{De}_a} \left( (1 - \alpha) + \alpha \frac{E}{1 - y_3} x_3 \right) \left( \frac{E}{1 - y_3} x_3 - 1 \right) \tag{3.14}
$$

$$
g_4 := - \frac{x_4}{x_1} y_1 - \frac{1 - y_3}{x_1 \text{De}_a} \left( (1 - \alpha) + \alpha \frac{E}{1 - y_3} x_4 \right) \left( \frac{E}{1 - y_3} x_4 - 1 \right) \tag{3.15}
$$

where $\text{tr} = (E/(1 - y_3)) (x_3 + 2x_4) - 3 + 9\text{De}_{sc} y_2 y_1$.

Vector function **h** is:

$$
h_1 := \frac{\text{num}_2}{\text{den}_2} \tag{3.16}
$$

$$
h_2 := 2 \frac{y_2}{x_1} y_1 - \frac{\sigma}{x_1 \text{De}_{sc}} y_2 + \frac{2}{3} \frac{1}{x_1} y_1 - 2 \frac{1 - q}{x_1} \left( \frac{2}{15} + \frac{11}{14} y_2 \right) y_1 - 3 \frac{q}{x_1} y_2 \left( y_2 + \frac{1}{3} \right) y_1 \tag{3.17}
$$

$$
h_3 := \frac{1}{x_1} K^* (1 - y_3) \exp(\psi \text{tr}) \tag{3.18}
$$

where $q = 1 - 27(y_2 + 1/3)(-y_2/2 + 1/3)^2$ and

$$
\text{den}_2 = \frac{1}{v_z} \left( 6\text{De}_{sc} (1 - q) \left( \frac{3}{15} + \frac{3}{7} y_2 \right) + \frac{27}{2} \text{De}_{sc} q y_2^2 \right)
$$

$$
\text{num}_2 = \frac{1}{v_z^2} q (\tau_{zz} - \tau_{rr}) + \frac{1}{v_z} Q_3 + D_1 q + D_2 \frac{(v_z - v_r)^2}{\sqrt{v_z}} - \frac{D_3}{v_z} + D_4 v_z^{-3/2} q.
$$

Here $Q_3$ is given by,

$$
\begin{aligned}
Q_3 = &-\frac{1}{1-y_3}\frac{\partial E}{\partial z}(x_3 - x_4) - \frac{E}{(1-y_3)^2}(x_3 - x_4)\frac{\partial y_3}{\partial z} - \frac{E}{1-y_3}\left(\frac{\partial x_3}{\partial z} - \frac{\partial x_4}{\partial z}\right) \\
&-\frac{9}{2}\frac{\partial y_2}{\partial z} - 6\frac{\partial \lambda_{sc}}{\partial z}\frac{v_0}{L}(1-q)\left(\frac{3}{15} + \frac{3}{7}y_2\right)y_1 + 6\mathrm{De}_{sc}\frac{\partial q}{\partial z}\left(\frac{3}{15} + \frac{3}{7}y_2\right)y_1 \\
&-\frac{18}{7}\mathrm{De}_{sc}(1-q)\frac{\partial y_2}{\partial z}y_1 - \frac{27}{2}\frac{\partial \lambda_{sc}}{\partial z}\frac{v_0}{L}qy_2^2 y_1 - \frac{27}{2}\mathrm{De}_{sc}\frac{\partial q}{\partial z}y_2^2 y_1 \\
&-27\mathrm{De}_{sc}\,q\frac{\partial y_2}{\partial z}\,y_2\,y_1.
\end{aligned}
$$

In the above expressions the derivatives with respect to $z$ can be written explicitly in terms of $(\mathbf{x}, \mathbf{y})$. In order to avoid longer formulae we have not shown them here.

The stress difference $\tau_{zz} - \tau_{rr}$ is given by:

$$
\tau_{zz} - \tau_{rr} = \frac{E}{1-y_3}(x_3 - x_4) + \frac{9}{2}y_2 + 6\,\mathrm{De}_{sc}(1-q)\left(\frac{3}{15} + \frac{3}{7}y_2\right)y_1 + \frac{27}{2}\mathrm{De}_{sc}\,q\,y_2^2\,y_1.
$$

**Remark 3.1** *The problem can be formulated in other ways. For example, as a first order system of differential equations with a discontinuous right hand side or a system of DAEs with a changing index. But it was found that there does not exist any theory that could be applied to such systems.*

**Remark 3.2** *From now onwards we shall be using the ODE systems with variables in their original notation (i.e $v_z$, $T$, $c_{zz}$,...) in order to be able to relate to their physical behaviour easily.*

## 3.2   Discussion of parameter sizes

Parameter sizes play an important role in the numerics. Some of the typical parameters of the melt spinning process are given in Tables 3.1, 3.2, 3.3 and 3.4. The values of the parameters in Table 3.2 are got after doing the simulations. In Table 3.2, "const" and "var" represent constant and variable parameters respectively and their dependence on the variables is indicated in the bracket. Range of the variable parameters is specified as they vary across the spinline.

| Parameter | Description | Value | Unit |
|-----------|-------------|-------|------|
| $D_0$ | Initial spinneret diameter | 0.02 | cm |
| $T_0$ | Polymer temperature at spinneret exit | 300 | °C |
| $W$ | Mass throughput | 1.5 -3.6 | g/min |
| $v_L$ | Take up velocity | 1000-6500 | m/min |
| $L$ | Spin length | 135 | cm |
| $T_a$ | Quench air temperature | 24 | °C |
| $v_c$ | Cross velocity of quench air | 1 | ft/s |

Table 3.1: *Typical processing conditions*

| Parameter | Description | Type | Value |
|-----------|-------------|------|-------|
| $D_1$ | Force due to inertia | const | $4.9 \cdot 10^{-3}$ |
| $D_2$ | Force due to air drag | var $(v_z, T)$ | $10^{-4}$ |
| $D_3$ | Force due to gravity | const | $1.7 \cdot 10^{-1}$ |
| $D_4$ | Force due to surface tension | const | $1.3 \cdot 10^{-3}$ |
| $D_5$ | Exchange of energy between air and fibre | var $(T, x, v_z)$ | 4.3 |
| $D_6$ | Viscous dissipation | var $(T, x)$ | $10^{-4}$ |
| $D_7$ | Latent heat of crystallization | var $(T, x)$ | 0.18 |
| $\text{De}_a$ | Weisenberg no. in amorphous phase | var $(T, x)$ | $10^{-3} - 10^{-7}$ |
| $\text{De}_{sc}$ | Weisenberg no. in semi-crystalline phase | var$(T, x)$ | $1 - 10^{20}$ |
| $E$ | Nonlinear force factor | var$(c_{zz}, c_{rr}, x)$ | $1 - 10^6$ |

Table 3.2: *Typical model parameters*

| Parameter | Equation | value |
|-----------|----------|-------|
| $F$ | (2.8) | 60 |
| $c$ | (2.8) | 0.001 |
| $\sigma$ | (2.22) | 1 |
| $\phi_\infty$ | (2.23) | 0.45 |
| $\alpha$ | (2.16), (2.17) | 0.4 |
| $\psi$ | (2.23) | 0.06 |

Table 3.3: *Typical values of model parameters for Nylon-66*

A general description of the factor $E$ has been given in Section 1.3.2.

| Parameter | Description | Value | Unit |
|:---:|:---|:---:|:---:|
| $\rho$ | Density | 0.98 | $g/\text{cm}^3$ |
| $\eta_0$ | Zero-shear viscosity at $280^0 C$ | 163 | pa s |
| $G$ | Melt shear modulus | $1.1 \cdot 10^5$ | pa |
| $N_0$ | Number of statistical links per chain | 200 | $-$ |
| $T_m$ | Melting temperature | 265 | $^\circ$C |
| $k$ | Thermal conductivity | $5 \cdot 10^{-4}$ | $^\circ$C |
| $s$ | Surface tension | 36 | dyn/cm |

Table 3.4: *Physical and rheological properties of Nylon-66 melt used in simulations*

Refer to Eqs.(3.1) and (3.2).

$$\lim_{e \to 0} E(e) = \lim_{e \to 0} \frac{L^{-1}(e)}{3e} \quad = \quad \lim_{e \to 0} \frac{1}{3e}(3e + \frac{9}{5}e^3 + \frac{297}{175}e^5 + ...) = 1 \quad (3.19)$$

$$\lim_{e \to 1} E(e) = \lim_{e \to 1} \frac{L^{-1}(e)}{3e} \quad = \quad \lim_{e \to 1} \frac{1}{3e}(\frac{1}{1-e}) = \infty \quad\quad\quad (3.20)$$

Therefore $1 \leq E \leq \infty$. [2].

## 3.3   Properties of system BOC

In this section we investigate the system BOC in detail. We first study the possible singularities in the system and then investigate the existence of solution to the initial value problem associated with it.

### 3.3.1   Singularities in system BOC

For a solution to exist for system of equations (3.5), it is necessary to investigate the singularities in the system. For equations (3.8) to (3.11), the following could be the possible singularities or parameters which could blow up the solution:

- $v_z = 0$

- $\text{De}_a = 0$ From section Section 2.3.1 and Appendix A, we see that for the phase BOC, $\text{De}_a \neq 0$. But it could be very small ($O(10^{-6})$ for very

high temperatures making the system very stiff. Refer to Table 3.2 for typical values of $\text{De}_a$.

- $e \to 1$

  As seen from the previous section, as $e \to 1$ parameter $E$ tends to infinity.

- $\text{Den} = 0$.

We observe that it is very difficult to prove the existence of a global solution to the IVP BOC because of the potential singularities in the system. Therefore, we make some remarks about the expected behaviour of the solution and restrict our class of solutions to that which shows the expected behaviour of the fibre. We expect that:

- axial velocity increases monotonically along the spinline.

- starting from the initial temperature greater than the melting temperature, the temperature decreases monotonically along the spinline. This is crucial in order to determine the point of onset of crystallization $\xi$ since $T(\xi) = T_m$.

- variables $c_{zz}$ and $c_{rr}$ are positive along the spinline.

Now, we make some definitions:

**Definition 3.1** *The set of all initial conditions $(c_{zz}(0), c_{rr}(0))$ such that $dv_z/dz > 0, dT/dz < 0, dc_{zz}/dz > 0, dc_{rr}/dz < 0$ at $z = 0$ is called the set of plausible initial conditions.*

Let such a set be denoted by $J$. It can be easily proved that $J$ is non-empty. The set of all plausible conditions guarantees that at least in the neighbourhood of the point $z = 0$, the solution behaves as expected. Any initial conditions not in $J$ yield solutions that are unrealistic and hence of no use.

Any pair of $(c_{zz}(0), c_{rr}(0)) \notin J$ is called *aphysical initial condition*.

**Definition 3.2** *The set of solutions $(v_z, T, c_{zz}, c_{rr})$ of IVP BOC such that $c_{zz} > 0, \ c_{rr} > 0, \ T \geq T_m$ and $v_z > 0 \ \forall z \in [0, z^*], z^* < \infty$ is called the set of physically acceptable solutions in the interval $[0, z^*]$.*

Let us denote this set by $P$. Any solution not belonging to set $P$ will be called an *aphysical solution*. It can be easily proved that $P$ is non-empty. Positivity of $c_{zz}$ and $c_{rr}$ is an important property of the solution. More about this will be discussed later.

## 3.3.2   Local analysis of a simplified model

Motivation of this section is to show that even with a plausible set of initial conditions as given by Def.(3.1), it is possible that a singularity occurs. Therefore, even a restricted set of initial conditions cannot guarantee the global existence of the solution of IVP BOC. To show this, we do a local analysis of the model equations in the neighbourhood of $z = 0$ and show with the help of numerics how the solution blows up.

Let us simplify the model by letting $D_2 = D_3 = D_4 = 0$, $E = 1$, $\alpha = 0$ and $De_a = 1$ in Eq.(3.8), where $D_2$ represents the force due to air drag, $D_3$ is the force due to gravity, $D_4$ denotes the surface tension and $De_a$ is the Weisenberg number of the amorphous melt. See Section 2.5 for the corresponding formulae. By doing this we get the simplest form of the momentum equation consisting of only inertia force denoted by $D_1$ and the tensile stress. Then the momentum equation, (3.8) takes the following form:

$$\frac{dv_z}{dz} = \frac{c_{zz} - c_{rr}}{c_{zz} + 2c_{rr} - D_1 v_z^2}. \tag{3.21}$$

Let us denote the denominator of the equation by $\text{Den} = -D_1 v_z^2 + c_{zz} + 2c_{rr}$.

Now, consider the simplified evolution equations of $c_{zz}$ and $c_{rr}$.

$$\frac{dc_{zz}}{dz} = 2\frac{c_{zz}}{v_z}\frac{dv_z}{dz} - \frac{1}{v_z}\left(c_{zz} - 1\right) \tag{3.22}$$

$$\frac{dc_{rr}}{dz} = -\frac{c_{rr}}{v_z}\frac{dv_z}{dz} - \frac{1}{v_z}\left(c_{rr} - 1\right). \tag{3.23}$$

**Remark 3.3** *In the numerics, we first solve the IVP BOC using the guessed initial condition for $c_{zz}$ at $z = 0$. We determine the point of onset of crystallization $\xi$ and switch to system AOC. Using the boundary conditions specified at $z = \xi$ we calculate the solution to this system and match the final velocity*

*got numerically to the prescribed final velocity. We determine the next approximation to the correct initial condition and keep following the procedure till the numerical final velocity matches the prescribed one.*

Since we are working with non-dimensionalised variables as explained in Chapter 2, we have $v_z(0) = 1$, $T(0) = 1$. Let $c_{zz}(0) > 1$ and $0 < c_{rr}(0) < 1$. A typical value of $D_1$ is 0.004, see Table3.2. Then, from Eq.(3.21) we get $dv_z/dz > 0$ at $z = 0$. We assume the initial conditions are chosen such that at $z = 0$, $dc_{zz}/dz > 0$ and $dc_{rr}/dz < 0$. Therefore, $(c_{zz}(0), c_{rr}(0)) \in J$ are plausible initial conditions.

For $c_{zz} > 1$ and $\frac{dv_z}{dz} > 0$, from Eq.(3.22) we get the differential inequality

$$\frac{dc_{zz}}{dz} < 2\frac{c_{zz}}{v_z}\frac{dv_z}{dz}.$$

Solving the above differential inequality we get

$$c_{zz}(z) < Kv_z(z)^2, \quad K > 1. \tag{3.24}$$

This shows that under the mentioned conditions $c_{zz}$ has a quadratic profile with respect to velocity. Now, consider the denominator of the Eq.(3.21) given by Den $= -D_1v_z^2 + c_{zz} + 2c_{rr}$. Since we have chosen plausible initial conditions we know that in the neighbourhood of $z = 0$, $v_z$ and $c_{zz}$ grow and $c_{rr}$ becomes small. From numerics we observe that $c_{zz} + 2c_{rr} \rightarrow c_{zz}$. See Fig.3.1. Hence in Den we approximate the term $c_{zz} + 2c_{rr}$ with $c_{zz}$.
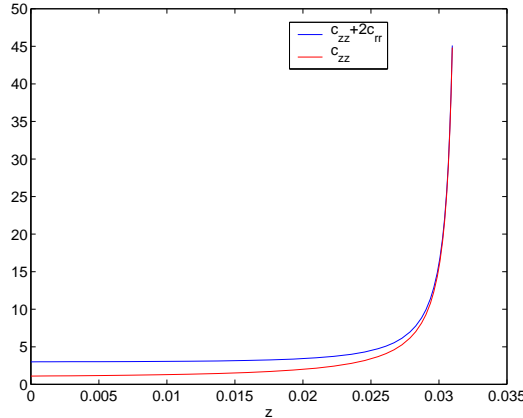


Figure 3.1: *Comparison of $c_{zz}$ and $c_{zz} + 2c_{rr}$*

Moreover, since $c_{zz}$ also has a quadratic profile as seen from Eq.(3.24), we

make a comparison of $D_1 v_z^2$ and $c_{zz}$ in Den. From numerics we observe that $D_1 v_z^2 \to c_{zz}$ as velocity $v_z$ becomes high. Fig.3.2 shows the plots of $D_1 v_z^2$ and $c_{zz}$ against $v_z$. In the first plot, distinct curves of the two terms can be seen for velocity not in very high regime. In the second plot one sees that as velocity becomes very high the two curves almost overlap making $dv_z/dz$ singular.
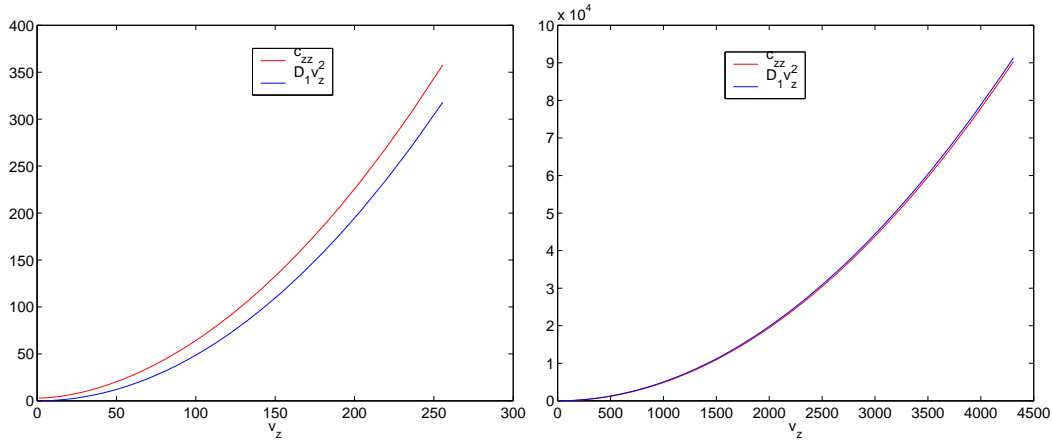


Figure 3.2: Left: *Comparison of $c_{zz}$ and $D_1 v_z^2$ in low velocity regime.* Right: *Comparison of $c_{zz}$ and $D_1 v_z^2$ in high velocity regime.*

**Remark 3.4** *The example given in this section is a very specific example with a special set of initial conditions. One could choose such a set of initial conditions for which a global solution to the problem exists. But from our numerical simulations with realistic data we found that in most cases a global solution to the system BOC does not exist. That is, even for the plausible set of initial conditions with which the melting temperature can also be reached, a global solution to the system BOC does not necessarily exist.*

From the above example, we conclude that global existence of the solution even for the phase BOC cannot be proved. However, we do not require a global solution for the phase BOC. We need the solution only till the point of onset of crystallization $\xi$, where we switch over to the system AOC. Therefore, we try to find the maximal interval in which the solution of IVP BOC exists.

### 3.3.3   Existence of a maximal solution for the IVP BOC.

Consider again the system:

$$\begin{aligned}
\mathbf{x}' &= \mathbf{f}(\mathbf{x}) \\
\mathbf{x}(0) &= \mathbf{x_0}
\end{aligned}$$

From well known basic theorems in ordinary differential equations, we conclude that on every interval $I = [0, z^*], z^* \leq 1$, which does not contain singularities, a unique global solution to the above problem exists. Moreover, if $\mathbf{f}$ has a singularity at $z_s \in (0, 1]$, then $|\mathbf{x}(\mathbf{z})| \to \infty$ as $z \to z_s$. The interval $[0, z_s)$ is the maximal interval in which the solution exists and the corresponding solution is called the maximal solution.

## 3.4   Temperature estimate

Existence of $\xi$ depends on the temperature since $\xi = T^{-1}(T_m)$. Since the initial temperature $T_0$ is always assumed to be greater than or equal to the melting temperature $T_m$ we need to investigate under what conditions T is monotonically decreasing. Let us consider the temperature equation:

$$\frac{dT}{dz} = -D_5 \frac{T - T_r}{\sqrt{v_z}} + D_6 \frac{E(c_{zz} - c_{rr})}{v_z} \frac{dv_z}{dz}. \tag{3.25}$$

**Physical interpretation**:
The first term on the right hand side describes the exchange of heat between the fibre and the surrounding air where as the second term describes the heat released due to the friction or viscous dissipation. The model for the zero-shear viscosity is given by, Eq.(1) in Appendix A:

$$\mu = \eta_0 \exp \left[ \frac{13500(280 - T)}{1099.2(T + 273.2)} \right].$$

Assuming that initially the temperature decreases, from the above relation we see that the viscosity increases, making the fibre solid. But if there are very high velocity gradients (which is expected in high speed melt spinning and which induces the strain hardening of the melt) then the force due to friction starts dominating the first term in the temperature equation. This results in the increase of temperature. Now, as the temperature starts increasing the viscosity starts decreasing becoming very small. In other words, the

relaxation time of the fluid given by $\lambda = \mu/G$ tends to zero. This reduces the viscoelastic model, which is given by the evolution equations of $c_{zz}$ and $c_{rr}$, to a model for a viscous fluid as explained in Section 1.1.3, thereby inducing a singularity in the equations for $c_{zz}$ and $c_{rr}$. Hence we see that the temperature can not only increase but this increase could even induce singularities in the model. For this we try to find bounds for the mechanical energy released due to friction as represented by the second term in the temperature equation. Therefore, we first get estimates for $c_{zz}$ and $c_{rr}$ in terms of the axial velocity $v_z$.

### 3.4.1  Estimate for conformation tensor variables $c_{zz}$ and $c_{rr}$

**Lemma 3.1** *Assume:* $\frac{dv_z}{dz} > 0$ *,* $v_z > 0$   $\forall z$. *If in addition,* $c_{zz} > \frac{1}{E}$ $\forall z$ *then*

$$c_{zz} < K_1 v_z^2$$

*for some constant* $K_1 \in \mathbb{R}^+$ *depending on the BC at* $z = 0$.

Proof: Consider the evolution equation of $c_{zz}$

$$\frac{dc_{zz}}{dz} = 2\frac{c_{zz}}{v_z}\frac{dv_z}{dz} - \frac{1}{v_z \mathrm{De}_a}\left(1 - \alpha + \alpha E c_{zz}\right)\left(E c_{zz} - 1\right)$$

Assuming that $c_{zz} > \frac{1}{E}$, we have the following differential inequality

$$\frac{dc_{zz}}{dz} < 2\frac{c_{zz}}{v_z}\frac{dv_z}{dz}$$

Solving the above differential inequality we get

$$c_{zz} < K_1 v_z^2$$

where $K_1$ is some constant depending on the BC at $z = 0$.

**Theorem 3.1** *If* $\frac{dv_z}{dz} > 0$ *,* $v_z > 0$   $\forall z$, *then*

$$c_{zz} \leq \max\{K_1 v_z^2, \frac{1}{E}\}$$

Proof : Suppose $c_{zz} > \max\{K_1 v_z^2, \frac{1}{E}\}$
Then,

- Case1. If $K_1 v_z^2 > \frac{1}{E}$

$$\Rightarrow c_{zz} > \frac{1}{E}$$

  Then, from lemma 3.1 we get

$$c_{zz} < K v_z^2$$

  which is a contradiction to our assumption.

- Case2. If $K_1 v_z^2 \leq \frac{1}{E}$, then

$$c_{zz} > \frac{1}{E}$$

  From lemma 3.1 we get

$$
\begin{aligned}
c_{zz} &< K_1 v_z^2 \\
\Rightarrow c_{zz} &< \frac{1}{E}
\end{aligned}
$$

  which is a again a contradiction

**Lemma 3.2** *Assume:* $\frac{dv_z}{dz} > 0$ *,* $v_z > 0$ $\forall z$. *If in addition,* $c_{rr} < \frac{1}{E}$ $\forall z$, *then*

$$c_{rr} > \frac{K_2}{v_z}$$

*for some constant $K_2$ depending on the BC at $z = 0$.*

Proof: Consider the evolution equation of $c_{rr}$

$$\frac{dc_{rr}}{dz} = -\frac{c_{rr}}{v_z}\frac{dv_z}{dz} - \frac{1}{v_z \mathrm{De}_a}\left(1 - \alpha + \alpha E c_{rr}\right)\left(E c_{rr} - 1\right)$$

Assuming that $c_{rr} < \frac{1}{E}$, we have the following inequality

$$\frac{dc_{rr}}{dz} > -\frac{c_{rr}}{v_z}\frac{dv_z}{dz}$$

Solving the above differential inequality we get,

$$c_{rr} > \frac{K_2}{v_z}$$

for some $K_2$ depending on the BC at $z = 0$.

**Theorem 3.2** *If $\frac{dv_z}{dz} > 0$ , $v_z > 0$   $\forall z$, then*

$$c_{rr} \geq \min\{\frac{K_2}{v_z}, \frac{1}{E}\}$$

Proof : Suppose $c_{rr} < \min\{\frac{K_2}{v_z}, \frac{1}{E}\}$
Then,

- Case1. If $\frac{K_2}{v_z} < \frac{1}{E}$

$$\Rightarrow c_{rr} < \frac{K_2}{v_z} < \frac{1}{E} \tag{3.26}$$

  But from lemma 3.2, $c_{rr} < \frac{1}{E} \Rightarrow c_{rr} > \frac{K_2}{v_z}$ which is a contradiction to our assumption.

- Case2. If $\frac{1}{E} \leq \frac{K_2}{v_z}$, then from our assumption,

$$c_{rr} < \frac{1}{E}$$

  But from lemma 3.2, we have $c_{rr} > \frac{K_2}{v_z}$. This implies that $c_{rr} < \frac{1}{E}$ which is a contradiction.

We want to get estimates for the second term in the temperature equation. Consider once more Eq.(3.25). Now following cases arise:

- $c_{zz} \leq \frac{1}{E}$ and $c_{rr} \geq \frac{1}{E}$

- $c_{zz} \leq K_1 v_z^2$ and $c_{rr} \geq \frac{1}{E}$

- $c_{zz} \leq \frac{1}{E}$ and $c_{rr} \geq \frac{K_2}{v_z}$

- $c_{zz} \leq K_1 v_z^2$ and $c_{rr} \geq \frac{K_2}{v_z}$

In the first case we get $c_{zz} - c_{rr} \leq 0$, in which case have $\frac{dT}{dz} < 0$ which shows that the temperature is monotonically decreasing.

We study the fourth case here since second and third cases are similar. That means now we have

$$c_{zz} - c_{rr} \leq K_1 v_z^2 - \frac{K_2}{v_z} \tag{3.27}$$

**Theorem 3.3** *Let $I = [0, z^T) \subset [0, 1]$ be such that $T(z) > T_m \quad \forall z \in I$ and $E(z) < \overline{E} < \infty$. In addition assume that $v_z > 0$ and $dv_z/dz > 0 \ \forall z$. Then,*

$$T(z) < T(0) + \left[ \overline{E} \left( \frac{K_1 v_z^2}{2} + \frac{K_2}{v_z} \right) \right]_0^{z^T} - \overline{D}_6 \int_0^{z_T} \frac{g(v_z)}{\sqrt{v_z}(T_m - T_r)} dz. \quad (3.28)$$

*where $\overline{D}_6 = \max(D_6(T))$, g is some function depending on $v_z$ and $K_1$ and $K_2$ are constants depending on the boundary conditions at $z = 0$.*

Proof: Consider once more the temperature equation:

$$\frac{dT}{dz} = -D_5 \frac{T - T_r}{\sqrt{v_z}} + D_6 \frac{E(c_{zz} - c_{rr})}{v_z} \frac{dv_z}{dz}.$$

This can be re-rewritten as:

$$\frac{dT}{dz} = D_6 \left( \underbrace{-\frac{D_5}{D_6} \frac{T - T_r}{\sqrt{v_z}} + \frac{E(c_{zz} - c_{rr})}{v_z} \frac{dv_z}{dz}}_{f} \right).$$

From the form of the parameters $D_5$ and $D_6$, as in Section(2.5), we see that $D_5/D_6$ is independent of $T$. (For parameter dependencies refer to Table 3.2). Let $g := \frac{D_5}{D_6}$. Then g is a function of $v_z$. Moreover, $0 < D_6 < \overline{D}_6 < \infty$. Also, assume that $|f| > 0$.
Using Theorems 3.1 and 3.5 we estimate the second term in the temperature equation in terms of the axial velocity using inequality (3.27):

$$\frac{E(c_{zz} - c_{rr})}{v_z} < \frac{\overline{E}(K_1 v_z^2 - \frac{K_2}{v_z})}{v_z}$$

Hence we have,

$$\frac{dT}{dz} < \overline{D}_6 \left( \frac{-g(T_m - T_r)}{\sqrt{v_z}} + \overline{E}(K_1 v_z - \frac{K_2}{v_z^2}) \frac{dv_z}{dz} \right)$$

Integrating the above inequality with respect to $z$ we get,

$$T(z^T) < T(0) + \overline{D}_6 \left[ \overline{E} \left( \frac{K_1 v_z^2}{2} + \frac{K_2}{v_z} \right) \right]_0^{z^T} - \int_0^{z^T} \frac{g}{\sqrt{v_z}(T_m - T_r)} dz.$$

The above theorem gives us an estimate for the temperature in terms of the boundary conditions and the axial velocity. In order to get a more precise

estimate for the temperature one would have to get an estimate for the axial velocity which is very difficult because of coupling between all variables and the complicated form of the equations.

Further we show some properties of the solution which will help us in proving the existence of a physically acceptable solution.

## 3.5  Positive definiteness of conformation tensor

In this section we will show the positive definiteness of the conformation tensor variables.

**Lemma 3.3** *For the IVP*

$$\frac{du}{dz} = f(u), \quad u(0) = u_0$$

*Assume, $u : [0, Z) \to R$, $0 < Z \leq +\infty$, is a solution.*
*Then:*

- *if $\exists\ m \in \mathbb{R}$ such that $f(m) < 0\ \ \forall z \in [0, Z)$ and if $u_0 < m$ then $u(z) < m\ \ \forall\ 0 \leq z < Z$*

- *if $\exists\ N \in \mathbb{R}$ such that $f(N) > 0\ \ \forall z \in [0, Z)$ and if $u_0 > N$, then $u(z) > N\ \forall\ 0 \leq z < Z$.*

We do not prove the above lemma since the proof is obvious. A geometrical interpretation of the lemma is given in Fig.3.3.

**Theorem 3.4** *Assume that $\frac{dv_z}{dz} < \lambda < \infty$, $v_z > 0\ \forall z \in [0, z^*)$ and $1 \leq E \leq \infty$ then*

- $c_{zz}(0) > 0 \Rightarrow c_{zz} > 0\ \ \forall z \in [0, z^*)$

- $c_{rr}(0) > 0 \Rightarrow c_{rr} > 0\ \ \forall z \in [0, z^*)$
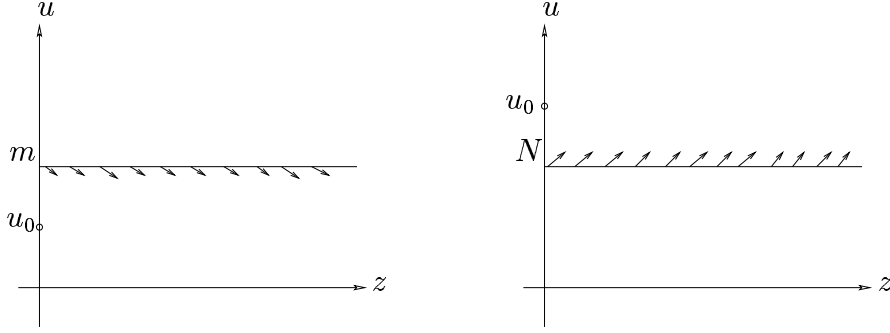
Figure 3.3: Left:*Geometric description of first statement of lemma 3.3.* Right:*Geometric description of second statement of lemma 3.3.*

Proof: For convenience we put $w = dv_z/dz$. Consider the evolution equation of $c_{zz}$

$$\frac{dc_{zz}}{dz} = 2\frac{c_{zz}}{v_z}w - \frac{1}{v_z\mathrm{De}_a}\left((1-\alpha) + \alpha E c_{zz}\right)\left(E c_{zz} - 1\right)$$

This can be re-written as:

$$\frac{dc_{zz}}{dz} = \frac{1}{v_z\mathrm{De}_a}\underbrace{\left(-\alpha E^2 c_{zz}^2 + (2w\mathrm{De}_a + (2\alpha - 1)E)c_{zz} + (1-\alpha)\right)}_{f}$$

Roots of $f$ are

$$c_{1,2}(z) = \frac{\underbrace{-(2w\mathrm{De}_a + (2\alpha - 1)E)}_{b} \pm \sqrt{(2w\mathrm{De}_a + (2\alpha - 1)E)^2 + \underbrace{4\alpha(1-\alpha)E^2}_{d}}}{-2\alpha E^2}$$

Since $0 < \alpha \le 1$, we have $d \ge 0$. Hence, it implies that $c_1(z) \le 0 \le c_2(z)$ $\forall z$. That is, $f$ always has one positive and one negative root for all points $z$.

At any point $z$, $f$ has an "inverted" parabolic profile. Therefore for $c_1 < c_{zz} < c_2$, we have $f(c_{zz}) > 0$. In particular, let $N = 0$. Then, $f(N) > 0$ $\forall z$. From Lemma 3.3, it follows that if we choose $c_{zz}(0) > N$ then $c_{zz} > 0$ $\forall z$. Applying similar arguments to the evolution equation for $c_{rr}$ we find that if we choose the initial condition of $c_{rr}$ such that $c_{rr}(0) > 0$ then it follows that $c_{rr} > 0$ $\forall z$.
Moreover, let $m = \max(c_2(z)) + \epsilon$, $\epsilon > 0$. It is easy to see that $c_2$ is bounded and a maximum exists. Then we see that $f(m) < 0$ $\forall z$. Again applying Lemma 3.3, we get that for $c_{zz}(0) < m$, it follows that $c_{zz} < m$, $\forall z$. A maximum bound can also be found for $c_{rr}$ in a similar way.

From the above theorem we see that the conformation tensor **c** is bounded. This also proves that if we start with an initial condition for **c** such that **c**$(0) > 0$, then **c** remains positive definite in the whole domain. Viewing **c** as representing the conformation of a dumbbell, the negative-definiteness of **c** is not only hard to imagine but also unrealistic,[2]. According to Beris and Edwards, " in the numerical simulations, loss of positive- definiteness of **c** could be due to numerical error". Hence it a property of the solution which should be checked during the course of computations. In case of non-stationary equations, the positive definiteness of **c** is associated with the evolutionarity (well-posedness) of the governing equations. According to Hulsen's theorem, [2] "the steady state solutions of the models which correspond to a negative definite conformation tensor need to be dismissed as aphysical." In this context we prove the following lemma.

**Lemma 3.4** *If $\exists$ a unique maximal solution for IVP BOC in $I = [0, z^*)$, with the initial conditions $c_{zz}(0) > 0$, $c_{rr}(0) > 0$ and if $\xi \in I$, then the solution restricted to $I^* = [0, \xi] \subset I$ is a physically acceptable solution.*

Proof: Since a unique maximal solution exists for the IVP BOC, $v_z > 0$ and $dv_z/dz < \infty \ \forall z \in I$. (If $v_z(\tilde{z}) = 0$ for some $\tilde{z} \in (0, z^*)$, then right hand side of system BOC (Eqs.(3.8- 3.11) would become singular at $\tilde{z}$ and a solution would not exist). Moreover, since $c_{zz}(0) > 0$, $c_{rr}(0) > 0$, applying Thm.3.4 we get $c_{zz} > 0$ $c_{rr} > 0 \ \forall z \in I$. Hence in $I^*$, the conditions for the solution to be physically acceptable are satisfied.

## 3.6 Properties of system AOC

We write down the system AOC once more:

$$\mathbf{u}'(z) = \mathbf{g}(\mathbf{u}) \quad \mathbf{u}(\xi) = \mathbf{u}_\xi \ \forall z \in (\xi, 1]$$

Here $\mathbf{u} = [v_z, T, c_{zz}, c_{rr}, w = dv_z/dz, S_{zz}, x]$ and the boundary conditions are $\mathbf{u}_\xi = [v_z(\xi), T(\xi), c_{zz}(\xi), c_{rr}(\xi), 0, 0, 0]$ where continuity of solution gives the boundary values for $v_z, T, c_{zz}$ and $c_{rr}$ and the BCs for $w, S_{zz}$ and $x$ are prescribed and as explained in the previous chapter.

Lemma 3.3 of the previous section can be applied to the variables $c_{zz}$ and $c_{rr}$ once again in phase AOC to show that under the same conditions they remain bounded. More precisely, under the assumptions $v_z > 0$, $dv_z/dz <$

$\infty$ $\forall z \in [\xi, 1]$, if $c_{zz}(\xi) > 0$, $c_{rr}(\xi) > 0$ then $c_{zz} > 0$, $c_{rr} > 0$ $\forall z \in [\xi, 1]$. The evolution equations of $c_{zz}$ and $c_{rr}$ (Eq.(2.20), (2.21)), are coupled with the rate of crystallinity $x$. However, the term $1 - x$ which could possibly induce a singularity while calculating the roots of $f$ as in Lemma3.3, appears only in the numerator. Therefore, it is straightforward to carry over the same techniques as in Thm3.4 to $c_{zz}$ and $c_{rr}$ in phase AOC.

## 3.6.1   Singularities in system AOC

After a careful examination of the system of equations AOC given by Eqs.(3.12) to (3.18), the following were found to be the possible singularities:

- $v_z = 0$.

- Weisenberg number $\text{De}_{sc}$
  From the form of $\text{De}_{sc}$ one sees that for parameter $c \neq 0$, $\text{De}_{sc} \neq 0$ because of its exponential form. But for large values of $F$, it could become arbitrarily high. (Check out the numerical value of $\text{De}_{sc}$ in Table3.2).

- $x = 1$
  From the form of $\text{De}_a$, one observes that for $x \to 1$, $\text{De}_a$ goes to zero thus inducing a singularity in the equations of $c_{zz}$ and $c_{rr}$. Apart from that, the term $1/(1 - x)$ appears in many terms on the right hand side of system AOC, (Eqs.(3.12) to (3.18)).

- $e = 1$.

The above are so to say the "potential" singularities. Below we investigate the singularity $x = 1$.

**Proposition 1** *Assume that $\frac{dv_z}{dz} < \infty, v_z > 0, e < 1$ $\forall z \in [\xi, 1]$. If $c_{zz}(\xi) > 0, c_{rr}(\xi) > 0, x(\xi) < 1$, then $x < 1$   $\forall z \in [\xi, 1]$.*

Proof: From the assumption $e < 1$ we have,

$$\frac{1}{1 - x} \sqrt{\frac{c_{zz} + 2c_{rr}}{3N_0}} \quad < \quad 1 \tag{3.29}$$

$$\Rightarrow c_{zz} + 2c_{rr} \quad < \quad 3N_0(1 - x)^2. \tag{3.30}$$

Assume that $x = 1$ for some $z^* \in (\xi, 1]$ then from above we have,

$$c_{zz}(z^*) + 2c_{rr}(z^*) < 0$$

But we know that for $c_{zz}(\xi), c_{rr}(\xi) > 0$ we have $c_{zz}, c_{rr} > 0 \forall z \in [\xi, 1]$ (By applying Lemma.3.3 as explained earlier in this section). Therefore we have a contradiction. Hence $x < 1 \quad \forall z \in [\xi, 1]$.

As long as we have a bound on $c_{zz} + 2c_{rr}$ in terms of the parameter $N_0$, we can avoid the singularities. In the absence of singularities, applying standard basic theorems of ordinary differential equations one can prove the existence of a unique global solution to the IVP AOC. We now show that with the appropriate choice of the initial conditions for IVP BOC, it is possible to prove the existence of a unique physically acceptable solution for IVP AOC. For this, we first define a physically acceptable solution for AOC.

## 3.6.2   Existence of a physically acceptable solution

**Definition 3.3** *The set of solutions* $(v_z, T, c_{zz}, c_{rr}, w, S_{zz}, x)$ *of IVP AOC, such that* $v_z > 0$, $c_{zz} > 0$, $c_{rr} > 0$, $x < 1 \,\forall z \in [\xi, z^*], z^* \leq 1$ *is called the set of physically acceptable solutions in* $[\xi, z^*]$.

**Theorem 3.5** *If* $\exists$ *a unique physically acceptable solution of IVP BOC in* $[0, \xi]$ *and* $dv_z/dz < \infty$, $v_z > 0$, $e < 1 \,\forall z \in (\xi, 1]$, *then* $\exists$ *a unique physically acceptable solution for IVP AOC.*

Proof: Let $(v_z, T, c_{zz}, c_{rr})$ be the physically acceptable solution of IVP BOC. Then we have $v_z(\xi) > 0$, $T(\xi) = T_m, c_{zz}(\xi) > 0, c_{rr}(\xi) > 0$. From the assumptions in the theorem, we can apply Lemma 3.3 to variables $c_{zz}$ and $c_{rr}$ to get $c_{zz} > 0$, $c_{rr} > 0 \,\forall z \in [\xi, 1]$. Moreover, from Prop.1 we get $x(z) < 1 \,\forall z \in [\xi, 1]$. Since $v_z > 0$ by assumption and $x < 1$, therefore the right hand side of system AOC (Eqs.(3.12) to (3.18)) is Lipschitz continuous. Therefore, a unique solution exists for IVP AOC in $[\xi, 1]$. Moreover, the solutions satisfy the properties of a physically acceptable solution as described by Defn3.3.

We can go further to say that if a unique maximal solution exists for IVP BOC with the initial conditions $c_{zz}(0) > 0$, $c_{rr}(0) > 0$, such that $\xi$ can be determined then under the conditions $v_z > 0, dv_z/dz < \infty$ and $e < 1$, there exists a unique physically acceptable solution for IVP AOC. This gives a

connection between the existence of solution of IVP AOC and the choice of initial conditions for IVP BOC. We will see more about the choice of initial conditions in Chapter 5.

However, analysis of the complete boundary value problem is far too difficult at the moment because of lack of techniques even to analyse simpler nonlinear differential equations.

# Chapter 4

# Mathematical Analysis Part II: Hamiltonian Mechanics

*This chapter is intended to give a deeper understanding of the mechanics of 1-d, elongational flow of a viscoelastic fluid. Appropriate Poisson brackets are derived for the 1-d, elongational flow and using these Poisson and Dissipative brackets, cross-sectionally averaged mass and momentum equations of melt spinning along with the constitutive microstructural equations are derived.*

In the last few years interest in Poisson bracket formalism has increased because of application of Hamiltonian mechanics to continuous systems. In the 1980s a lot of work was done in developing non-canonical Poisson brackets for ideal fluid flow [22], [21]. However these studies were limited to conservative phenomena. But during the last few decades with progress in theory of irreversible thermodynamics and extension of Hamiltonian methods to dissipative media, there has been progress in the development of a so called *Dissipative bracket*. Beris and Edwards first introduced the *generalised bracket* consisting of the Poisson and dissipative brackets in order to express the dynamics in nonlinear elastic media and viscoelastic media in Hamiltonian form,[14]. Marsden *et al*(1984) have also determined the non-canonical Poisson brackets for elasticity. In this chapter we show the application of Hamiltonian mechanics aided with Poisson and Dissipative brackets to the specific case of a 1-d, uniaxial flow of a viscoelastic fluid in a cylindrical domain with a free boundary. We first derive the appropriate Poisson bracket for this special flow and then show that cross-sectionally averaged mass,momentum

and constitutive stress equations of melt spinning can be derived using this technique.

The Hamiltonian finds it's usefulness in analysis of differential equations and proving existence and uniqueness of solutions. By proving that the action integral has an extremum it is possible to prove that a solution exists for the corresponding system. Although, such an approach is a difficult one for complicated systems like the one we have seen in the last chapter, it is worthwhile to find the Hamiltonian for our system. From the previous chapter is was seen that to prove existence of solution is not only a highly complicated task, but under certain conditions even impossible. In this chapter we try to understand the underlying thermodynamics and transport phenomena within this highly structured media. Our work is based on the derivation of Poisson brackets for the 3-d viscoelastic flow as done by Beris and Edwards in [2], [14]. We apply the same techniques to our special case of a 1-d elongational viscoelastic flow.

# 4.1   Introduction to Hamiltonian-Poisson bracket theory

From classical mechanics we know that for a discreet particle system, the phase space $P$ is defined to be the space of all pairs $(\mathbf{p}, \mathbf{q})$ of positions $\mathbf{q}$ and momenta $\mathbf{p}$ of the particles. By writing down the action integral for this system of particles it is possible to find the Hamiltonian of the system. From the Hamiltonian it is then possible to write down the equations of motion of the system.

**Definition 4.1** *The canonical Poisson bracket $\{.,.\}$ is a map* $\{.,.\} : C^1(P, \mathbb{R}) \times C^1(P, \mathbb{R}) \to C^1(P, \mathbb{R})$ *defined as follows:*

$$\{F, G\} := \frac{\partial F}{\partial q} \frac{\partial G}{\partial p} - \frac{\partial F}{\partial p} \frac{\partial G}{\partial q}$$

The dynamical equation for any arbitrary functional F can be expressed as following.

$$\frac{dF}{dt} = [\{F, H\}]$$

where H is the Hamiltonian of the system and $\{[.,.]\}$ is the generalised bracket. The generalised bracket describes both conservative and non-conservative

effects. It is decomposed into two sub-brackets as follows

$$\{[F, H]\} = \{F, H\} + [F, H]$$

where $\{.,.\}$ is the Poisson bracket describing the conservative effects and $[.,.]$ is the Dissipative bracket describing the non-conservative effects.

### 4.1.1   Properties of Poisson bracket

For any arbitrary functions $f(\mathbf{p}, \mathbf{q})$ and $g(\mathbf{p}, \mathbf{q})$, the following properties should be satisfied by the Poisson bracket:

- Antisymmetry
  $\{f, g\} = -\{g, f\}$ In the special case where $f = h$, where h denotes the Hamiltonian, for conservative systems it is required that

$$\frac{dh}{dt} = \{h, h\} = 0$$

  This shows that the total energy is conserved.

- Bilinearity
  $\{\alpha f + \beta g, h\} = \alpha\{f, h\} + \beta\{g, h\}, \quad \alpha, \beta \in \mathbb{R} \text{ or } \mathbb{C}$

- Jacobi identity
  $\{f, \{g, f\}\} + \{g, \{h, f\}\} + \{h, \{f, g\}\} = 0$

### 4.1.2   Poisson brackets in continuous media

As the number of discreet particles increase to infinity, instead of determining the individual trajectories $x_i(t)$, $i = 1.., N$ $N \to \infty$, of discreet particles, one determines a single continuous vector function $Y(\mathbf{x}, t)$ which indicates the position of a fluid particle at time t with reference position $\mathbf{x}$ at time $t = 0$, [2].

## 4.2   Derivation of Poisson brackets for 1-d elongational viscoelastic flow

In this section we determine the Poisson bracket for a cross sectionally averaged 1-d viscoelastic fibre. We start with the canonical, material Poisson

bracket and derive from it the equivalent spatial Poisson bracket. Subsequently the spatial equations of melt spinning can be derived.

## 4.2.1  Canonical brackets (Lagrangian description)

Let us consider our fibre (domain) to be cylindrical with coordinates $(r, \theta, z)$. In the 1-d Lagrangian description we follow a certain fluid particle labelled by the position variable $z$, along it's trajectory given by $Y(z, t) \in \mathbb{R}$. At time $t = 0$, the fluid occupies a region $\Omega$ with boundary $\partial\Omega$ and the initial condition on the fluid particle under observation is $Y(z, 0) = z$. At time $t$ it occupies a region $\Omega'$ with boundary $\partial\Omega'$. But we assume that $\partial\Omega = \partial\Omega'$ for all times, i.e length of the fibre is fixed.

Since we want to work in 1-d, we take all the quantities of interest to be cross-sectionally integrated. If $\rho$ is the mass density then we define a new variable $\tilde{\rho}$ as follows.

$$\tilde{\rho} = \int\limits_{0}^{2\pi} \int\limits_{0}^{R(z,t)} \rho r \, dr = \rho \pi R^2(z, t) = \rho A(z, t) \tag{4.1}$$

where $R(z, t)$ is the radius of the fibre at point $z$ and time $t$ and $A(z, t) = \pi R(z, t)^2$ denotes the corresponding cross sectional area. Later on we will drop the dependencies while writing $A$. Note that since the free surface $r = R(z, t)$ is unknown, the new density $\tilde{\rho}$ is not constant.

The distribution of mass at $t = 0$ can be described by the density function $\rho_0 = \rho(z, 0)$. Since the mass of the fluid is conserved, the mass density at any $Y(z, t)$ must satisfy the conservation equation.

$$
\begin{aligned}
\tilde{\rho} dY &= \tilde{\rho}_0 dz \\
\tilde{\rho}(Y, t) dY &= \tilde{\rho}_0(z, 0) dz \\
\tilde{\rho}(Y, t) &= \tilde{\rho}_0 \frac{dz}{dY(z, t)} \\
&= \frac{\tilde{\rho}_0(z)}{J}
\end{aligned}
$$

where $J = dY(z, t)/dz$
The Lagrangian for this system can be expressed in terms of the dynamical

variables $Y(z)$ and $\dot{Y}(z)$ as follows:

$$
\begin{aligned}
L &= \int_\Omega \tilde{\rho}\left(\frac{\dot{Y}^2}{2} - U[\tilde{\rho}, \tilde{s}_0]\right) dY \\
&= \int_\Omega \tilde{\rho}_0(z)\left(\frac{\dot{Y}^2}{2} - U[\tilde{\rho}, \tilde{s}_0]\right) dz
\end{aligned}
$$

where $U$ depends on the initial entropy density $\tilde{s}_0 = \rho_0 s$. With this Lagrangian, the action integral for this system can be written as follows.

$$
I = \int_{t_1}^{t_2} L \, dt
$$

Before we go further, we introduce the notation for the functional derivative. The functional derivative of a functional $F[Y(z)]$ is always represented by means of the $L_2$ pairing on the appropriate space of functions:

$$
\frac{\delta F}{\delta Y}\delta Y = \int_\Omega \frac{\widehat{\delta F}}{\delta Y}[Y](z)\delta Y(z) dz
$$

Thus, $\frac{\widehat{\delta F}}{\delta Y}$ denotes the associated function representing the derivative $\frac{\delta F}{\delta Y}$ with respect to the $L_2$ pairing.

Conjugate momentum is defined as

$$
\pi(z) = \frac{\widehat{\delta L}}{\delta \dot{Y}} = \tilde{\rho}_0(z)\dot{Y}(z)
$$

The Hamiltonian is the sum of the kinetic and potential energies:

$$
H[Y, \pi] = \int_\Omega \left[\frac{\pi^2}{2\tilde{\rho}_0} + \tilde{\rho}_0 \, U[\tilde{\rho}(Y), s_0(z)]\right] dz
$$

The equation of motion for the 1-d fluid in the Lagrangian description can be written as follows

$$
\begin{aligned}
\dot{Y}(z) &= \frac{\widehat{\delta H}[Y, \pi]}{\delta \pi} = \frac{\pi(z)}{\tilde{\rho}_0} \\
\dot{\pi}(z) &= -\frac{\widehat{\delta H}[Y, \pi]}{\delta Y}
\end{aligned}
$$

**Definition 4.2** *The phase space $P$ for the infinite dimensional case is defined as :*

$$P := \{(Y, \pi) \in C^1(I, \mathbb{R}) \times C^1(I, \mathbb{R})\}$$

*where $I$ is an appropriate set of Lagrange parameters.*
The canonical Poisson bracket is defined as follows:

$$\{F, G\}[Y, \pi] := \int_\Omega \left( \frac{\widehat{\delta F}}{\delta Y}[Y, \pi](z) \frac{\widehat{\delta G}}{\delta \pi}[Y, \pi](z) - \frac{\widehat{\delta F}}{\delta \pi}[Y, \pi](z) \frac{\widehat{\delta G}}{\delta Y}[Y, \pi](z) \right) dz$$

**Remark 4.1** *When $F$ and $G$ are function valued, the formula has to be modified. However, for each function value of $F$ and $G$, the above formula applies:*

$$\{F, G\}[Y, \pi](x, x') := \{F(x), G(x')\}[Y, \pi] =$$

$$\int_\Omega \left( \frac{\widehat{\delta F(x)}}{\delta Y}[Y, \pi](z) \frac{\widehat{\delta G(x')}}{\delta \pi}[Y, \pi](z) - \frac{\widehat{\delta F(x)}}{\delta \pi}[Y, \pi](z) \frac{\widehat{\delta G(x')}}{\delta Y}[Y, \pi](z) \right) dz$$

$$(4.2)$$

## 4.2.2 Non-canonical brackets (Spatial description)

In the spatial description, we consider a fixed coordinate in space $x$, for which the length element is given by $dx$.

$$z = Y(R(x, \tilde{t}), \tilde{t})$$

$R(x, \tilde{t})$ is a material label for the fluid particle which has position x at time t.
We first define the following quaties: Momentum density:

$$\tilde{\mathbf{M}} = \int_0^{2\pi} \int_0^{R(z,t)} \rho \mathbf{v} r \, dr = \rho \mathbf{v} \pi R^2(z, t) = \rho \mathbf{v} A = \tilde{\rho} \mathbf{v}$$

Although the conformation tensor is a microstructural variable, on the macroscopic scale it can be interpreted as the Cauchy strain tensor. i.e $\mathbf{c} = \mathbf{F^T F}$ where $\mathbf{F}$ is the displacement gradient tensor,[27]. For elongational flow, the tensor $\mathbf{F}$ has the following form [4]. Let $\epsilon = dv_z/dz$ denote the elongation rate of the fibre.

$$\mathbf{F} = \begin{pmatrix} e^{\int \epsilon dt} & 0 & 0 \\ 0 & e^{-\int \frac{\epsilon}{2} dt} & 0 \\ 0 & 0 & e^{-\int \frac{\epsilon}{2} dt} \end{pmatrix} \qquad (4.3)$$

From above, we have $c_{zz} = F_{zz}^2, c_{rr} = F_{rr}^2 = \frac{1}{F_{zz}} = c_{\theta\theta}$, where $F_{zz}, F_{rr}, F_{\theta\theta}$ denote the diagonal components of the strain matrix.

Because we deal with a uniaxial stretching of the fibre along the axial direction, $\mathbf{c}$ is a diagonal tensor. But in 1-d we treat $c_{zz} \in \mathbb{R}, c_{rr} \in \mathbb{R}$ and $c_{\theta\theta} \in \mathbb{R}$ as separate scalar quantities.

Analogous to the density and momentum, we define the following:

$$\tilde{C}_{zz} = \rho c_{zz} A, \quad \tilde{C}_{rr} = \rho c_{rr} A, \quad \tilde{C}_{\theta\theta} = \rho c_{\theta\theta} A$$

We observe that $\tilde{C}_{rr} = \tilde{C}_{\theta\theta}$ and they can be expressed as functions of $F_{zz}$. We take into account the internal energy density of the fibre:

$$\tilde{U} = \int\limits_{0}^{2\pi} \int\limits_{0}^{R(z,t)} \rho U r dr = \rho U A = \tilde{\rho} U$$

where $U$ is the internal energy per unit mass. Thus the phase space $P_E$ consists of the following variables.

$$\begin{aligned}
\tilde{\rho}(x) &\in & C([0, L], \mathbb{R}) \\
\tilde{M}_z(x) &\in & C([0, L], \mathbb{R}) \quad M_z = 0 \text{ for } x = 0, x = L \\
\tilde{C}_{zz}(x) &\in & C([0, L], \mathbb{R}) \\
\tilde{C}_{rr}(x) &\in & C([0, L], \mathbb{R}) \\
\tilde{s}(x) &\in & C([0, L], \mathbb{R})
\end{aligned}$$

The Hamiltonian can be written as follows.

$$H[\tilde{\rho}, \tilde{M}_z, \tilde{C}_{zz}, \tilde{C}_{rr}] = \int\limits_{\Omega'} \left[ \frac{\tilde{M}_z^2}{2\tilde{\rho}} + \tilde{U}(\tilde{\rho}, \tilde{C}_{zz}, \tilde{C}_{rr}, \tilde{s}) \right] dz \qquad (4.4)$$

with $\tilde{U} = \tilde{a} + T\tilde{s}$ where $\tilde{a}$ is the elastic potential energy density of the viscoelastic fluid and $\tilde{s}$ is the entropy density. The viscoelastic model under consideration is the Giesekus model. The elastic potential energy for this model is given as follows: [2]

$$\begin{aligned}
\tilde{a} = &\frac{1}{2} nK(\tilde{C}_{zz} + 2\tilde{C}_{rr}) \left( E + \frac{1}{3e^2} ln \left( \frac{3eE}{\sinh(3eE)} \right) \right) \\
&- \frac{1}{2} n\tilde{\rho} k_B T \ln \left( \left( \frac{K}{\tilde{\rho}} \right)^3 \tilde{C}_{zz} \tilde{C}_{rr}^2 \right)
\end{aligned}$$

where

$K$    —    spring constant

$k_B$    —    Boltzmann constant

$n$    —    number of chains per unit length

$e$    —    extension of chain with respect to it's length (see section (1.3.2))

$E$    —    nonlinear force factor.

$T$    —    absolute temperature

Consider an arbitrary functional F, of the dynamical variables $\tilde{\rho}$, $\tilde{M}_z$, $\tilde{C}_{zz}$, $\tilde{C}_{rr}$ and $\tilde{s}$:

$$F[\tilde{\rho}, \tilde{M}_z, \tilde{C}_{zz}, \tilde{C}_{rr}, \tilde{s}] = \int_{\Omega} f(\tilde{\rho}, \tilde{M}_z, \tilde{C}_{zz}, \tilde{C}_{rr}, \tilde{s}) dz$$

Then the dynamical equation for this functional can be written as

$$\frac{dF}{dt} = \int_{\Omega} \left[ \frac{\widehat{\delta} F}{\delta \tilde{\rho}} \frac{\partial \tilde{\rho}}{\partial t} + \frac{\widehat{\delta} F}{\delta \tilde{M}_z} \frac{\partial \tilde{M}_z}{\partial t} + \frac{\widehat{\delta} F}{\delta \tilde{C}_{zz}} \frac{\partial \tilde{C}_{zz}}{\partial t} + \frac{\widehat{\delta} F}{\delta \tilde{C}_{rr}} \frac{\partial \tilde{C}_{rr}}{\partial t} + \frac{\widehat{\delta} F}{\delta \tilde{s}} \frac{\partial \tilde{s}}{\partial t} \right] dz \quad (4.5)$$

We need to derive the Poisson bracket in the spatial description. For this, the spatial variables are written in terms of the material variables. The transformation of a material variable $g_L$ to its corresponding spatial description $g_E$ is given by :

$$\int_{\Omega} g_L(z) \delta[Y(z) - x] dz \equiv g_E(x) \quad (4.6)$$

Thus we define the following variables from their material counterparts:

$$\tilde{\rho}[Y, \pi](x) \quad := \quad \int_{\Omega} \tilde{\rho}_0(z) \delta[Y(z) - x] dz \quad (4.7)$$

$$\tilde{M}_z[Y, \pi](x) \quad := \quad \int_{\Omega} \Pi(z) \delta[Y(z) - x] dz \quad (4.8)$$

$$\tilde{C}_{zz}[Y, \pi](x) \quad := \quad \int_{\Omega} \tilde{\rho}_0 c_{zz}(F_{zz}(z), t) \delta[Y(z) - x] dz \quad (4.9)$$

$$\tilde{C}_{rr}[Y, \pi](x) \quad := \quad \int_{\Omega} \tilde{\rho}_0 c_{rr}(F_{zz}(z), t) \delta[Y(z) - x] dz \quad (4.10)$$

$$\tilde{s}[Y, \pi](x) \quad := \quad \int_{\Omega} \tilde{\rho}_0(z) s \delta[Y(z) - x] dz \quad (4.11)$$

where $F_{zz}$ is the strain component as explained in Section 4.2.1. To evaluate the Poisson bracket in the Eulerian description, we need to define the functional derivatives using the chain rule for differentiation. For an arbitrary functional $F[\tilde{\rho}(x), \tilde{M}_z(x), \tilde{C}_{zz}(x), \tilde{C}_{rr}(x), \tilde{s}(x)]$, we have

$$
\begin{aligned}
\frac{\widehat{\delta F}}{\delta Y}[Y, \pi](x) &= \int_\Omega \left( \frac{\widehat{\delta F}}{\delta \tilde{\rho}}[\tilde{\rho}[Y, \pi]](x) \frac{\widehat{\delta \tilde{\rho}}}{\delta Y}[Y, \pi](x, x') + \frac{\widehat{\delta F}}{\delta \tilde{M}_z} \frac{\widehat{\delta \tilde{M}_z}}{\delta Y} + \frac{\widehat{\delta F}}{\delta \tilde{C}_{zz}} \frac{\widehat{\delta \tilde{C}_{zz}}}{\delta Y} \right. \\
&\quad \left. + \frac{\widehat{\delta F}}{\delta \tilde{C}_{rr}} \frac{\widehat{\delta \tilde{C}_{rr}}}{\delta Y} + \frac{\widehat{\delta F}}{\delta \tilde{s}} \frac{\widehat{\delta \tilde{s}}}{\delta Y} \right) dz \\
\frac{\widehat{\delta F}}{\delta \Pi}[Y, \pi](x) &= \int_\Omega \left( \frac{\delta F}{\delta \tilde{\rho}} \frac{\widehat{\delta \tilde{\rho}}}{\delta \Pi} + \frac{\delta F}{\delta \tilde{M}_z} \frac{\widehat{\delta \tilde{M}_z}}{\delta \Pi} + \frac{\delta F}{\delta \tilde{C}_{zz}} \frac{\widehat{\delta \tilde{C}_{zz}}}{\delta \Pi} \right. \\
&\quad \left. + \frac{\widehat{\delta F}}{\delta \tilde{C}_{rr}} \frac{\widehat{\delta \tilde{C}_{rr}}}{\delta \Pi} + \frac{\widehat{\delta F}}{\delta \tilde{s}} \frac{\widehat{\delta \tilde{s}}}{\delta \pi} \right) dz
\end{aligned}
$$

where the functional dependence has been shown only in the first term in the RHS of the first equation. The same dependencies follow for the rest of the terms. Now, suppose $F = F_E \circ \mathbf{X}$, 1.e $F_E$ is the spatial counterpart of $F$ and $\mathbf{X}$ is the vector of spatial variables then:

$$
\begin{aligned}
\{F, G\}_L &= \int_\Omega \left( \frac{\widehat{\delta F}}{\delta Y}[Y, \pi](z) \frac{\widehat{\delta G}}{\delta \pi}[Y, \pi](z) - \frac{\widehat{\delta F}}{\delta \pi}[Y, \pi](z) \frac{\widehat{\delta G}}{\delta Y}[Y, \pi](z) \right) dz \\
&= \int_\Omega \left( \frac{\widehat{\delta(F_E \circ X)}}{\delta Y}[Y, \pi](z) \frac{\widehat{\delta(G_E \circ X)}}{\delta \pi}[Y, \pi](z) - \curvearrowleft \right) dz \\
&= \int_\Omega \left( \int_\Omega \Sigma_i \frac{\widehat{\delta F_E}}{\delta X_i}[X_i[Y, \pi]](z') \frac{\widehat{\delta X_i}}{\delta Y}[Y, \pi](z', z) dz' \right. \\
&\quad \left. \cdot \int_\Omega \Sigma_j \frac{\widehat{\delta G_E}}{\delta X_j}[X_j[Y, \pi]](z'') \frac{\widehat{\delta X_i}}{\delta \pi}[Y, \pi](z'', z) dz'' - \curvearrowright \right) dz \\
&= \int_\Omega \Sigma_{i,j} \left( \int_\Omega \int_\Omega \frac{\widehat{\delta F_E}}{\delta X_i}[X_i(Y, \pi)](z') \frac{\widehat{\delta G_E}}{\delta X_j}[X_j(Y, \pi)](z'')
\end{aligned}
$$

$$
\cdot \frac{\widehat{X}_i}{\delta Y}[Y, \pi](z', z) \frac{\widehat{\delta X_j}}{\delta \pi}[Y, \pi](z'', z) dz' dz'' - \curvearrowright \bigg) dz
$$

$$
= \int_\Omega \Sigma_{i,j} \int_\Omega \int_\Omega \frac{\widehat{\delta F_E}}{\delta X_i}(z') \frac{\widehat{\delta G_E}}{\delta X_j}(z'') \left( \frac{\widehat{\delta X_i}}{\delta Y}(z', z) \frac{\widehat{\delta X_j}}{\delta \pi}(z'', z) \right.
$$

$$
\left. - \frac{\widehat{\delta X_i}}{\delta \pi}(z', z) \frac{\widehat{\delta X_j}}{\delta Y}(z'', z) \right) dz' dz'' dz
$$

$$
= \Sigma_{i<j} \int_\Omega \int_\Omega \left( \frac{\widehat{\delta F_E}}{\delta X_i}(z') \frac{\widehat{\delta G_E}}{\delta X_j}(z'') - \frac{\widehat{\delta F_E}}{\delta X_j}(z'') \frac{\widehat{\delta G_E}}{\delta X_i}(z') \right)
$$

$$
\{X_i(z', \cdot), X_j(z'', \cdot)\}_L dz' dz'' \tag{4.12}
$$

Substituting the above in the Poisson brackets, for two arbitrary functionals $F$ and $G$ of our spatial variables we get:

$$
\{F, G\}_E
$$

$$
= \int_\Omega \int_\Omega \left[ \frac{\widehat{\delta F}}{\delta \tilde\rho(x)} \frac{\widehat{\delta G}}{\delta \tilde M_z(x')} - \frac{\widehat{\delta G}}{\delta \tilde\rho(x)} \frac{\widehat{\delta F}}{\delta \tilde M_z(x')} \right] \{\tilde\rho(x), \tilde M_z(x')\}_L dx' dx
$$

$$
+ \int_\Omega \int_\Omega \left[ \frac{\widehat{\delta F}}{\delta \tilde M_z(x)} \frac{\widehat{\delta G}}{\delta \tilde M_z(x')} - \frac{\widehat{\delta G}}{\delta \tilde M_z(x)} \frac{\widehat{\delta F}}{\delta \tilde M_z(x')} \right] \{\tilde M_z(x), \tilde M_z(x')\}_L dx' dx
$$

$$
+ \int_\Omega \int_\Omega \left[ \frac{\widehat{\delta F}}{\delta \tilde C_{zz}(x)} \frac{\widehat{\delta G}}{\delta \tilde M_z(x')} - \frac{\widehat{\delta G}}{\delta \tilde C_{zz}(x)} \frac{\widehat{\delta F}}{\delta \tilde M_z(x')} \right] \{\tilde C_{zz}(x), \tilde M_z(x')\}_L dx' dx
$$

$$
+ 2 \int_\Omega \int_\Omega \left[ \frac{\widehat{\delta F}}{\delta \tilde C_{rr}(x)} \frac{\widehat{\delta G}}{\delta \tilde M_z(x')} - \frac{\widehat{\delta G}}{\delta \tilde C_{rr}(x)} \frac{\widehat{\delta F}}{\delta \tilde M_z(x')} \right] \{\tilde C_{rr}(x), \tilde M_z(x')\}_L dx' dx
$$

$$
+ \int_\Omega \int_\Omega \left[ \frac{\widehat{\delta F}}{\delta \tilde s(x)} \frac{\widehat{\delta G}}{\delta \tilde M_z(x')} - \frac{\widehat{\delta G}}{\delta \tilde s(x)} \frac{\widehat{\delta F}}{\delta \tilde M_z(x')} \right] \{\tilde s(x), \tilde M_z(x')\}_L dx' dx \tag{4.13}
$$

The factor 2 in the second last term appears to take into account $\tilde C_{\theta\theta}$ which we know is equal to $\tilde C_{rr}$.

In order to evaluate the canonical poisson brackets appearing in the above equation, we need to evaluate the corresponding functional derivatives. Using the definition of functional derivative as given in Section 4.2.1, we get:

$$
\frac{\widehat{\delta \tilde\rho}}{\delta Y}[Y, \pi](x) = \tilde\rho_0(z) \frac{\partial \delta[Y(z) - x]}{\partial Y}, \frac{\widehat{\delta \tilde\rho}}{\delta \Pi}[Y, \pi](z) = 0 \tag{4.14}
$$

$$\frac{\widehat{\delta \tilde{M}_z}}{\delta Y} = \tilde{\Pi}(z)\frac{\partial \delta[Y(z) - x]}{\partial Y}, \frac{\widehat{\delta \tilde{M}_z}}{\delta \Pi} = \delta[Y(z) - x] \tag{4.15}$$

$$\frac{\widehat{\delta \tilde{C}_{zz}}}{\delta Y} = \tilde{\rho}_0 c_{zz}\frac{\partial \delta[Y - x]}{\partial Y} - \frac{\partial}{\partial z}\left(\tilde{\rho}_0 \delta[Y - x]\frac{\partial c_{zz}}{\partial F_{zz}}\right), \frac{\widehat{\delta \tilde{C}_{zz}}}{\delta \Pi} = 0 \tag{4.16}$$

$$\frac{\widehat{\delta \tilde{C}_{rr}}}{\delta Y} = \tilde{\rho}_0 c_{rr}\frac{\partial \delta[Y - x]}{\partial Y} - \frac{\partial}{\partial z}\left(\tilde{\rho}_0 \delta[Y - x]\frac{\partial c_{rr}}{\partial F_{zz}}\right), \frac{\widehat{\delta \tilde{C}_{rr}}}{\delta \Pi} = 0 \tag{4.17}$$

$$\frac{\widehat{\delta \tilde{s}}}{\delta Y} = \tilde{\rho}_0 s(z)\frac{\partial \delta[Y - x]}{\partial Y}, \frac{\widehat{\delta \tilde{s}}}{\delta \Pi} = 0 \tag{4.18}$$

with the functional dependence for all the equations as in (4.14).
We now show the derivation only of $\{\tilde{C}_{zz}(x), \tilde{M}_z(x')\}_L$ which appears in Eq.(4.13).

$$\{\tilde{C}_{zz}(x, t), \tilde{M}_z(x', t)\}_L = \int_\Omega \left(\frac{\widehat{\delta \tilde{C}_{zz}}}{\delta Y}\frac{\widehat{\delta \tilde{M}_z}}{\delta \Pi} - \frac{\widehat{\delta \tilde{C}_{zz}}}{\delta \Pi}\frac{\widehat{\delta \tilde{M}_z}}{\delta Y}\right) dx$$

Substituting the functional derivatives given by Eqs.(4.14) to (4.18), we get

$$\{\tilde{C}_{zz}(x), \tilde{M}_z(x')\}_L$$
$$= \int_\Omega \left[\tilde{\rho}_0 c_{zz}\frac{\partial \delta[Y - x]}{\partial Y} - \frac{\partial}{\partial z}\left(\tilde{\rho}_0 \delta[Y - x]\frac{\partial c_{zz}}{\partial F_{zz}}\right)\right]\delta[Y - x']dx$$
$$= \int_\Omega \left(\rho c_{zz}\frac{\partial \delta[Y - x]}{\partial Y} - \frac{1}{J}\frac{\partial}{\partial z}(\rho J\delta[Y - x]2F_{zz})\right)\delta[Y - x']dY$$
$$= \int_\Omega \left(\rho c_{zz}\frac{\partial \delta[Y - x]}{\partial Y} - \frac{1}{J}\frac{\partial Y}{\partial z}\frac{\partial}{\partial Y}(\rho J\delta[Y - x]2F_{zz})\right)\delta[Y - x']dY$$
$$= \tilde{C}_{zz}(x', t)\frac{\partial \delta[x' - x]}{\partial x'} - \frac{\partial}{\partial x'}(\delta[x' - x]2\tilde{C}_{zz}(x', t)) \tag{4.19}$$

It is here that one takes into account that the flow we are dealing with is an elongational flow. For such a flow the deformation gradient tensor and consequently the strain tensor has the diagonal form. Also, $c_{zz}$ and $c_{rr}$ depend on $F_{zz}$. This is the main step in all the calculations which gives us the correct Poisson bracket for the 1-d viscoelastic fibre.

Similarly, the other Poisson brackets can be evaluated and shown to be

$$\{\tilde{C}_{rr}(x), \tilde{M}_z(x')\}_L = \tilde{C}_{rr}(x')\frac{\partial\delta[x'-x]}{\partial x'} + \frac{\partial}{\partial x'}(\delta[x'-x]\tilde{C}_{rr}(x')) \qquad (4.20)$$

$$\{\tilde{\rho}(x), \tilde{M}_z(x')\}_L = \tilde{\rho}(x')\frac{\partial\delta[x'-x]}{\partial x'} \qquad (4.21)$$

$$\{\tilde{M}_z(x), \tilde{M}_z(x')\}_L = \tilde{M}_z(x')\frac{\partial\delta[x'-x]}{\partial x'} - \tilde{M}_z(x)\frac{\partial\delta[x-x']}{\partial x} \qquad (4.22)$$

$$\{\tilde{s}(x), M_z(x')\}_L = s(x')\frac{\partial\delta[x-x']}{\partial x} \qquad (4.23)$$

After substituting the above expressions in Eq.(4.13) and after a few manipulations the following Poisson bracket in the Eulerian description can be derived.

$$\{F, G\}_E = -\int_\Omega \left[\frac{\hat{\delta}F}{\delta\tilde{\rho}}\frac{\partial}{\partial z}\left(\frac{\hat{\delta}G}{\delta\tilde{M}_z}\tilde{\rho}\right) - \frac{\hat{\delta}G}{\delta\tilde{\rho}}\frac{\partial}{\partial z}\left(\frac{\hat{\delta}F}{\delta\tilde{M}_z}\tilde{\rho}\right)\right] dz$$

$$-\int_\Omega \left[\frac{\hat{\delta}F}{\delta\tilde{M}_z}\frac{\partial}{\partial z}\left(\frac{\hat{\delta}G}{\delta\tilde{M}_z}\tilde{M}_z\right) - \frac{\hat{\delta}G}{\delta\tilde{M}_z}\frac{\partial}{\partial z}\left(\frac{\hat{\delta}F}{\delta\tilde{M}_z}\tilde{M}_z\right)\right] dz$$

$$-\int_\Omega \left[\frac{\hat{\delta}F}{\delta\tilde{C}_{zz}}\frac{\partial}{\partial z}\left(\frac{\hat{\delta}G}{\delta\tilde{M}_z}\tilde{C}_{zz}\right) - \frac{\hat{\delta}G}{\delta\tilde{C}_{zz}}\frac{\partial}{\partial z}\left(\frac{\hat{\delta}F}{\delta\tilde{M}_z}\tilde{C}_{zz}\right)\right] dz$$

$$-\int_\Omega 2\tilde{C}_{zz}\left[\frac{\hat{\delta}G}{\delta C_{zz}}\frac{\partial}{\partial z}\left(\frac{\delta F}{\delta\tilde{M}_z}\right) - \frac{\hat{\delta}F}{\delta\tilde{C}_{zz}}\frac{\partial}{\partial z}\left(\frac{\hat{\delta}G}{\delta\tilde{M}_z}\right)\right] dz$$

$$-2\int_\Omega \left[\frac{\hat{\delta}F}{\delta\tilde{C}_{rr}}\frac{\partial}{\partial z}\left(\frac{\hat{\delta}G}{\delta\tilde{M}_z}\tilde{C}_{rr}\right) - \frac{\hat{\delta}G}{\delta\tilde{C}_{rr}}\frac{\partial}{\partial z}\left(\frac{\hat{\delta}F}{\delta\tilde{M}_z}\tilde{C}_{rr}\right)\right] dz$$

$$-2\int_\Omega C_{rr}\left[\frac{\hat{\delta}F}{\delta\tilde{C}_{rr}}\frac{\partial}{\partial z}\left(\frac{\hat{\delta}G}{\delta\tilde{M}_z}\right) - \frac{\hat{\delta}G}{\delta C_{rr}}\frac{\partial}{\partial z}\left(\frac{\hat{\delta}F}{\delta\tilde{M}_z}\right)\right] dz$$

$$-\int_\Omega \left[\frac{\hat{\delta}F}{\delta\tilde{s}}\frac{\partial}{\partial z}\left(\frac{\hat{\delta}G}{\delta\tilde{M}_z}\tilde{s}\right) - \frac{\hat{\delta}G}{\delta\tilde{s}}\frac{\partial}{\partial z}\left(\frac{\delta\hat{F}}{\delta\tilde{M}_z}\tilde{s}\right)\right] dz \qquad (4.24)$$

Since in future we will derive evolution equations with $z$ as the independent variable therefore for convenience of notation, x has been replaced by z in the above Poisson bracket.

The above Poisson bracket can be shown to satisfy the properties of a Poisson bracket mentioned in Section 4.1.1.

## 4.3    Dissipation bracket

In the last few years significant progress has taken place in the study of irreversible phenomena leading to the development of the dissipation bracket. This bracket describes the non-conservative processes.  Beris and Edward were the first ones to develop this bracket and to use it to derive dynamical equations for non-linear elasticity and viscoelastic flow [14]. The dissipative bracket is phenomenological in nature and there seems to be no rigorous theory behind it as yet.  But still, it is now being used extensively in the study of dissipative phenomena. We will not go into the details of the theory and development of this bracket but will use the relevant dissipation bracket to derive our equations.

Starting from the 3-d dissipation bracket for viscoelastic flow given in [2], using our integrated variables and the considering the special flow (elongational) in consideration, we get the following form of dissipation bracket.

$$
[F,G] = -\int_\Omega \left( \Lambda_z \frac{\widehat{\delta F}}{\delta \tilde{C}_{zz}} \frac{\widehat{\delta G}}{\delta \tilde{C}_{zz}} + \Lambda_r \frac{\widehat{\delta F}}{\delta \tilde{C}_{rr}} \frac{\widehat{\delta G}}{\delta \tilde{C}_{rr}} \right.
$$
$$
\left. + \frac{1}{T} \frac{\widehat{\delta F}}{\delta \tilde{s}} \Lambda_z \frac{\widehat{\delta G}}{\delta \tilde{C}_{zz}} \frac{\widehat{\delta G}}{\tilde{C}_{zz}} + \frac{1}{T} \frac{\widehat{\delta F}}{\delta \tilde{s}} \Lambda_r \frac{\widehat{\delta G}}{\delta \tilde{C}_{rr}} \frac{\widehat{\delta G}}{\tilde{C}_{rr}} \right) dz \qquad (4.25)
$$

where $\Lambda_z$ and $\Lambda_r$ are the relaxation parameters. For the particular model in consideration (Giesekus model) $\Lambda_z$ has the following form :

$$
\Lambda_z = \frac{\tilde{\rho}}{2\lambda_a n K} \left[ (1-\alpha)4\tilde{C}_{zz} + 4\alpha \frac{KE}{k_B T} \tilde{C}_{zz}^2 \right]. \qquad (4.26)
$$

$\Lambda_r$ is defined analogously. For the form of the relaxation matrix for a 3-d flow refer to [2]. The dissipation bracket has to satisfy certain properties. In the special case of $F = H$, we have

$$
\frac{dH}{dt} = \{H, H\} + [H, H] = 0.
$$

which shows conservation of the total energy.  From antisymmetry of the Poisson we have $\{H, H\} = 0$ and therefore it follows that:

$$
[H, H] = 0.
$$

## 4.4    Derivation of Evolution equations

Using the derived Poisson brackets given by Eq.(4.24) and the dissipative brackets given by Eq.(4.25), we can derive the evolution equations of the fibre. The dynamical equation for the functional $F$ can be written as follows

$$\frac{dF}{dt} = \{F, H\} + [F, H].$$

From the Hamiltonian as given by Eq.(4.4) the functional derivatives can be evaluated to be:

$$\frac{\widehat{\delta} H}{\delta \tilde{M}_z} = \frac{\tilde{M}_z}{\tilde{\rho}} = v_z$$

$$\frac{\widehat{\delta} H}{\delta \tilde{\rho}} = -\frac{\tilde{M}_z^2}{2\tilde{\rho}^2} + \frac{d\tilde{a}}{d\tilde{\rho}}$$

$$\frac{\widehat{\delta} H}{\delta \tilde{s}} = \frac{\partial \tilde{U}}{\partial \tilde{s}} = T$$

$$\frac{\widehat{\delta} H}{\delta \tilde{C}_{zz}} = \frac{\partial \tilde{a}}{\partial \tilde{C}_{zz}} = \frac{EnK}{2} - \frac{\tilde{\rho} n k_B T}{2\tilde{C}_{zz}}$$

$$\frac{\widehat{\delta} H}{\delta \tilde{C}_{rr}} = \frac{\partial \tilde{a}}{\partial \tilde{C}_{rr}} = EnK - \frac{\tilde{\rho} n k_B T}{\tilde{C}_{rr}} \tag{4.27}$$

Substituting these derivatives in Eqs.(4.5), (4.24) and (4.25), we get the following equations:

$$\frac{\partial \tilde{\rho}}{\partial t} = -\frac{\partial}{\partial z}\left(\frac{\delta H}{\delta \tilde{M}_z}\tilde{\rho}\right)$$

$$\frac{\partial \tilde{s}}{\partial t} = -\frac{\partial}{\partial z}\left(\frac{\delta H}{\delta \tilde{M}_z}\tilde{s}\right) + \frac{1}{T}\Lambda_z \frac{\delta H}{\delta \tilde{C}_{zz}}\frac{\delta H}{\delta \tilde{C}_{zz}} + \frac{1}{T}\Lambda_r \frac{\delta H}{\delta \tilde{C}_{rr}}\frac{\delta H}{\delta \tilde{C}_{rr}}$$

$$\frac{\partial \tilde{M}_z}{\partial t} = -\tilde{\rho}\frac{\partial}{\partial z}\left(\frac{\delta H}{\delta \tilde{\rho}}\right) - \frac{\partial}{\partial z}\left(\frac{\delta H}{\delta \tilde{M}_z}\tilde{M}_z\right) - \tilde{M}_z\frac{\partial}{\partial z}\left(\frac{\delta H}{\delta \tilde{M}_z}\right) - s\frac{\partial}{\partial z}\left(\frac{\delta H}{\delta \tilde{s}}\right)$$

$$-\tilde{C}_{zz}\frac{\partial}{\partial z}\left(\frac{\delta H}{\delta \tilde{C}_{zz}}\right) + \tilde{C}_{rr}\frac{\partial}{\partial z}\left(\frac{\delta H}{\delta \tilde{C}_{rr}}\right) + \frac{\partial}{\partial z}2\tilde{C}_{zz}\frac{\delta H}{\partial \tilde{C}_{zz}} - 2\frac{\partial}{\partial z}\left(\tilde{C}_{rr}\frac{\delta H}{\delta \tilde{C}_{rr}}\right)$$

$$\frac{\partial \tilde{C}_{zz}}{\partial t} = -\frac{\partial}{\partial z}\left(\tilde{C}_{zz}\frac{\delta H}{\delta \tilde{M}_z}\right) + 2\frac{\partial}{\partial z}\frac{\delta H}{\delta \tilde{M}_z}\tilde{C}_{zz} - \Lambda_z\frac{\delta H}{\delta \tilde{C}_{zz}}$$

$$\frac{\partial \tilde{C}_{rr}}{\partial t} = -\frac{\partial}{\partial z}\left(\tilde{C}_{rr}\frac{\delta H}{\delta \tilde{M}_z}\right) - \frac{\partial}{\partial z}\frac{\delta H}{\delta \tilde{M}_z}\tilde{C}_{rr} - \Lambda_r\frac{\delta H}{\delta \tilde{C}_{rr}}$$

After substituting the corresponding functional derivatives in the above equations and performing calculations (see Appendix B), one finally gets the following 1-d system of equations:

- Equation of continuity

$$\frac{\partial}{\partial t}(\rho A) = -\frac{\partial}{\partial z}(\rho v_z A).\tag{4.28}$$

- Momentum equation

$$\rho A \frac{\partial v_z}{\partial t} = -\rho A v_z \frac{\partial v_z}{\partial z} + \rho \frac{\partial}{\partial z}(A(\tau_{zz} - \tau_{rr})).\tag{4.29}$$

where $\tau_{zz} = Ec_{zz} - 1$ and $\tau_{rr} = Ec_{rr} - 1$, [2].

- Equations of $c_{zz}$ and $c_{rr}$

$$\frac{\partial c_{zz}}{\partial t} = -v_z \frac{\partial c_{zz}}{\partial z} + 2c_{zz} \frac{\partial v_z}{\partial z} - \frac{c_{zz}}{\lambda_a nK}\left(1 - \alpha + \frac{KEc_{zz}}{k_B T}\right)(c_{zz}EnK - nk_B T)$$
$$\tag{4.30}$$

$$\frac{\partial c_{rr}}{\partial t} = -v_z \frac{\partial c_{rr}}{\partial z} - c_{rr} \frac{\partial v_z}{\partial z} - \frac{c_{rr}}{\lambda_a nK}\left(1 - \alpha + \frac{KEc_{rr}}{k_B T}\right)(c_{rr}EnK - nk_B T)$$
$$\tag{4.31}$$

At present, the temperature equation cannot be obtained directly from the Hamiltonian. From the entropy equation one can get the equation for internal energy and subsequently the temperature equation.

## 4.4.1    Energy Dissipation

In the last section we saw the derivation of the equations of melt spinning from the Poisson-Dissipation bracket formalism. We could derive the 1-d, cross sectionally averaged equations from the 1-d Hamiltonian. The dynamical equation of Hamiltonian written as:

$$\frac{dH}{dt} = \{H, H\} + [H, H] = 0$$

shows the conservation of total energy. In case we consider force due to shear stress at the fibre surface (air drag), then we would have:

$$\frac{dH}{dt} = -\int_\Omega \frac{1}{2}DC_D v_z (v_z - v_d)^2 dz.$$

In such a case the total energy would dissipate with time.

From the analysis done in this chapter we conclude that the problem of fibre spinning can be expressed in the general framework of classical mechanics.

# Chapter 5

# Numerics

*In this chapter we discuss the numerical procedure used to solve the boundary value problem. Some case studies are also presented to show the sensitivity of the equations with respect to parameters. Finally results of the numerical simulations are presented.*

## 5.1  Numerical scheme: Shooting method

Numerical simulations of the free boundary value problem have been done using a shooting method. Two initial value problems have to be solved. Both of these problems are coupled through boundary values. We consider the domain to be $\Omega = [0, 1]$. One of the boundary conditions at the point $z = 0$ is not specified. Instead the final velocity is prescribed at $z = 1$. Therefore, a shooting technique is used to match the velocity got from the simulation with the prescribed final velocity. For convenience we write down the systems BOC and AOC once more.

The system BOC (Before the onset of crystallisation) reads

$$\begin{aligned} \mathbf{u}'(z) &= \mathbf{f}(\mathbf{u}(z)) \quad \forall z \in [0, \xi) \\ \mathbf{u}(0) &= \mathbf{u}_0 \end{aligned}$$

where $\mathbf{u} \in R^4$.

The system AOC (After the onset of crystallization) reads

$$\begin{aligned} \mathbf{v}'(z) &= \mathbf{g}(\mathbf{v}(z)) \quad \forall z \in (\xi, 1] \\ \mathbf{v}(\xi) &= \mathbf{v}_\xi \end{aligned}$$

where $\mathbf{v} \in R^7$.

**Remark 5.1** *We work with the dimensionless equations as given in Section 2.5.*
We give below the main steps of the shooting algotrithm and discuss the steps in detail in the following subsection.

## Algorithm

- Step 1.
  Let the vector of initial conditions for the system BOC be denoted by $s$ where $s = [u_1(0), u_2(0), c_{zz,0}, c_{rr,0}]$. Here $c_{zz,0}$ is guessed and $c_{rr,0}$ is obtained by solving $\tilde{h}(c_{zz,0}, c_{rr,0}) = 0$ as given by Eq(3.7). Let $s^{(i)}$ and $c_{zz,0}^{(i)}$ denote the $i^{th}$ iteration values of $s$ and $c_{zz,0}$ respectively.

    - initialise the index variable $i$ to 2.
    - guess two initial values $c_{zz,0}^{(i-1)}$ and $c_{zz,0}^{(i)}$.

- Step 2.
  Solve the system BOC using the two IC vectors $s^{(i-1)}$ and $s^{(i)}$. Denote the solutions of the two systems by $u(s^{(i-1)})$ and $u(s^{(i)})$ respectively.

- Step 3.
  Determine the points of onset of crystallization $\xi_{i-1}$ and $\xi_i$ for the two systems using the condition $u_2(s^{(k)}, \xi_k) = T_m, \quad k = i - 1, i$.

- Step 4.
  Solve the system AOC using the interface conditions given by the vector

$$
\begin{aligned}
v_{0,k} \quad := \quad & [v_1(s^{(k)}, \xi_k) = u_1(s^{(k)}, \xi_k), \quad v_2(s^{(k)}, \xi_k) = 0, \\
& v_3(s^{(k)}, \xi_k) = u_2(s^{(k)}, \xi_k), \quad v_4(s^{(k)}, \xi_k) = u_3(s^{(k)}, \xi_k), \\
& v_5(s^{(k)}, \xi_k) = u_4(s^{(k)}, \xi_k), \quad v_6(s^{(k)}, \xi_k) = 0, \\
& v_7(s^{(k)}, \xi_k) = 0]
\end{aligned}
$$

for $k = i - 1, i$.

- Step 5.
  Determine the error
  $$\epsilon = |v_l - v_7(L, s^{(i)})|$$
  where $v_l$ is the draw ratio (prescribed final velocity/initial velocity).

- Step 6.
  Let Tol denote a prescribed tolerance.
  If $\epsilon > $ Tol then

  - Determine the new value of $c_{zz,0}$ using the secant method

    $$c_{zz,0}^{i+1} = c_{zz,0}^{i-1} + (c_{zz,0}^{i} - c_{zz,0}^{i-1})\frac{v_l - v(s^{i-1}, 1)}{v(s^i, 1) - v(s^{i-1}, 1)}$$

  - Update $i = i + 1$.

  - Go to Step 2 and follow the procedure only for the latest value of $i$.

  Else
  Stop


## 5.1.1  Guessing the initial condition

The initial value of $c_{zz}$ at $z = 0$ needs to be guessed. According to the DMM model, at the spinneret exit, the melt exhibits a Newtonian behaviour [12] which is modelled as:

$$\frac{\tau_{rr,0}}{\tau_{zz,0}} = \frac{E_0 c_{rr,0} - 1}{E_0 c_{zz,0} - 1} = -0.5.$$

Solving the above equation we get the following expression for $E_0$:

$$E_0 = \frac{3}{2c_{rr,0} + c_{zz,0}} \tag{5.1}$$

where $E_0, c_{zz,0}, c_{rr,0}$ represent the values of $E, c_{zz}$ and $c_{rr}$ at $z = 0$. From Chapter3 we know that,

$$e_0 = \sqrt{\frac{c_{zz,0} + 2c_{rr,0}}{3N_0}}. \tag{5.2}$$

Substituting the above in Eq.(5.1), we get $E_0$ in terms of $e_0$:

$$E_0 = \frac{1}{e_0^2 N_0}. \tag{5.3}$$

Once the value of $c_{zz,0}$ is guessed, then $c_{rr,0}$ can be computed using the definition of $E$ as given by:

$$E_0 = \frac{L^{-1}(e_0)}{3e_0}$$

Substituting the Langevin function, we have

$$\coth(3e_0 E_0) - \frac{1}{3e_0 E_0} - e_0 = 0. \tag{5.4}$$

Substituting Eq.(5.3) in Eq.(5.4), we get

$$f(e_0, N_0) = \coth\left(\frac{3}{e_0 N_0}\right) - \frac{e_0 N_0}{3} - e_0 = 0. \tag{5.5}$$

Let us fix the value of the parameter $N_0 = 200$ which we shall be using for all our future simulations. (Each polymer molecule is composed of 200 links). Now, we can determine the roots of the function $f$ using the Newton Raphson method. The root of $f(e)$ is $e = 0.0706$. From Eq.(5.2) we have

$$
\begin{aligned}
c_{zz,o} + 2c_{rr,0} &= 3N_0 e^2 = 2.9906 \\
c_{zz,o} + 2c_{rr,0} &\approx 3 \\
c_{rr,0} &\approx \frac{3 - c_{zz,0}}{2}
\end{aligned}
\tag{5.6}
$$

Negative values of $c_{zz}$ and $c_{rr}$ are not realistic as discussed in Chapter3. Moreover, according to Def 3.1, $c_{zz}(0) \leq 0$, $c_{rr}(0) \leq 0$ are aphysical initial conditions. Therefore, we put the restriction that $c_{zz,0} \geq 0$ and $c_{rr,0} \geq 0$. From Eq.(5.6), we see that
Case 1.: for $c_{zz,0} < 1$,     $c_{rr,0} > 1 \Rightarrow c_{zz,0} - c_{rr,0} < 0$
Case 2.: for $c_{zz,0} \geq 1$,     $c_{rr,0} \leq 1 \Rightarrow c_{zz,0} - c_{rr,0} \geq 0$


We know that $\tau_{zz} - \tau_{rr} = E(c_{zz} - c_{rr})$. Since $E$ is always positive (Section 3.2), a negative value of $c_{zz,0} - c_{rr,0}$ implies a negative normal stress difference. In general, for a unaxial stretching the normal stress difference is expected to be positive. For a uniaxial extensional flow the normal stress difference is written as

$$\tau_{zz} - \tau_{rr} = \eta_T \epsilon$$

where $\eta_T$ is the elongational viscosity and $\epsilon$ denotes the elongation rate which in our case is $dv_z/dz$. A negative stress difference would imply a negative elongation rate and a decreasing velocity. From the physical point of view, this seems to be an unrealistic behaviour. Moreover, from Defn 3.1 an initial condition for which $dv_z/dz < 0$ at $z = 0$ is an "aphysical initial condition". Hence, we restrict the value of $c_{zz,0}$ to be greater than or equal to 1.

The condition $c_{rr,0} \geq 0$ gives us an upper bound for $c_{zz,0}$ namely, $c_{zz,0} \lessapprox 3$ The bounds for $c_{zz,0}$ can be written as

$$1 \leq c_{zz,0} \lessapprox 3$$

**Remark 5.2** *Although the given bound is a very rough estimate, in the absence of any other information about the choice of the initial condition, this actually proves to be useful. Numerically it is seen that for any choice of the numerous parameters that this model has, the value of $c_{zz,0} < 1$ is a disaster as the numerics break down completely. From the numerics it is also seen that $1 < c_{zz,0} < 1.02$ is the observed bound for $c_{zz,0}$. In all our simulations it has never exceeded this range.*

**Remark 5.3** *From a physical point of view, a value of $c_{zz}(0) \approx 1$ shows that the melt is in equilibrium near the spinneret. The polymer chains are coiled in the equilibrium configuration, [27].*

## 5.1.2 Calculation of $c_{rr}(0)$ and E

Once, we choose the value of $c_{zz,0}$, the value of $c_{rr,0}$ can be calculated in the following way.
In Eq.(5.5), replace $e_0$ by $c_{zz,0} + 2c_{rr,0}$ and solve the equation using Newton Raphsons method for $c_{rr,0}$.
The value of $E_0$ is determined by solving Eq.(5.4) by again using the Newton Raphson method. But at each point $z$ down the spinline, for each value of $c_{zz}$ and $c_{rr}$, a new value of $E$ has to be computed and this is done by solving the same Eq.(5.4) for current values of $c_{zz}$ and $c_{rr}$.

**Remark 5.4** *For $c_{zz}(0) \geq 1$, we get $c_{rr}(0)$ such that these are plausible initial conditions.*

### 5.1.3   Nature of the ODE systems

### 5.1.4   Note on implementation

The system BOC was solved using the Matlab routine ode23tb. This routine uses the implicit method with backward differentiation to solve stiff differential equations. It is an implementation of TR-BDF2 [24], an implicit 2 stage Runge-Kutta formula where the first stage is a trapezoidal rule step and the second stage is a backward differentiation formula of order two.

The system AOC was solved using the MATLAB routine ode15s which is again an implicit method for solving stiff ODEs. It is a quasi-constant step size implementation of the numerical differentiation formulas in terms of backward differences, [25].

**Observations**

The orders of magnitude of some of the parameters in system BOC are: $De_a \sim O(10^{-10})$, $E \sim O(10^4)$ and it was seen that $e \to 1$. The condition number of the Jacobian of the system was observed to be of the order $10^7$. From this, we see that system BOC is very stiff. Even though efficient implicit methods have been applied, the solution exists only in a certain range.

The order of magnitude of some of the parameters in system AOC are: $D_{sc} \sim O(10^{20})$, $D_{ea} \sim O(10^{-6})$. The variable representing the rate of crystallization $x$ tends to 1. The Jacobian of the ODE system is of order of magnitude $10^{20}$ showing again a highly stiff system. The routine ode15s solves DAE systems also. Due to the observed orders of magnitudes of parameters, one can guess that the ODE system could become a DAE system. In both the routines ode23tb and ode15s the control parameters had to be changed suitably in order to get the desired results since the ODE systems were exceptionally stiff.

### 5.1.5   Calculation of the point of onset of crystallization $\xi$

The criteria for determination of the point $\xi$ is $T(\xi) = T_m$. Since we assume that the temperature at the spinneret exit, i.e at $(z = 0)$, denoted by $T_0$ is

always greater than or equal to the melting temperature $T_m$, the determination of $\xi$ depends on the monotonicity of T. Two questions arise which are of importance for determining $\xi$.

- Does T always decrease monotonically?

- Is it possible that the solution explodes before reaching the point $\xi$?

The answer to the first question is "no" and to the second question is "maybe"! The details about the analysis of the temperature equation have already been treated in Chapter 3. Here, we just show some numerical examples which support the analysis done there.

Determination of $\xi$ depends on the existence of solution of the system BOC. As explained in the previous section, solution of the system BOC may not necessarily exist globally. But we require the solution only in the interval $(0, \xi)$. This means that as soon as we determine $\xi$ we can terminate the simulation for BOC.

Fig.5.1 shows the relation between the initial condition and the minimum and maximum temperatures reached by the system BOC during the course of simulations. In particular Fig.5.1(top) shows the relation between the initial guess for $c_{zz}(0)$ and the minimum temperature. One sees how in a short range of the initial guess the minimum temperature reached changes. Since the determination of the point $\xi$ depends on whether the melting temperature is reached or not, it is important to observe the values of the minimum temperature. Suppose the melting temperature of the fibre happens to be below the minimum temperature, then the point $\xi$ will never be reached. Moreover, from Fig.5.1(bottom) one can see that the temperature certainly does not always decrease monotonically with the maximum temperature far exceeding the initial temperature $T_0$.

## 5.2  Some numerical case studies

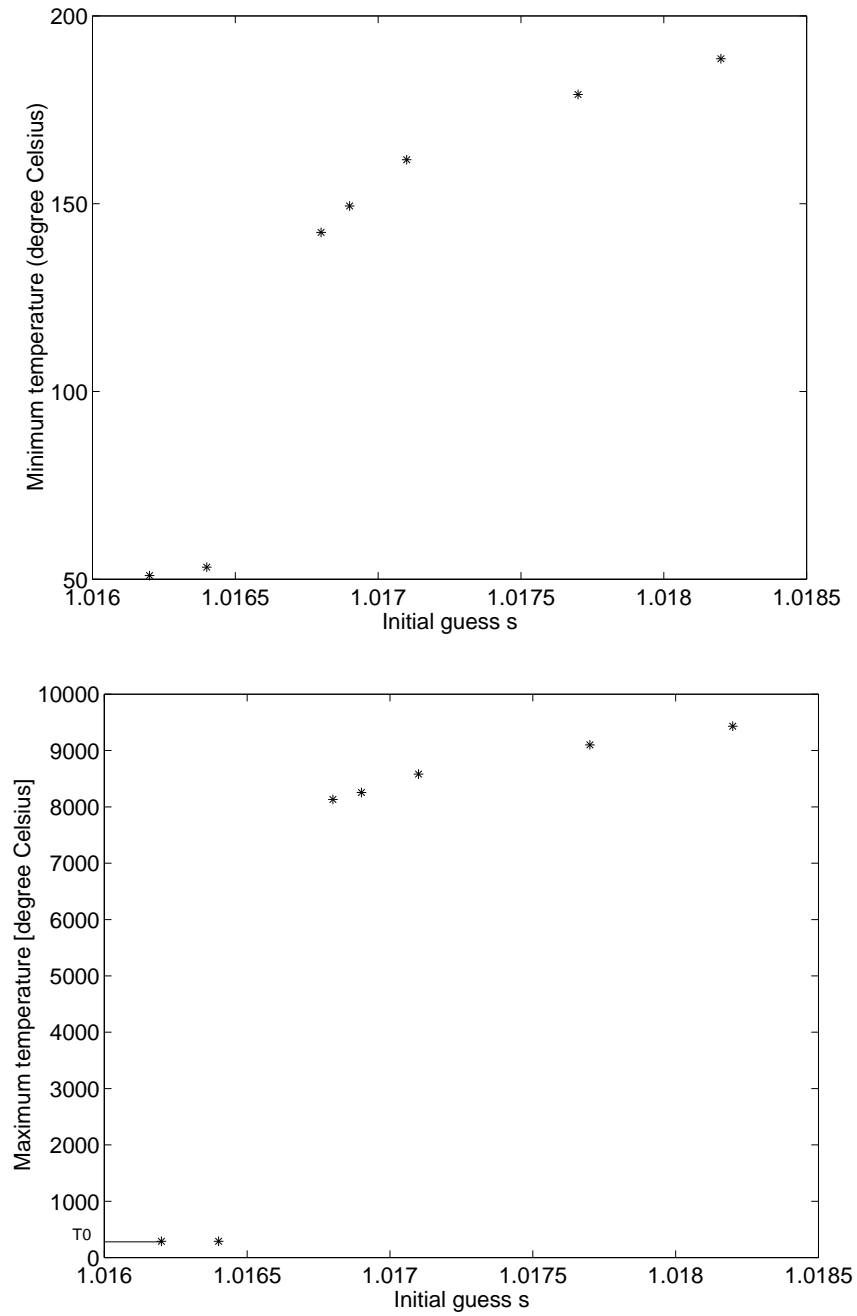Difficulties in simulations owing to stiffness of the system motivated us to do some numerical case studies.

Figure 5.1: Top: *Minimum temperature versus initial guess*, Bottom: *Maximum temperature versus initial guess*
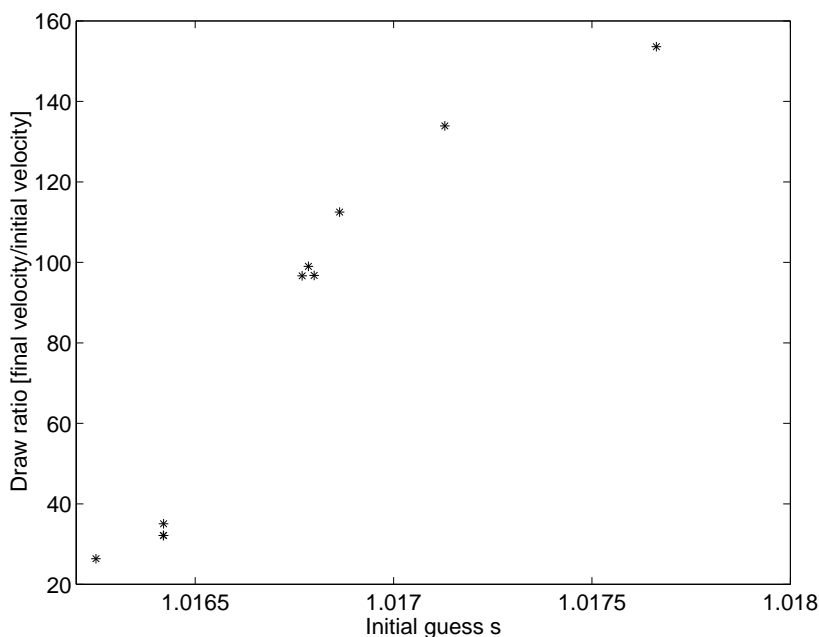
Figure 5.2: *Draw ratio versus initial guess*

## 5.2.1 Relation between initial guess and draw ratio

Fig.5.2 visualises the sensitivity of the ODE system with respect to a change in the initial guess for $c_{zz}$. In a small range of initial guess one sees that the draw ratio changes from around 20 to around 140. This not only emphasises the need for a good initial guess but also an efficient algorithm for the shooting method. Stiffness of the problem can also be measured by the magnitudes of parameters in the system. The Weisenberg number for the semi-crystalline phase was found to be $2.3 \cdot 10^{23}$ and for the amorphous part in the semi-crystalline phase was found to be $2.2 \cdot 10^{-05}$ in one particular simulation.

## 5.2.2 Dependence on parameters

Some numerical experiments are performed to study the sensitivity of system BOC with respect to parameters.

Consider the momentum equation

$$D_1 \frac{dv_z}{dz} = \frac{d}{dz} \left[ \frac{\tau_{zz} - \tau_{rr}}{v_z} \right] - D_2 \frac{(v_z - v_r)^2}{\sqrt{(v_z)}} + \frac{D_3}{v_z} - D_4 (v_z)^{-3/2} \frac{dv_z}{dz}$$

- Let $D_1 = D_2 = D_3 = D_4 = 0$
  We neglect all the parameters representing force due to inertia ($D_1$), air drag ($D_2$), gravity ($D_3$) and surface tension ($D_4$), in the momentum equation so that we are left with the simplest form of the momentum equation. The shooting method converges and we see that the solution of IVP BOC exists continuously even in $[0, 1]$.

- Let $D_1 \neq 0, D_2 = D_3 = D_4 = 0$
  Now we consider the momentum equation with just one parameter representing inertial force. Solution of IVP BOC explodes after reaching $\xi$. But since $\xi$ is reached, shooting method converges.

- Let $D_1 = 0, D_2 \neq 0, D_3 \neq 0, D_4 \neq 0$
  Now, we consider the momentum equation with all the parameters except the inertial term. Shooting method converges and the solution for BOC exists over the whole domain $[0, 1]$.

**Remark 5.5** *In Section 3.1.1, we showed how $D_1$ could lead to a possible singularity making the RHS of the momentum equation singular.*

According to the above numerical experiments it seems that $D_1 = \rho v_0 / L$ representing the force acting on the fibre due to inertia is the parameter which is quite sensitive to the simulations for the phase BOC. In Fig.5.3 one can see the relation between $D_1$ and the draw ratio which is obtained by solving first BOC and then AOC. Keeping all other parameters the same and using the same initial condition for different values of $D_1$ ranging from $D_1 = 0.0040$ to $D_1 = 0.0050$, the value of the final velocity reached at $z = 1$ is plotted.

### Dependence on ODE coefficients

It is seen that just by changing the order of magnitude of some ODE coefficients, the solution either explodes or exists continuously over the domain. We consider for example, the evolution equation of $c_{zz}$

$$\frac{dc_{zz}}{dz} = a \frac{c_{zz}}{v_z} \frac{dv_z}{dz} - \frac{1}{v_z De_a} \left( (1 - \alpha) + \alpha E c_{zz} \right) \left( E c_{zz} - 1 \right)$$
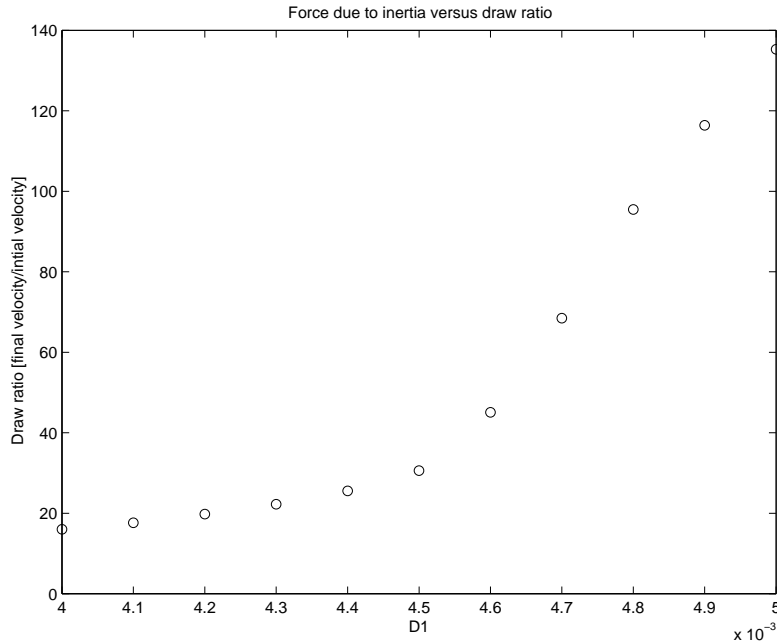
Figure 5.3: *Draw ratio versus $D_1$.*

where $a = 2$ is the actual coefficient in the differential equation. By putting $a = 1.9871$, we perform numerical simulations to study the effect of this change on the system. The results with the different coefficients, calculated with the same initial conditions are shown in the Fig.5.4. The plots reveal to us the lack of any structure in the system. Just by perturbing the ODE coefficient slightly we get very different results. This example throws light on the complexity of the ODE system and infact shows us that the problem is ill-posed.

## 5.3   Results

Figs.5.5 to 5.9 show the numerical results obtained on the basis of data given in Chapter 3 . Results are plotted for take-up velocities ranging from 1000m/min to 7500 m/min.
The results are in good agreement with the expected behaviour of the fibre. We make the following observations from the results.

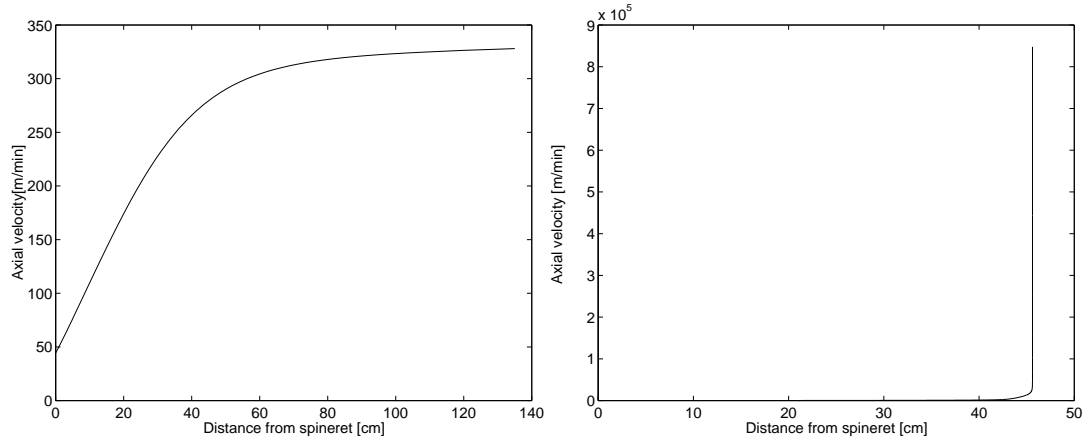- Axial velocity and diameter profiles (Figs 5.5, 5.6)

Figure 5.4: *Axial velocity versus spinlength* Left: *a=1.9871* Right: *a=2*

For high take-up velocities the velocity increases at a higher rate. This sudden increase in the axial velocity results in a sharp decrease in the diameter of the fibre. The region showing this decrease of diameter is the so called " neck" region. As the take up velocity increase this region becomes thinner as seen in Fig.5.6. At low speeds necking is not so visible. The point on the spinline where the axial velocity reaches the take up velocity is called the "freeze point". With increasing take-up velocity the freeze point moves towards the spinneret.

- Temperature profile
  In the temperature plot Fig.5.7 one sees a jump in the temperature owing to the heat released due to crystallization. This increase in temperature takes place just near the freeze point when crystallization is complete.

- $c_{zz}$ and $c_{rr}$ profiles
  Figs.5.8 and 5.9 show the behaviour of the microstructural variables $c_{zz}$ and $c_{rr}$. As crystallization proceeds, due to the transformation from amorphous to semi-crystalline phase, the variables $c_{zz}$ and $c_{rr}$ representing the conformation of the amorphous melt go to zero. At the macroscopic level, these variables can be understood as the corresponding strain tensor components. As crystallization proceeds and the fibre becomes rigid, the strain tends to zero.

- Rate of crystallization
  Fig.5.10 shows the profile of crystallization. One can observe that rate of crystallization is very slow near the point of onset of crystallization
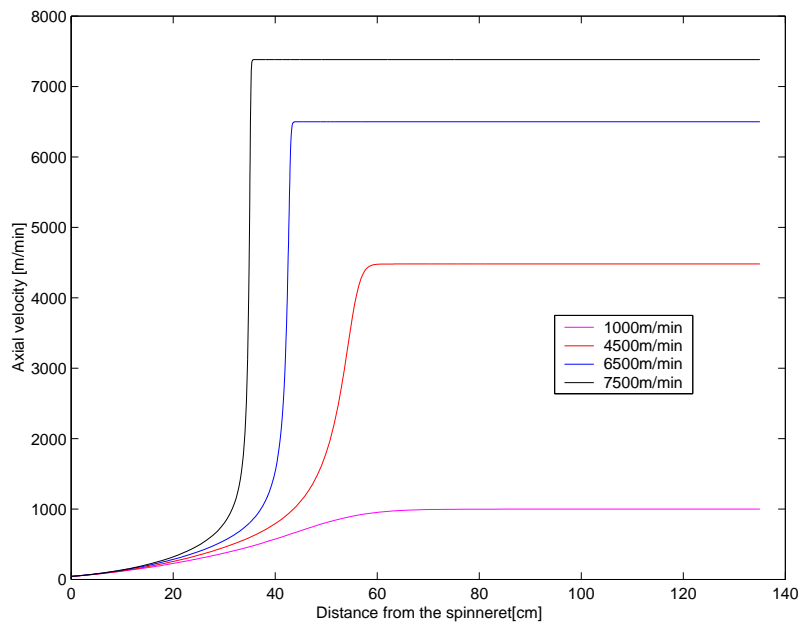
Figure 5.5: *Axial velocity profiles for different take-up velocities.*
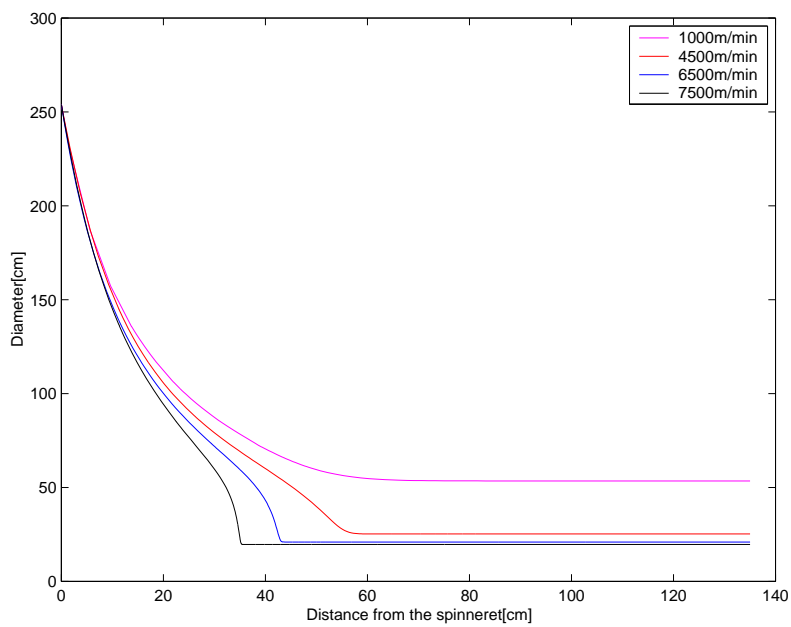


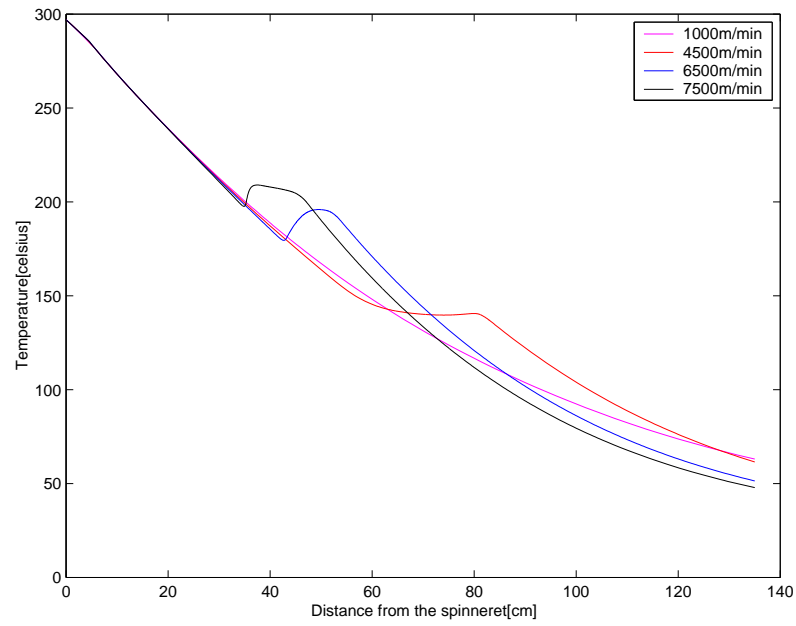Figure 5.6: *Effect of take-up velocity on diameter profiles*

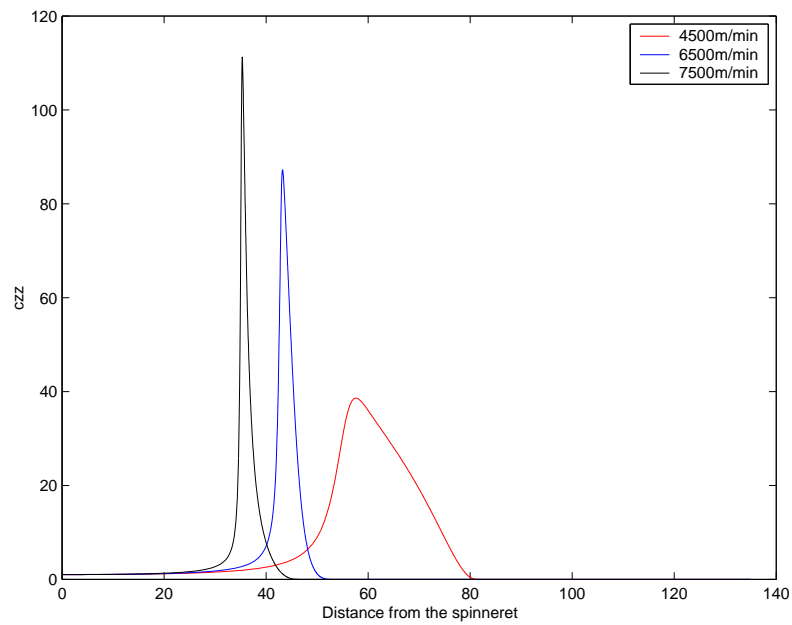Figure 5.7: *Effect of take-up velocity on the temperature profiles*



Figure 5.8: *Effect of take-up velocity on profiles of $c_{zz}$*
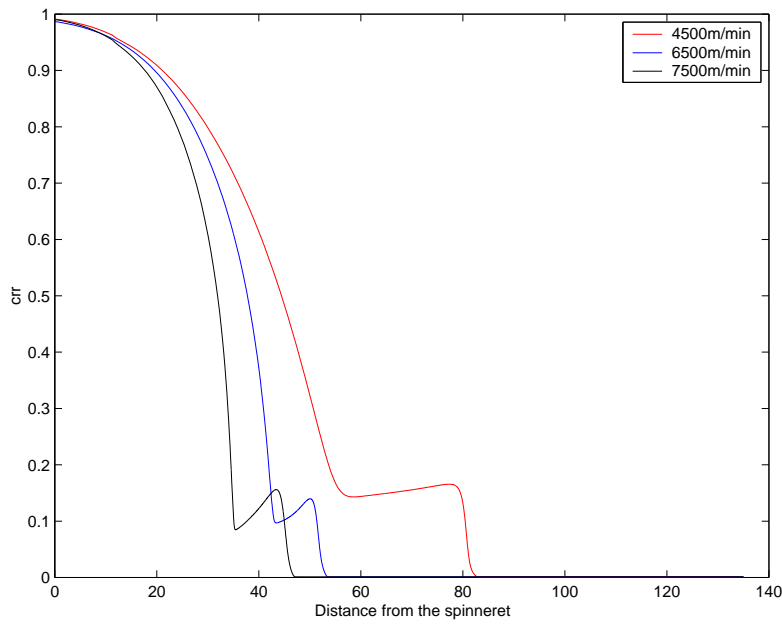
Figure 5.9: *Effect of take-up velocity on profiles of $c_{rr}$*
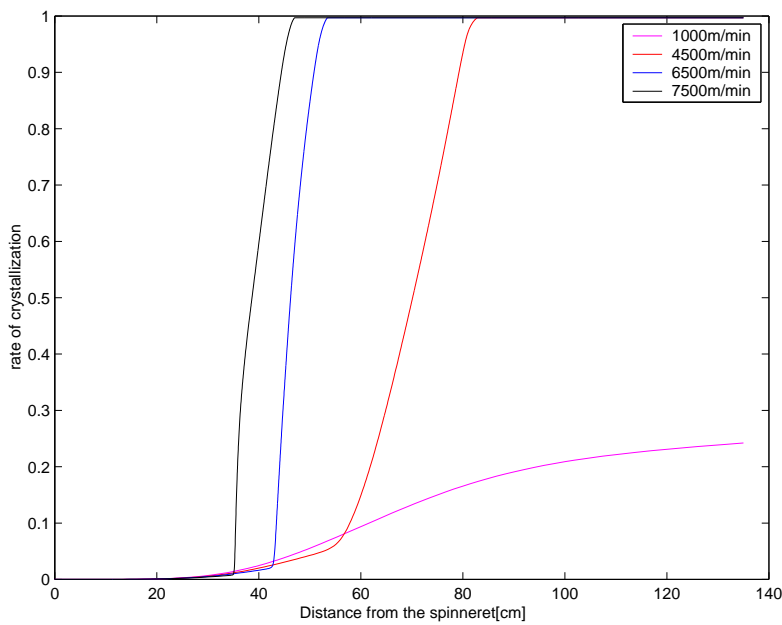


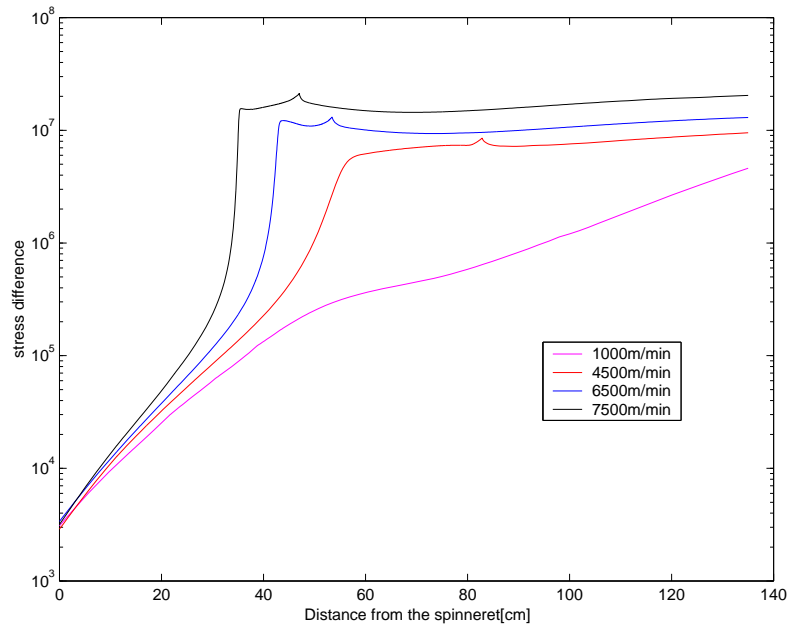Figure 5.10: *Effect of take-up velocity on the crystallization profiles*

Figure 5.11: *Effect of take-up velocity on tensile stress profiles*
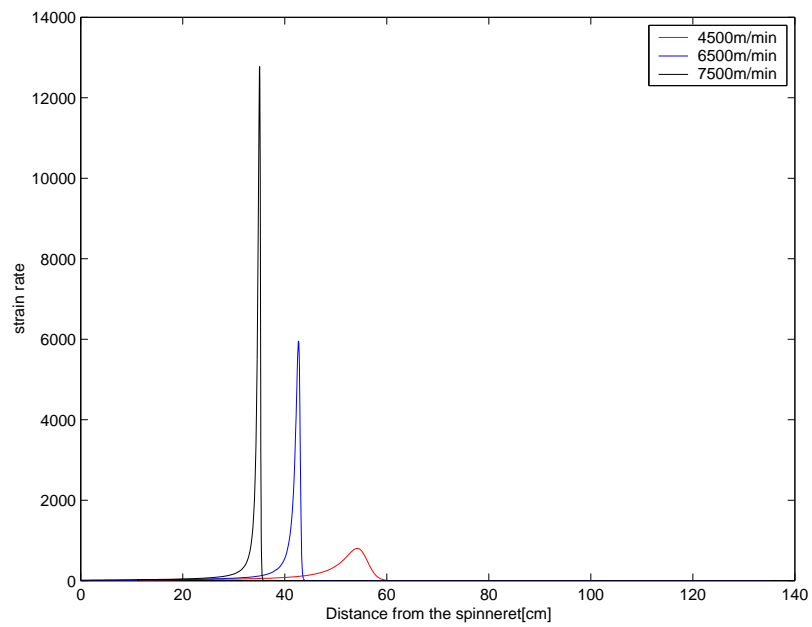


Figure 5.12: *Effect of take-up velocity on strain rate profiles*

which was measured to be approximately 14cm for all take up velocities. It increases suddenly to reach the freeze point exhibiting the "necking phenomena".

- Stress difference
  Fig.5.11 shows the profile of stress difference against distance from the spinneret. This plot has a logarithmic scale. In these profiles necking is indicated by a strong increase of tensile stress just before the freeze point.

- Strain rate
  Fig.5.12 shows the profile of the strain rate $dv_z/dz$. One observes that for high take up velocities the strain rate shoots up near the freeze point and then decays gradually to zero.

In all the plots, one observes that the sudden increase or decrease in variables takes place just near the freeze point. At the point of onset of crystallization which is about 14cm from the spinneret exit, there is no noticeable change in any of the variables.

The advantage of this model seems to lie firstly in the fact that it has taken into account effects like crystallization and necking along with forces like air drag, inertia, gravity and surface tension. In this sense the model is complete. From the numerics, it has been shown that the model is valid for medium to high speed spinning conditions. The results, as will be seen in the next chapter are in good agreement with experimental data. Moreover the freeze point arises naturally here as opposed to other models where it has to be artificially induced. The disadvantage is the highly stiff system of equations that arise from the model. Choosing the initial guess in the first challenge. To apply efficient numerical solvers to the stiff system of ODEs is the next challenge. The third challenge lies in fitting the model parameters to the experimental profiles. However, we have done the simulations for take-up velocities as high as 7500m/min which have not been done earlier using this model to our knowledge. Usually, the higher is the take-up velocity, more difficult are the numerical simulations. In this context, this model has proved to be very robust.

**Remark 5.6** *The change induced in the original DMM model in terms of the interface condition at the point of onset of crystallization was not found to influence the result significantly.*

**Remark 5.7** *All the simulations in this chapter have been done with constant model parameters as given in chapter3*

# Chapter 6

# Industrial Application

*In this chapter we present a comparison of our simulation results based on given industrial data by* Freudenberg & Co *with the experimental profiles provided by them. In particular, we compare the axial velocity profile of the fibre with the experimentally measured profile under different spinning conditions.*

## 6.1 Simulations and comparisons with experimental data

Simulations have been performed for four sets of data and the material used is PET. The material properties of PET are tabulated below.

| Property | Value | Units |
|---:|:---:|:---:|
| Density | 0.98 | g/cm$^3$ |
| Zero shear viscosity | 163 | Pa s |
| Thermal conductivity | 20900 | calories /cm s °C |
| Melt shear modulus | 952000 | Pa |

Table 6.1: *Material properties of PET*

85

| Process parameter (units) | Data1 | Data2 | Data3 | Data4 |
|---|---|---|---|---|
| Diameter (mm) | 0.5 | 0.5 | 0.5 | 0.5 |
| Melting temperature (°C) | 300 | 290 | 290 | 290 |
| Velocity of quench air (m/s) | 0.5 | 0.4 | 0.4 | 0.4 |
| Temperature of quench air (°C) | 70 | 27 | 27 | 27 |
| Take up velocity (m/s) | 83.2 | 51.04 | 58.65 | 64.82 |
| Length of the fibre (mm) | 2000 | 750 | 750 | 750 |
| Mass throughput (gr/min) | 1.16 | 0.63 | 0.86 | 0.86 |
| Distance for quench air (mm) | 300 | 50-400 | 50-400 | 50-400 |

Table 6.2: *Table of data*

We observe that for various processing conditions, the numerical results are in very good agreement with the experimental profiles. We must remember the sensitivity of the numerics to the process parameters. These simulations have been done for spinlength ranging from 750mm to 2000mm, quench air temperatures as different as 70 °C and 27 °C and take-up velocities ranging from 51.04 m/s to 83.2 m/s. In Fig.6.4 we see a slight disparity of the numerical profile from the experimental one. This could also be attributed to error is measurements as will be described in the next section. However, it should be observed that the freeze point has been predicted to be fairly close to its experimental value in all the cases.

## 6.2   Note on experimental measurements

The experimental profiles that have been shown here are only the mean values of the various sets of measurements taken at different points down the spin line. Therefore, they can by no means be regarded as the most accurate measurement of velocity down the spinline. Also since the measurement takes place in the presence of hundreds of other fibres, error in measurement cannot be excluded. This could account for the disparity in the experimental and numerical profiles at some places.

**Remark 6.1** *For these simulations we had to change some of the model parameter values which we took from [11]. The correct choice of parameters is a matter of fitting the parameters to experimental profiles. Due to the lack of such data we did not perform such a fitting. Much work has been done by Doufas et al, [11], [13], in this regard.*
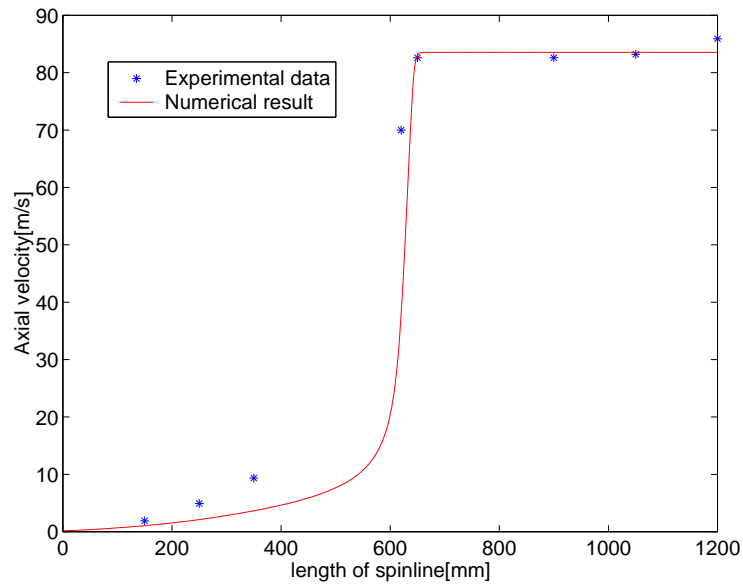
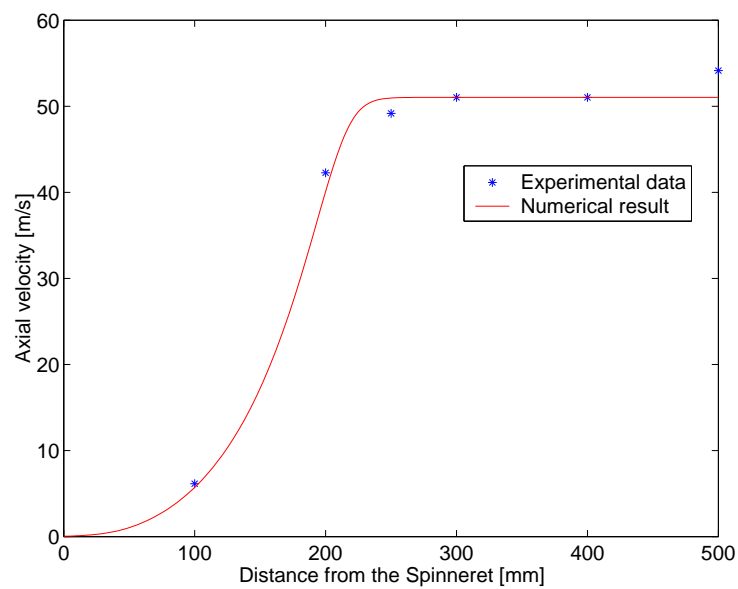Figure 6.1: *Comparison of axial velocity profiles for Data 1.*



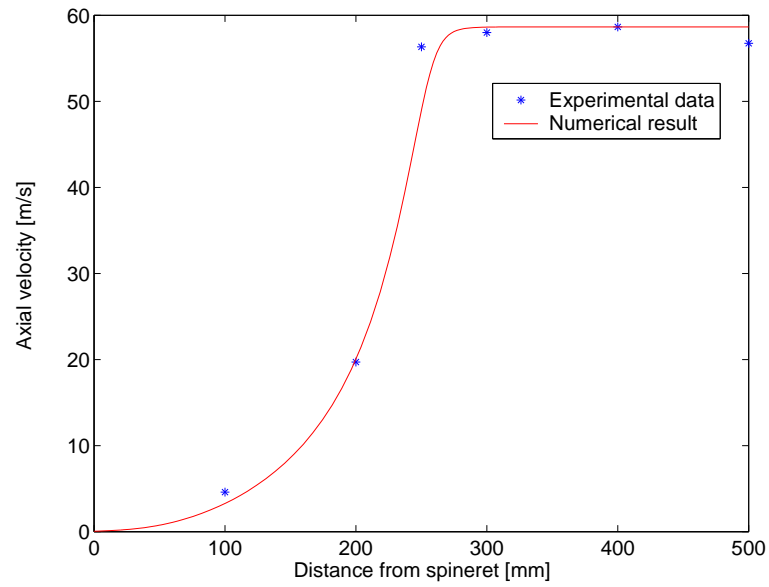Figure 6.2: *Comparison of axial velocity profiles for Data 2*

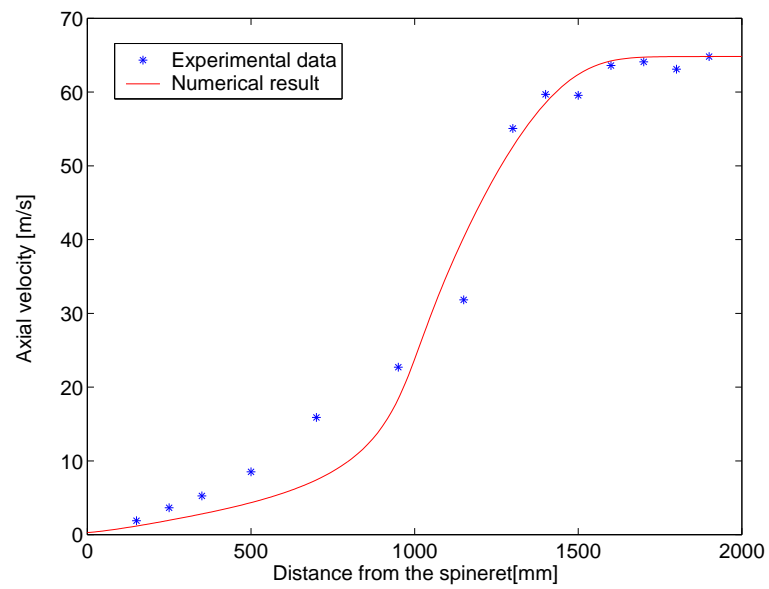Figure 6.3: *Comparison of axial velocity profiles for Data 3*



Figure 6.4: *Comparison of axial velocity profiles for Data 4*

# Conclusion

We did an investigation of the DMM model of melt spinning which takes into account effects of inertia, air drag, gravity and surface tension in the momentum equation, heat exchange between air and fibre surface and viscous dissipation in the temperature equation and crystallization. Moreover, the model has a complicated coupling with microstructural equations in the two phases BOC and AOC. We made two changes in DMM model concerning the air drag and an interface condition. However these changes did not influence the results in a big way. The mathematical problem associated with the model is a non-linear, coupled, free boundary value problem. The analysis showed that the solution depended heavily on the parameters and initial conditions. We showed that a global solution of IVP BOC in general does not exist. Therefore we were led to look for a maximal solution. By defining a *physically acceptable solution*, it was shown that for a more restricted set of initial conditions, if a unique solution exists for IVP BOC then it is a physically acceptable solution. For this we proved the important property of positivity of the conformation tensor. Further, we showed that if a physically acceptable solution exists for IVP BOC, then under certain conditions it also exists for IVP AOC. This gives an important connection between the initial conditions of IVP BOC and the existence of solution of IVP AOC.

A new investigation was done for the melt spinning problem in the framework of classical mechanics. We derived appropriate Poisson brackets for the 1-d flow of viscoelastic fluid. From the 1-d Hamiltonian, we derived cross-sectionally averaged mass, momentum equations of melt spinning along with the microstructural equations. These studies show that the complicated problem of melt spinning coupled with microstructure can also be studied under the framework of classical mechanics. This work provides the basic ground work on which more investigations on the dynamics of a fibre could be done.

Numerical simulations were done in MATLAB using inbuilt routines to solve

the IVPs arising in the problem and applying a shooting method to solve the boundary value problem. We did some numerical case studies to study the sensitivity of the ODE systems with respect to the initial guess and parameters. These experiments support the analysis done and throw more light on the stiff nature and ill-posedness of the ODE systems which show that both numerics and analysis of such a system of equations is a very challenging task. However, to validate the model, simulations were performed on sets of data provided by the company *Freudenberg Nonwovens group* and comparison of the numerical result (axial velocity profile) was done with the experimental profiles provided by them. The numerical results were in very good agreement with the experimental profiles.

# Appendix A

## Polymer physical properties

In this appendix we give a summary of the models of material properties of polymer as taken from [12].

- Zero-shear viscosity of the melt

$$\eta_0 = \eta_0(280°C) \exp\left(\frac{E_A(280 - T)}{1099.2(T + 273.2)}\right) \quad (1)$$

  where $E_A$ is the activation energy typically taken as 13,500 cal/mol for Nylon. The relaxation time $\lambda_{a,0}$ is calculated from Eq.(1) using the relation $\lambda_{a,0} = \eta_0/G$.

- Heat capacity
  The heat capacity $C_p$ is a function of temperature and crystallinity

$$C_p = C_s x\phi_\infty + C_1(1 - x\phi_\infty)$$

  where $C_s$ is the heat capacity of the crystalline region and $C_1$ is that of the amorphous region.

$$C_s(T) = C_{s1} + C_{s2}T + C_{s3}(T)^2 \quad (2)$$
$$C_1(T) = C_{11} + C_{12}T + C_{13}(T)^2 \quad (3)$$

- Heat of fusion

$$\Delta H_f(T) = \Delta H_f(0) + (C_{11} - C_{s1})T + (C_{12} - C_{s2})\frac{T^2}{2} + (C_{13} - C_{s3})\frac{T^3}{3} \quad (4)$$

  where $\Delta H_f(0)$ is a reference heat of fusion taken to be equal to $50 cal/g$ for Nylon.

- Crystallization parameter
  The Avrami constant $K_{av}$ used in the evolution equation of rate of crystallization is described by:

$$K_{av}(T) = 1.47 \cdot 10^{-3} \left( \frac{4\pi N_u}{3\phi_{\infty,is}} \right)^{1/3} \exp\left( -\left( \frac{T - 141}{47.33} \right)^2 \right) \quad (5)$$

where $N_u$ represents the number density of nuclei initially present within the melt spinneret. A typical value of $N_u$ is taken to be $10^{10}$ per $cm^3$. The ultimate isotropic crystallinity $\phi_{\infty,is}$ is taken as 0.5.

- Physical properties of quench air

  - Density : $\rho_a = \frac{0.351}{T_f} (g/cm^3)$

  - Viscosity : $\mu_a = \frac{1.446 \cdot 10^{-5} T_f^{1.5}}{T_f + 113.9}$ (poise)

  - Thermal conductivity: $k_a = 4.49 \cdot 10^{-7} T_f^{0.866}$ (cal/cm $s \,^\circ C$)
    where $T_f(K)$ is the temperature defined as the arithmetic mean of the filament temperature and the quench air temperature.

The heat transfer coefficient is modelled as:

$$\beta = \frac{0.42 k_a}{D} \mathrm{Re}^{0.334} \left[ 1 + \left( \frac{8 v_c}{v_z - v_d} \right)^2 \right]^{0.167} \quad (6)$$

where $v_c$ is the horizontal component of the velocity and $v_d$ the downward component of velocity.

# Appendix B

## Derivation of fibre spinning equations from hamiltonian

The functional derivatives with repect to the Hamiltonian Eq.(4.4) are as given in Section (4.4). To understand the steps of the calculations better we repeat those equations got by susbtituting the derivatives in the dynamical equation for $F$ :

$$\frac{\partial \tilde{\rho}}{\partial t} = -\frac{\partial}{\partial z}\left(\frac{\delta H}{\delta \tilde{M}_z}\tilde{\rho}\right) \tag{7}$$

$$\frac{\partial \tilde{s}}{\partial t} = -\frac{\partial}{\partial z}\left(\frac{\delta H}{\delta \tilde{M}_z}s\right) + \frac{1}{T}\Lambda_z\frac{\delta H}{\delta \tilde{C}_{zz}}\frac{\delta H}{\delta \tilde{C}_{zz}} + \frac{1}{T}\Lambda_r\frac{\delta H}{\delta \tilde{C}_{rr}}\frac{\delta H}{\delta \tilde{C}_{rr}} \tag{8}$$

$$\frac{\partial \tilde{M}_z}{\partial t} = -\tilde{\rho}\frac{\partial}{\partial z}\left(\frac{\delta H}{\delta \tilde{\rho}}\right) - \frac{\partial}{\partial z}\left(\frac{\delta H}{\delta \tilde{M}_z}\tilde{M}_z\right) - \tilde{M}_z\frac{\partial}{\partial z}\left(\frac{\delta H}{\delta \tilde{M}_z}\right) - s\frac{\partial}{\partial z}\left(\frac{\delta H}{\delta \tilde{s}}\right)$$
$$-\tilde{C}_{zz}\frac{\partial}{\partial z}\left(\frac{\delta H}{\delta \tilde{C}_{zz}}\right) + \tilde{C}_{rr}\frac{\partial}{\partial z}\left(\frac{\delta H}{\delta \tilde{C}_{rr}}\right) + \frac{\partial}{\partial z}2\tilde{C}_{zz}\frac{\delta H}{\partial \tilde{C}_{zz}} - 2\frac{\partial}{\partial z}\left(\tilde{C}_{rr}\frac{\delta H}{\delta \tilde{C}_{rr}}\right) \tag{9}$$

$$\frac{\partial \tilde{C}_{zz}}{\partial t} = -\frac{\partial}{\partial z}\left(\tilde{C}_{zz}\frac{\delta H}{\delta \tilde{M}_z}\right) + 2\frac{\partial}{\partial z}\frac{\delta H}{\delta \tilde{M}_z}\tilde{C}_{zz} - \Lambda_z\frac{\delta H}{\delta \tilde{C}_{zz}} \tag{10}$$

$$\frac{\partial \tilde{C}_{rr}}{\partial t} = -\frac{\partial}{\partial z}\left(\tilde{C}_{rr}\frac{\delta H}{\delta \tilde{M}_z}\right) - \frac{\partial}{\partial z}\frac{\delta H}{\delta \tilde{M}_z}\tilde{C}_{rr} - \Lambda_r\frac{\delta H}{\delta \tilde{C}_{rr}} \tag{11}$$

Now, let us consider the above equations one by one. First consider Eq.(7). Substituting for the functional derivatives, one obtains

$$\frac{\partial \tilde{\rho}}{\partial t} = -\frac{\partial}{\partial z}(\tilde{\rho}v_z).$$

Substituting $\tilde{\rho} = \rho A$ in the above equation one gets the continuity equation.

$$\frac{\partial}{\partial t}(\rho A) = -\frac{\partial}{\partial z}(\rho v_z A) \tag{12}$$

Now consider Eq.(8). Substituting the functional derivatives in the equation one gets

$$\frac{d\tilde{M}_z}{dt} = -\tilde{\rho}\frac{\partial}{\partial z}\left(-\frac{\tilde{M}_z^2}{2\tilde{\rho}^2}\right) - \tilde{\rho}\frac{\partial}{\partial z}\left(\frac{\partial \tilde{U}}{\partial \tilde{\rho}}\right) - \frac{\partial}{\partial z}\left(\frac{\tilde{M}_z^2}{\tilde{\rho}}\right) - M_z\frac{\partial}{\partial z}\left(\frac{\tilde{M}_z}{\tilde{\rho}}\right)$$
$$- s\frac{\partial}{\partial z}\left(\frac{\partial \tilde{U}}{\partial \tilde{s}}\right) - \tilde{C}_{zz}\frac{\partial}{\partial z}\left(\frac{\partial \tilde{U}}{\partial \tilde{C}_{zz}}\right) - \tilde{C}_{rr}\frac{\partial}{\partial z}\left(\frac{\partial \tilde{U}}{\partial \tilde{C}_{rr}}\right) + \frac{\partial}{\partial z}\left(2\tilde{C}_{zz}\frac{\partial \tilde{U}}{\partial \tilde{C}_{zz}}\right)$$
$$- \frac{\partial}{\partial z}\left(2\tilde{C}_{rr}\frac{\delta \tilde{U}}{\delta \tilde{C}_{rr}}\right)$$

$$\tag{13}$$

The second, fifth, sixth and seventh terms in the above equation can be written as follows:

$$-\tilde{\rho}\frac{\partial}{\partial z}\left(\frac{\partial \tilde{U}}{\partial \tilde{\rho}}\right) - s\frac{\partial}{\partial z}\left(\frac{\partial \tilde{U}}{\partial \tilde{s}}\right) - \tilde{C}_{\alpha\alpha}\frac{\partial}{\partial z}\left(\frac{\partial \tilde{U}}{\partial \tilde{C}_{\alpha\alpha}}\right)$$
$$= -\frac{\partial}{\partial z}\left(-\tilde{\rho}\frac{\partial \tilde{U}}{\partial \tilde{\rho}} - s\frac{\partial \tilde{U}}{\partial \tilde{s}} - \tilde{C}_{\alpha\alpha}\frac{\partial \tilde{U}}{\partial \tilde{C}_{\alpha\alpha}}\right) + \frac{\partial \tilde{U}}{\partial \tilde{\rho}}\frac{\partial \tilde{\rho}}{\partial z} + \frac{\partial \tilde{U}}{\partial \tilde{s}}\frac{\partial \tilde{s}}{\partial z} + \frac{\partial \tilde{U}}{\partial \tilde{C}_{\alpha\alpha}}\frac{\partial \tilde{C}_{\alpha\alpha}}{\partial z}$$
$$= -\frac{\partial}{\partial z}\left(-\tilde{\rho}\frac{\partial \tilde{U}}{\partial \tilde{\rho}} - s\frac{\partial \tilde{U}}{\partial \tilde{s}} - \tilde{C}_{\alpha\alpha}\frac{\partial \tilde{U}}{\partial \tilde{C}_{\alpha\alpha}} - \tilde{U}\right) \tag{14}$$

In the above equation the term with $\tilde{C}_{\alpha\alpha}$ represents the sum of corresponding terms with $\alpha = z, r$. After expanding Eq.(14) one can verify that:

$$-\tilde{\rho}\frac{\partial}{\partial z}\left(\frac{\partial \tilde{U}}{\partial \tilde{\rho}}\right) - s\frac{\partial}{\partial z}\left(\frac{\partial \tilde{U}}{\partial \tilde{s}}\right) - \tilde{C}_{\alpha\alpha}\frac{\partial}{\partial z}\left(\frac{\partial \tilde{U}}{\partial \tilde{C}_{\alpha\alpha}}\right) = 0$$

After doing some more manipulations we get the following momentum equation:

$$\frac{\partial \tilde{M}_z}{\partial t} = -\frac{\partial}{\partial z}(\tilde{\rho}v_z^2) + 2\frac{\partial}{\partial z}\left(\tilde{C}_{zz}\frac{\partial \tilde{U}}{\partial \tilde{C}_{zz}}\right) - 2\frac{\partial}{\partial z}\left(\tilde{C}_{rr}\frac{\partial \tilde{U}}{\partial \tilde{C}_{rr}}\right)$$

Substituting $\tilde{\tau}_{\alpha\alpha} = 2\tilde{C}_{\alpha\alpha}\frac{\delta \tilde{U}}{\delta \tilde{C}_{\alpha\alpha}}$ we get

$$\frac{\partial \tilde{M}_z}{\partial t} = -\frac{\partial}{\partial z}(\tilde{\rho}v_z^2) + \frac{\partial \tilde{\tau}_{zz}}{\partial z} - \frac{\partial \tilde{\tau}_{rr}}{\partial z}$$

Using the continuity equation one can get the momentum equation as follows:

$$\rho A \frac{\partial v_z}{\partial t} = -\rho A v_z \frac{\partial v_z}{\partial z} + \rho \frac{\partial}{\partial z}(A(\tau_{zz} - \tau_{rr})) \tag{15}$$

The evolution equations for $c_{zz}$ and $c_{rr}$, after substituting for the relaxation parameters in Eqs.(9) and (10) and using the continuity equation are the following:

$$\frac{\partial c_{zz}}{\partial t} = -v_z \frac{\partial c_{zz}}{\partial z} + 2c_{zz} \frac{\partial v_z}{\partial z} - \frac{c_{zz}}{\lambda_a nK}\left(1 - \alpha + \frac{KEc_{zz}}{k_B T}\right)(c_{zz}EnK - nk_B T) \tag{16}$$

$$\frac{\partial c_{rr}}{\partial t} = -v_z \frac{\partial c_{rr}}{\partial z} - c_{rr} \frac{\partial v_z}{\partial z} - \frac{c_{rr}}{\lambda_a nK}\left(1 - \alpha + \frac{KEc_{rr}}{k_B T}\right)(c_{rr}EnK - nk_B T). \tag{17}$$

# Notations

As general conventions, scalar-valued quantities are denoted by normal-sized letters ($x$), vectors and tensors by bold face letters ($\mathbf{n}$).
Furthermore, we have used the following notations:

## Variables

| | | | |
|---|---|---|---|
| $z$ | z-coordinate | $\boldsymbol{\sigma}$ | stress tensor |
| $r$ | r-coordinate | $\boldsymbol{\tau}$ | shear stress tensor |
| $\theta$ | $\theta$-coordinate | $\mathbf{D}$ | deformation rate tensor |
| $v_\theta$ | velocity in $\theta$-direction | $\mathbf{c}$ | conformation tensor |
| $v_r$ | velocity in r-direction | $\mathbf{S}$ | orientation tensor |
| $v_z$ | velocity in z-direction | $\mathbf{n}$ | normal vector to the free surface of the fibre. |
| $D$ | diameter of the fibre | $\kappa_r$ | curvature of the fibre in r direction |
| $\sigma_s$ | surface tension | $\kappa_z$ | curvature of the fibre in z direction |

## Physical and rheological parameters

| | | | |
|---|---|---|---|
| $T_a$ | temperature of air | $G$ | melt shear modulus |
| $T_m$ | melting temperature of polymer | $C_p$ | heat capacity of the polymer |
| $v_d$ | downward component of quench air velocity | $g$ | acceleration due to gravity |
| $v_c$ | horizontal component of quench air velocity | $k_a$ | thermal conductivity of air |
| $\rho$ | density of polymer | $k$ | heat conduction coefficient |
| $\rho_a$ | density of air | $\beta$ | heat transfer coefficient |
| $\eta_0$ | zero shear viscosity of polymer | $\mu$ | viscosity of polymer |
| $N_0$ | number is statistical links | $\mu_a$ | viscosity of air |

## Processing conditions

$v_L$   take-up velocity
$v_l$   draw ratio
$W$   mass throughput
$T_0$   temperature at exit of spinneret
$D_0$   diameter at spinneret exit
$L$   length of the fibre

## Mathematical symbols

Dot product        $\mathbf{u} \cdot \mathbf{v} = \Sigma_i u_i v_i$
Dyadic product   $\mathbf{u} \otimes \mathbf{v} = [u_i v_j]_{i,j=1..3}$
Tensor product   $\boldsymbol{\tau} : \boldsymbol{\tau} = \Sigma_{i,j=1}^{3} \tau_{ij} \tau_{ij}$

## Numbers and constants

$\lambda_a$      relaxation time of amorphous phase
$\lambda_{sc}$   relaxation time of semi-crystalline phase
$\mathrm{De}_a$   Weisenberg number of amorphous phase
$\mathrm{De}_{sc}$   Weisenberg number of semi-crystalline phase
$C_d$      air drag coefficient
$k_B$      Boltzmann constant
$K$      Hookean spring constant
$l$      length of a statistical link

# References

[1] ADVANI, S.G., AND TUCKER, C.L, *Closure approximations for three-dimensional structure tensors*, J. Rheology. 34(3), 367–386 (1990)

[2] BERIS, A.N., EDWARDS, B.J., *Theromodynamics of flowing systems*, Oxford Science Publications (1994)

[3] BERIS, A.N., EDWARDS, B.J., *Non-canonical Poisson bracket for nonlinear elasticity with extensions to viscoelasticity*, J. Phys. A:Math. Gen.24 261-2480 (1991)

[4] BIRD, R.B., ARMSTRONG, R.C., AND HASSAGER, O., *Dynamics of polymeric liquids, volume 1, First edition*, John Wiley & Sons (1977)

[5] BIRD, R.B., ARMSTRONG, R.C., AND HASSAGER, O., *Dynamics of polymeric liquids, volume 1, Second edition*, John Wiley & Sons (1987)

[6] BIRD, R.B., CURTIS, C.F., ARMSTRONG, R.C., AND HASSAGER, O., *Dynamics of polymeric liquids, volume 2*, John Wiley & Sons (1987)

[7] CHOUMILINA, A., *Visco-Elastic models for fiber spinning*, Master thesis, Univerity of Kaiserslautern (2001)

[8] CODDINGTON, E.A., AND LEVINSON, N, *Theory of Ordinary Differential Equations*, McGraw-Hill Book Company (1955)

[9] DAEHLEN, M. AND TVEITO, A., *Numerical Methods and Software Tools in Industrial Mathematics*, Birkhaeuser (1997)

[10] DARBY, R., *Viscoelastic fluids*, Marcel, Dekker, INC. (1976)

[11] DOUFAS, A.K, *A microstructural model for flow-induced crystallization with applications to the simulation of polymer processes*, Dissertation,Urbana,Illinois (2000)

[12] DOUFAS, A.K.,MCHUGH, A.J. AND MILLER, C., *Simulation of melt spinning including flow-induced crystallization Part I. Model development and prediction*, J. Non-Newtonian Fluid Mech. 92, 27–66 (2000)

[13] DOUFAS, A.K.,MCHUGH, A.J. AND MILLER, C., *Simulation of melt spinning including flow-induced crystallization Part II. Quantitative comparisons with industrial spinline data*, J. Non-Newtonian Fluid Mech. 92, 81–103 (2000)

[14] EDWARDS, B.J. AND BERIS, A.N, *Non-canonical Poisson bracket for nonlinear elasticity with extensions to viscoelasticity*, J. Phys. A:Math. Gen.24, 2461–2480 (1991)

[15] FEISTAUER, M., *Mathematical methods in fluid dynamics*, Longman Scientific and Technical (1993)

[16] GOLDSTEIN, H., POOLE, C. AND SAFKO, J., *Classical mechanics third edition* Addison Wesley, (2002)

[17] HAGEN, T.C., *Elongational flows in polymer processing*, Doctoral thesis, Virginia Polytechnic Institute and State University (1998)

[18] HENRY, D.I.A., BROWN, R., AND YANG, Y.M, *Hamiltonian formulation of inviscid flows with free boundaries*, Phys. Fluids, Vol 31(10), (1988)

[19] KRONJAEGER, J., *Numerical studies of viscoelastic shear turbulence*, Diplomarbeit Department of Physics, Philipps-Universitaet Marburg(2001)

[20] LANGTANGEN, H.P, *Derivation of a Mathematical Model for Fibre Spinning*, Dept. of Mathematics, Mechanics Division, University of Oslo (1997)

[21] MORRISON, P.J, AND GREEN, J.M., *Noncanonical Hamltonian density formulation of hydrodynamics and ideal magnetohydrodynamics*, Phys, Rev, Lett.45:790-4;errata. ibid.48:569(1982)

[22] MORRISON, P.J, *The Maxwell-Vlasov equations as a continuous Hamiltonian system*, Phys. Lett.80A:383-6

[23] PHAN-THIEN, N., *A nonlinear network viscoelastic model*, J. Rheology. 22(3), 259–283 (1978)

[24] SHAMPINE, L.F. AND HOSEA, M.E, *Analysis and Implementation of TR-BDF2*, Applied Numerical mathematics 20,(1996)

[25] SHAMPINE, L.F. AND REICHELT, M.W., *The MATLAB ODE Suite*, SIAM Journal of Scientific Computing, Vol. 18, pp1–22(1997)

[26] SPANIER, J, AND OLDHAM, K.B, *An Atlas of Functions*, Hemisphere publishing corporation (1987)

[27] TANNER, R.I., *Engineering rheology*, Oxford Science Publications (1988)

[28] ZIABICKI, A., *Fundamentals of fibre formation*, John Wiley & Sons, New York (1976)

[29] ZIABICKI, A., AND KAWAI, H., *High-speed fibre spinning*, John Wiley & Sons, New York (1985)

# Curriculum Vitae

| | |
|---|---|
| 29.July 1975 | Born in Tamil Nadu (India) |
| 1981 – 1991 | Primary and middle school, Army school Srinagar (India) |
| 1991 – 1993 | High school at Kendriya Vidyalaya, Madras (India) |
| 1993 – 1996 | Bachelor of Science (Mathematics), Madras university, Madras (India) |
| 1996 – 1998 | Master of Science (Mathematics) IIT Madras, Madras (India) |
| Oct. 1998 – 2000 | Master of Science (Industrial Mathematics), Technical University of Kaiserslautern |
| Dec. 2001 – April 2005 | PhD (Department of Mathematics) Technical University of Kaiserslautern |